UNIVERSITÉ DE SHERBROOKE
Faculté de génie

PHOTOCORROSION DIGITALE DE MICROSTRUCTURES À SEMI-CONDUCTEURS QUANTIQUES : UNE MÉTHODE DE DIAGNOSTIQUE STRUCTURALE ET DE DÉTECTION DE MOLÉCULES CHARGÉES ÉLECTRIQUEMENT

DIGITAL PHOTOCORROSION OF QUANTUM SEMICONDUCTOR MICROSTRUCTURES: A METHOD FOR STRUCTURAL DIAGNOSTICS AND SENSING OF ELECTRICALLY CHARGED MOLECULES

Thèse de doctorat

Srivatsa AITHAL

Composition du jury :
Prof. Jan J. Dubowski, Université de Sherbrooke, directeur
Prof. Mohamed Chaker, Institute National de la Recherche Scientifique, expert externe
Prof. Eric H. Frost, Université de Sherbrooke, expert interne
Prof. Serge Charlebois, Université de Sherbrooke, rapporteur

Sherbrooke (Québec) Canada 18th Sept 2018

Dedicated to my father and mother

RÉSUMÉ

La fabrication de dispositifs à base de structures multicouches de semi-conducteurs exige une mesure de routine des épaisseurs et de la localisation des interfaces des couches formées. Ceci est souvent réalisé en utilisant des techniques coûteuses et compliquées telles que la microscopie à force atomique (AFM) ou la spectroscopie de photoélectrons à rayons X (XPS). Dans ce travail, la métrologie à température ambiante dans un environnement aqueux a été développée pour des tests de post-croissance des nano-hétérostructures (NHs) semi-conductrices. La méthode utilise le procédé de photocorrosion numérique (DIP) et la sensibilité de l'émission de photoluminescence (PL) aux états de surface révélés pendant la photocorrosion.

Le processus de photocorrosion des NHs semi-conducteurs GaAs/AlGaAs a été étudié en présence d'une excitation la bande interdite d'échantillons immergés dans différentes solutions aqueuses. Une photo-excitation de faible intensité au-dessus de la bande interdite (<105 mW/cm^2) a été appliquée en mode pulsé caractérisée par un duty cycle (DC) donné par $T_{ON}/(T_{ON} + T_{OFF})$. Ceci a produit des vitesses moyennes de gravure du matériau enleves à la précision de la sous-monocouche pendant chaque cycle DIP. En utilisant les techniques d'AFM et de XPS, il a été démontré que l'émission de la PL d'une NH GaAs/AlGaAs au cours de la DIP oscille en raison des couches de GaAs et d'AlGaAs révélées. Ces oscillations sont causées par la sensibilité de l'émission PL à la vitesse de recombinaison de surface des porteurs, qui diffère considérablement pour GaAs et AlGaAs. Le processus DIP a révélé une épaisseur de 1 nm de GaAs dans une structure de GaAs/AlGaAs, mais cela ne semble pas être une limite de résolution de cette approche.

Le potentiel de circuit ouvert (OCP) mesuré au cours du DIP diffère entre les jonctions d'électrolyte-GaAs et électrolyte-AlGaAs formées au cours du processus de la photocorrosion. Les différences de OCP sont interprétées comme pouvant provenir des photo-oxydes superficiels qui portent la charge électrique. Le dipôle formé par ces oxydes superficiels définit l'OCP mesuré. L'oscillation de l'OCP pourrait également être utilisée pour la métrologie des NHs. Cela ouvre la perspective d'étendre la métrologie DIP aux NHs semi-conducteurs avec un signal PL non existant ou négligeable.

Enfin, les entités chargées proches du voisinage d'une surface semi-conductrice affectent le taux de DIP. Cette propriété a été utilisée pour détecter la Legionella pneumophila qui est normalement chargée négativement au pH> 4. Les mesures de FTIR ont indiqué que les monocouches auto-assemblées (SAM) d'alkanethiol restent sur la surface semi-conductrice pendant le DIP. Cela a permis la détection de la Legionella pneumophila vivante à une concentration de 10^5 CFU/mL avec une architecture simple à base d'anticorps. Une discussion a été proposée suggérant des protocoles de biocapteurs possibles pour atteindre des limites de détection améliorées avec le biocapteur DIP.

Mots clés : Photoluminescence; Potentiel de circuit ouvert; Photocorrosion numérique; Les microstructures GaAs/AlGaAs; La métrologie des nano-hétérostructures; Biocapteur; Legionella pneumophila;

ABSTRACT

Fabrication of devices based on semiconductor multilayer structures demands routine measurement of thicknesses and location of the interfaces of the constituent layers. This is often achieved using expensive and complicated techniques such as scanning electron microscopy, secondary ion mass spectroscopy, atomic force microscopy (AFM) or x-ray photoelectron spectroscopy (XPS). In this work, room temperature metrology in water environment has been developed for post-growth testing of semiconductor nanoheterostructures (NHs). The method utilizes the process of digital photocorrosion (DIP) and the sensitivity of photoluminescence (PL) emission to surface states revealed during photocorrosion.

The photocorrosion process of GaAs/AlGaAs semiconductor NHs has been investigated in the presence of above bandgap excitation of samples immersed in different aqueous solutions. In order to achieve precise control over photocorrosion rates, the NH samples were placed in a flow cell with controlled aqueous environment. A low intensity above-bandgap photoexcitation (< 105 mW/cm^2) was incident in a pulse mode and characterized by a duty cycle (DC) given by $T_{ON}/(T_{ON} + T_{OFF})$. This has produced average etch rates of material removed at sub-monolayer precision during each DIP cycle. Using AFM and XPS, it has been demonstrated that the PL emission from a GaAs/AlGaAs NH during DIP oscillates owing to revealed GaAs and AlGaAs layers. These oscillations are caused by the sensitivity of the PL emission to the carrier surface recombination velocity, which drastically differs for GaAs and AlGaAs. The DIP process has revealed a 1 nm thick GaAs in a GaAs/AlGaAs NH structure, but this does not seem to be the resolution limit of this approach.

Open circuit potential (OCP) measured during DIP differs amongst GaAs-electrolyte and AlGaAs-electrolyte junctions formed during the photocorrosion process. The OCP oscillations were found in-phase with the PL oscillations measured during DIP. The differences of OCP are theorized to originate from the surficial photo-oxides that carry electric charge. The dipole formed by these surficial oxides define the measured OCP. The OCP oscillation could also be used for metrology of NHs. This opens the prospect of extending the DIP metrology to semiconductor NHs with non-existing or negligible PL signal.

Lastly, charged entities near the vicinity of a semiconductor surface affects the rate of DIP. This property has been utilized to detect *Legionella pneumophila* that normally are negatively charged at pH > 4. Fourier transform infrared spectroscopy measurements have indicated that alkanethiol self-assembled monolayers (SAMs) remain on the semiconductor surface during DIP. This has allowed for the detection of live *Legionella pneumophila* at 10^5 CFU/mL with a simple antibody-based architecture. A discussion has been provided suggesting possible biosensing protocols for achieving enhanced detection limits with the DIP biosensor.

Key words: Photoluminescence; Open circuit potential; Digital photocorrosion; GaAs/AlGaAs microstructures; Nanoheterostructure metrology; Biosensor; *Legionella pneumophila*;

ACKNOWLEDGEMENTS

I would like to sincerely thank my advisor Prof. Jan J. Dubowski for the invaluable guidance, financial and technical support during my PhD. Dr. Eric H. Frost has been important to my growth as a researcher, I thank and appreciate his support.

I greatly value and appreciate the time and effort taken by my committee members, Prof. Eric H. Frost, Prof. Serge Charlebois, and Prof. Mohamed Chaker to help improve my work.

I wish to thank Dr. Khalid Moumanis and Dr. Walid Hassen for all the support both inside and outside the lab.

This work would not be possible without the camaraderie, support and help from current and former members of QS group, Neng Liu, Mohammed Reza Aziziyan, Lilian Sirbu, Hemant Sharma, Xiaohuan Huang, Dominic Carrier and Elnaz Nazemi.

Finally, none of this work would be possible without the support of my late father, mother, bother and my long-suffering partner Dr. Nosrati. I cannot thank them enough.

TABLE OF CONTENTS

FIGURES

TABLES

ACRONYMS

BCE	Bacteria capture efficiency
CRP	C reactive protein
CFU	Colony forming units
DE	Digital etching
DI	Deionized
DIP	Digital photocorrosion
DNA	Deoxyribonucleic acid
ECL	Electro-chemiluminescence
EDC	1-Ethyl-3-(3-dimethylaminopropyl)-carbodiimide
FRET	Förster resonant energy transfer
FITC	Fluorescein 5(6)-isothiocyanate
HRP	Horse radish peroxidase
HI-PLM	Hyper-spectral imaging mapper
HUS	Hemolytic uremic syndrome
IgG	Immunoglobulin G
IPA	Isopropanol
LED	Light emitting diode
LOD	Limit of detection
MHDA	Mercapto hexadecenoic acid
NHs	Nano-heterostructure
NHS	N-hydroxy sulfo succinimide
pI	Isoelectric point

PE-CY7	FRET conjugate of Phycoerythrin and Cyanine 7 dye
PEG-B	Poly ethylene glycol thiol - Biotin
PSA	Prostate specific antigen
QSPB	Quantum semiconductor photonic biosensor
QSPBN	Quantum semiconductor and photon-based bionanotechnology
RNA	Ribonucleic acid
SAM	Self-assembled monolayer
SELEX	Systematic evolution of ligands by exponential enrichment
SERS	Surface-enhanced Raman spectroscopy
SPW	Surface plasma wave
SQUID	Superconducting quantum interference device
TTP	Thrombotic thrombocytopenic purpura
XPS	X-ray photoelectron spectroscopy

1 INTRODUCTION

This thesis is focused on investigation of a so-called digital photocorrosion (DIP) effect in GaAs/AlGaAs nano-heterostructures (NHs), and exploring its application for a) post epitaxial growth diagnostics, and b) detection of electrically charged molecules immobilized in the vicinity of such NH. The work describes the fundamental parameters of the DIP process and it demonstrates the potential of DIP in providing attractive information about structural parameters of semiconductor NH. The results of this work also clarify on some of the fundamental aspects concerning the quantum semiconductor photonic biosensing (QSPB) technology investigated by the Université de Sherbrooke Quantum Semiconductors (QS) Group.

Semiconductor devices based on multiple layers of thin semiconductors are ubiquitously used in consumer, defense and medical applications. Applications that require operation in radio frequencies such as cellphones, WiFi routers and solar cells for space applications use this multilayer semiconductor technology (Bhattacharya, Fornari, & Kamimura, 2011a; Dimroth et al., 2014; E Pettenpaul, 1998). Consistent and reproducible fabrication of multi-layer devices are affected by variation in thickness of layers, roughness at the interfaces, variation in carrier recombination rates and Schottky barrier height. Post-growth metrological tools are normally used to measure these parameters (Schroder, 2006). Etching is one of the critically important processes during fabrication of multilayer devices. This process usually involves removal of a material from photoresist patterned substrates. Since conventional plasma etching and wet etching techniques leave microscopically damaged surfaces, there has been an urgent need of developing alternative methods of nanostructuring of materials. One of the most advanced methods responding to this need is digital etching (DE) that allows processing of semiconducting materials with repeated, self-terminating cycles involving a gas phase reactants (Meguro & Aoyagi, 1997) or wet etching of the products of surface localized reactions (DeSalvo et al., 1996). In DE, etchant gas pulses and Ar ions are sequentially impinged onto the substrate surface to be etched. For GaAs, a typical etchant gas pulse is Cl_2 and the 0.5 monolayers or 0.142 nm of GaAs is removed in each cycle (Takashi et al., 1990). Due to lack of *in situ* monitoring techniques, these numbers are based on post-processing measurements. The application of the DIP process for etching of semiconductor NHs allows monitoring *in situ* position of the photocorrosion front with a sub-monolayer precision(Nazemi, Aithal, Hassen, Frost, & Dubowski, 2015). The investigation of fundamental parameters affecting DIP and application of this process for post-growth metrology of quantum well (QW) microstructures and selected NH represent the 1st axis of the research undertaken in the frame of this project.

The 2nd axis of the undertaken research concerns the investigation of the DIP process for detection of electrically charged molecules. Biomolecules are characterized by a pH and salt dependent electrical charge due to their constituent ionizable groups (Salgin, Salgin, & Bahadir, 2012; Salis et al., 2011). For example, Bovine serum albumin (BSA) has an overall negative charge of 18 electrons at pH 7 (Fologea, Ledden, McNabb, & Li, 2007). Isoelectric point (pI), the pH at which there is zero net charge, of many viruses lie between $3.5 < pI < 7$ (Michen & Graule, 2010). A vast majority of bacteria are negatively charged at pH 7 (A. T. Poortinga, Bos, Norde, & Busscher,

2002). Rapid detection of viruses, bacteria and other pathogenic biomolecules, including the assessment of the interaction between such biomolecules and living organisms are of a great interest to the modern life science sector that, despite of a tremendous progress demonstrated since the invention of the electrochemical biosensor in 1962 (Clark & Lyons, 1962) still suffers from the lack of an inexpensive, rapid and precise quantification method of biological entities. Biosensing is the science of recognition and quantification of an analyte, which includes unicellular organisms like bacteria and amoeba, virus, protein, DNA, RNA, or biologically relevant organic and inorganic molecules, hereafter referred to as analyte. Prototypical analytes for human diagnosis and prognosis include biomarkers such as, c-reactive protein (CRP), prostate-specific antigen (PSA) for prostate cancer and, troponin T and troponin I for cardiac events (Hamm et al., 1997).

Bacteria are unicellular microorganisms without a nucleus. Bacteria in the human body outnumber human cells by a factor of 10. Bacterial flora in human gut have increasing found to influence human health (Lynch & Pedersen, 2016). Many species of naturally occurring bacteria and other microorganisms are pathogenic, i.e. they induce disease in humans.

Among the conventional methods, the gold standard for routine detection of bacteria is culture, which in microbiology refers to the transfer of an organism from its ecological niche (e.g., water stream), transient vehicle (e.g., food), or storage medium (as in case of stock culture), into a growth-permitting laboratory medium. The inoculated medium is then incubated, under optimum growth conditions and for a suitable length of time, to allow cell multiplication, resulting in a culture of the organism (Zourob, Elwary, & Turner, 2008). In practice, a majority of the bacteria are not-culturable using standard methods (Vartoukian, Palmer, & Wade, 2010).

Environmental monitoring of microorganisms for drinking water require monitoring Cryptosporidium, Giardia lamblia, Legionella and *E. coli* among others. In many cases, 80% of the costs involved with hazardous place cleanup are for lab tests, for sampling and monitoring, microorganisms (Ho, Robinson, Miller, & Davis, 2005). *Legionella pneumophila* occurs at low levels in natural sources of water and soil. They multiplie in warm water conditions such as in cooling towers, evaporation condensers, humidifiers, warm water tanks and other water reservoirs. *L. pneumophila* typically forms biofilms, which provide a habitat and gradient for nutrients (Murga et al., 2001). Additionally, increased occurrence of *L. pneumophila* infected amoebae compared to natural sources have also been observed in the case of water from cooling towers (Berk et al., 2006). *L. pneumophila* is responsible for Legionnaire's disease, severe pneumonia and non-pneumonic Pontiac fever syndrome. The common methods for detection of *Legionella* in the environment include PCR and culture that is considered the "gold" standard for detection of bacteria, but due to the slow growing nature of *Legionella* (Stølhaug & Bergh, 2006), other methods are necessary. Bacterial biosensors often target the whole cell, DNA and RNA. Nucleic acid sensing requires a sample isolation and purification step. Whole cell sensors often face the challenge of bringing the bacteria to interact with the sensor surface. Techniques such as dielectrophoresis and chemotaxis are often used to overcome the whole cell transport limitation. (Burlage & Tillmann, 2017; W. Hassen et al., 2016). This activity represents a large effort of the QS Group towards rapid and automated detection of bacteria, such as *Escherichia*

coli and *Legionella pneumophila* bacteria that, under normal conditions (pH > 5), are characterized by a relatively strong negatively charged outer shell (Soni, Balasubramanian, Beskok, & Pillai, 2008).

2 STRUCTURAL DIAGNOSTICS OF SEMICONDUCTOR SURFACES AND HETEROSTRUCTURES

2.1 Conventional methods

Heterojunction semiconductor devices based on multilayer sandwiched of semiconductors find wide application in consumer electronics and photonics. Heterojunction bipolar transistors and high electron mobility transistors (Bhattacharya, Fornari, & Kamimura, 2011b) form the core technology enablers for RF components in ubiquitous devices such as mass-produced cellphones, satellite communication devices and car radars (E. Pettenpaul, 1998). High efficiency heterojunction solar cells used in concentrated photovoltaics (Dimroth et al., 2014) are examples of devices taking advantage of the semiconductor multilayer technology.

These devices are manufactured using photolithography, which involves deposition, patterning and etching of semiconducting materials. The successful fabrication of such devices depends on the quality of semiconductor wafers that relies on advanced diagnostic and metrology tools frequently employed as post-growth interrogation about such parameters as layer thickness, interfacial roughness, material composition, density of carriers and interface traps, or Schottky barrier height (Schroder, 2006). One or more of these parameters are critical for appropriate functioning of such devices. The most common methods employed for characterization of physical and chemical properties of semiconductor are summarized in table 1.

Table 1 Parameters measured, techniques used and references for characterization of semiconductors.

Property Measured	**Techniques**	**References**
Crystal quality	X-ray diffraction, transmission electron microscopy, scanning electron microscopy	(Gerardi, Giannini, Passaseo, & Tapfer, 1997; Nakashima & Tateno, 2004)
Interfacial roughness	Atomic Force Microscopy	(Oliver, 2008)
Composition	Secondary ion mass spectroscopy, x-ray photoelectron spectroscopy, Auger electron spectroscopy	(Gerardi et al., 1997; Herrmann, Lehnhardt, Strauß, Kamp, &

		Forchel, 2011; Liu & Dubowski, 2013)
Layer thicknesses	Scanning electron microscopy, transmission electron microscopy, reflectance spectroscopy,	(Linkov, Artemyev, Efimov, & Nabiev, 2013; Wośko et al., 2011)
Band structure, carrier concentration	Current-voltage (I-V), capacitance-voltage (C-V) measurements, photo-electrochemical profiling	(Blood, 1986; Fleetwood et al., 1993; Kaniewska & Slomka, 2001)
Band offsets	Photo-voltage spectroscopy	(Kronik & Shapira, 2001; Masut, Roth, Dubowski, & Lenchyshyn, 1986)
Surface defects	Electrochemical imaging	(Simpson & Rodríguez-López, 2015)

The thickness of semiconductor layers constituting heterostructure devices is one of the fundamental parameters determining functional characteristics of (QW) and other quantum confined microstructure based devices. Typical methods for determining this parameter are based on cross-section SEM or TEM imaging (Perovic et al., 1995), ellipsometric analysis (Erman, Theeten, Vodjdani, & Demay, 1983), depth profiling with Auger electron spectroscopy (J. J. Dubowski, D. F. Williams, P. B. Sewell, & Norman, 1985), SIMS (Liu, Poulin, & Dubowski, 2013) and x-ray diffraction techniques (Tapfer & Ploog, 1986). *In situ* monitoring the growth process of NH could be carried out with reflection high-energy electron diffraction technique (e.g., (Franke, Kreutzer, Zacher, Naumann, & Anton, 1998)), but no such diagnostics is available for *in situ* monitoring of material etched with a comparable (sub-monolayer) resolution.

Location of interfaces of QWs and quantum dots could be profiled using photo-electrochemical techniques. Owing to the small dimension of these devices, method with high etch rates cannot be readily applied in such applications (Fink & Osgood, 1993). For example, laser-induced

photoetch rates for GaAs and InP are in the range of 0.1 – 100 µm/min (Ruberto et al., 1991). Moreover, high surface roughness of the photoetched surface, over 15 nm (Kirchner et al., 2002), also limit ready application of photo-electrochemical techniques to these methods.

2.2 Photocorrosion of GaAs

Photocorrosion of bulk GaAs has been reported in literature as a "photowashing effect" (Ruberto et al., 1991). Upon photoexcitation, GaAs in contact with an electrolyte undergoes oxidation and photo-decomposition of n-type GaAs could be described by the following reactions:

$$\boldsymbol{GaAs + 5H_2O + 6h^+ \rightarrow Ga^{3+} + HAsO_2 + 3H^+}$$ Reaction 1

$$\boldsymbol{GaAs + 3e \rightarrow Ga^0 + As}$$ Reaction 2

where h^+ represents the holes in the semiconductor and H^+ is the proton in the solution, e represents the electron and Ga^0 denotes a reduced gallium atom. The water environment and excited holes arriving at the semiconductor surface lead to oxidation, and the reactions represented by equations (1) and (2) describe oxidation and dissolution of GaAs upon photo-excitation. The built-in potential at the liquid-solid junction drives the current that is responsible for the photocorrosion process. Application of bias to the semiconductor, presence of redox species in the liquid phase, pH of the solution, wavelength of incident light, dynamics of dissolution of corrosion products and presence of charged or ionizable species at the semiconductor-electrolyte junction affect the photocorrosion process.

2.3 Photoetching of semiconductor heterostructures

Application of photocorrosion as a wet etching process for AlGaAs/GaAs multilayer structures has been investigated by Fink and Osgood (Fink & Osgood, 1993). Photocorrosion was performed on MBE grown n-$Al_{0.3}Ga_{0.7}As$/n-GaAs in dilute nitric acid (HNO_3:H_2O = 1:20). The cyclic voltammetry curves (CV) for GaAs and AlGaAs, and temporal current density in constant current mode are given in figure 1.

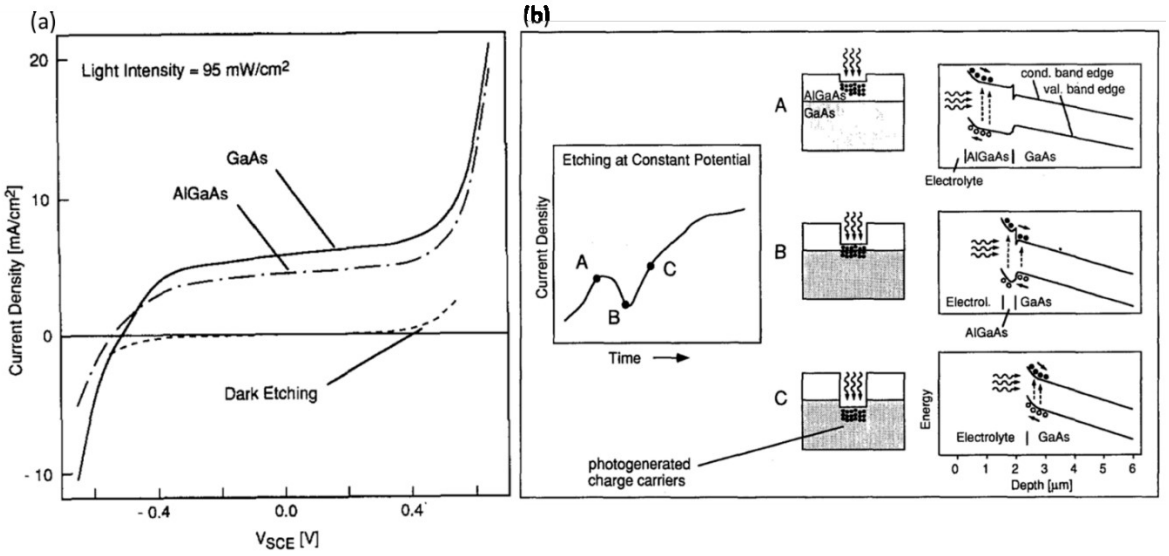

Fig. 1. (a) Cyclic voltammetry of GaAs and AlGaAs in dark and irradiated with halogen lamp of 95 mW/cm^2 continuous photoexcitation intensity. (b) Temporal current density during photoelectrical etching of AlGaAs/GaAs heterostructure (Fink & Osgood, 1993).

CV curves without photoexcitation for both GaAs and AlGaAs behave the same way and are indicated as “Dark Etching” in figure 1(a). The onset of anodic reaction starts after an overvoltage of +0.5 V and essentially follows Eq. 1 and, while hydrogen evolution starts at about -0.5 V.

With photoexcitation, the photogenerated carriers induce a current in the CV response of GaAs and AlGaAs within the -0.5 V to 0.5V window. Thus, only the illuminated portions of the sample were photocorroded. Energy band diagram, near the semiconductor-electrolyte interface, is shown in figure 3(b). The conduction and the valence bands are bent upwards and holes to accumulate at the surface of the heterostructure. At points ‘A’, ’B’ and ‘C’ indicated in the temporal current density plot, the variation in the current density could be attributed to the peculiarities of the band structure variations during etching. At points ‘A’ and ‘C’, photogenerated carriers are present in AlGaAs or GaAs, respectively, and there are no additional potential barriers for the holes to reach the semiconductor surface. Whereas at point ‘B’, photogenerated carriers appear both in GaAs and AlGaAs. The holes in GaAs experience a potential barrier formed by AlGaAs. The etch rate in this case, R (nm/min), has been relatively slow and followed the relation $R = 15 \times current\ density(mA/\text{cm}^2)$ dependence for both GaAs and AlGaAs layers.

Photocorrosion effect of PL emitting GaAs/AlGaAs heterostructures employed for monitoring biomolecular binding involving electrically charged molecules that allowed for a rapid detection of bacteria in aqueous solutions has been demonstrated recently (Aziziyan, Hassen, Morris, Frost, & Dubowski, 2016; Nazemi et al., 2015). This was possible thanks to creating conditions for uniform photocorrosion proceeding at typically under ~60 nm/min, which represent etch rates on the order of one monolayers for each cycle of photoexcitation. In the current work, we investigate the mechanisms of GaAs and AlGaAs photocorrosion in water and aqueous environment of NH_4OH, and we examine the conditions leading to the high-sensitive resolution of different material layers contributing to PL emission.

3 SENSING OF ELECTRICALLY CHARGED MOLECULES IN WATER

Biomolecules and biological entities such as lipids, proteins, carbohydrates, nucleic acids, virus, bacteria, cells, etc., are normally electrically charged (Salgin et al., 2012; Zhang et al., 2008). Charge and electrostatic interactions determine the structure, stability, binding affinity, chemical properties, and biological reactivity of proteins (Akke & Forsén, 2004; Chu et al., 2012; Sharp, 2002). Bacterial cell surfaces possess net negative electrostatic charge by virtue of ionized phosphoryl and carboxylate substituents on outer cell envelope of such macromolecules exposed to the extracellular environment (Wilson, Wade, Holman, & Champlin, 2001). This charge property of biomolecules has been used in conjunction with electric field-effect transistor based sensors for detection of DNA hybridization (Fritz, Cooper, Gaudet, Sorger, & Manalis, 2002) and antibody-antigen reaction in an immuno-field effect transistor (Immuno-FET) for Carcinoembryonic antigen, a cancer marker, has been developed using the AlGaN/GaN-based high-electron mobility transistor (HEMT) technology (Sarangadharan, Chu, Hsu, & Wang, 2015).

As discussed in section 1, biomolecules are charged at pH away from their isoelectric point (pI). Hence, biomolecular adsorption in the vicinity of a semiconductor can perturb the electrostatics of the semiconductor surface. This will typically result in the change of the built-in electric field in the proximity of the semiconductor surface, leading to the modulation of the surficial hole concentration and, consequently, perturbing the speed of the photocorrosion (Ruberto et al., 1991). The second channel of modulation of semiconductor surface properties is through charge transfer. It has been suggested that a charged entity such as bacteria could transfer some charge during adhesion to a semiconductor surface (A. Poortinga, Bos, & Busscher, 1999). These authors have claimed that *E. coli* adhering onto the indium tin oxide surface could be characterized with a charge totaling 10^{-14} C per bacterium, i.e., ~ 10^{5} electrons per bacterium. Transfer of the charge could also result in perturbation of the electric field near the semiconductor surface, thus affecting the photocorrosion process.

3.1 Biosensing

The International Union of Pure and Applied Chemistry (IUPAC) defines biosensor as a device that uses specific biochemical reactions mediated by isolated enzymes, immunosystems, tissues, organelles or whole cells to detect chemical compounds usually by electrical, thermal or optical signals (Nagel, Dellweg, & Gierasch, 1992). Biosensing process typically consists of two separate but related processes, recognition and transduction as illustrated in figure 2. Recognition is the selective affinity of the receptor to the analyte of interest, and transduction refers to conversion of this binding into an electrical or optical signal. Recognition is typically performed by naturally occurring receptor to the target of interest.

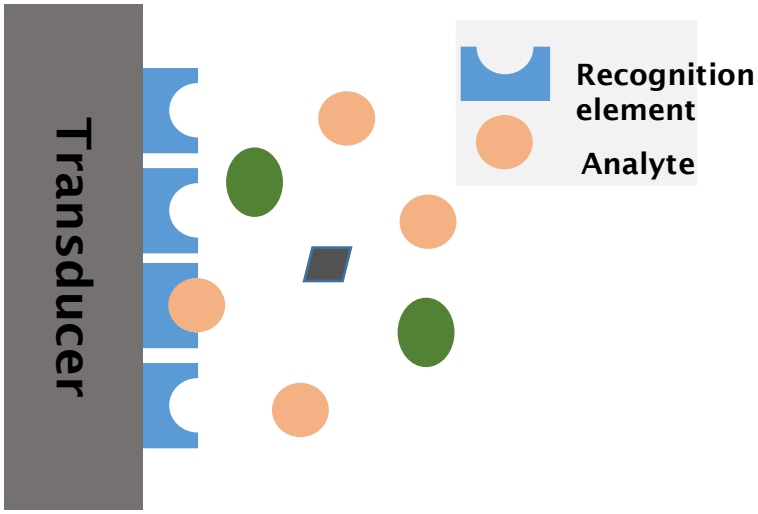

Fig. 2. Prototypical biosensing processes

3.2 Biosensing receptors

Receptors are chosen by their selective affinity to the analyte of interest. Common receptor analyte interactions include, nucleic acid interaction between complementary strands of DNA (hybridization) (Wang, 2002), antibody antigen interaction (Rowe, Scruggs, Feldstein, Golden, & Ligler, 1999) and, nucleic acid ligand interactions in aptamers (Subramanian et al., 2013).

Nucleic acids are central molecules in transmission, expression, and conservation of genetic information (Bloomfield & Crothers, 2000). They are present in all known forms of life. Two forms of nucleic acids are deoxyribonucleic acid (DNA) and ribonucleic acid (RNA), these two are known to carry information and allow for transcription of proteins. Nucleic acids have differential affinity to ligands such as small molecules, proteins, nucleic acids and cells. Repeated *in vitro* selection (SELEX - systematic evolution of ligands by exponential enrichment) allows for isolation of sequences with high affinity to the ligand of interest.

Antibodies are proteins produced by the immune system with the primary function of recognizing foreign targets. There are five classes of antibodies IgG, IgM, IgA, IgD and IgE, each of these have different structure, molecular weight and number of “binding sites”. Their foreign targets include proteins, small molecules and bacteria. An antibody can be divided into two distinct regions, variable and constant regions as shown in figure 3.

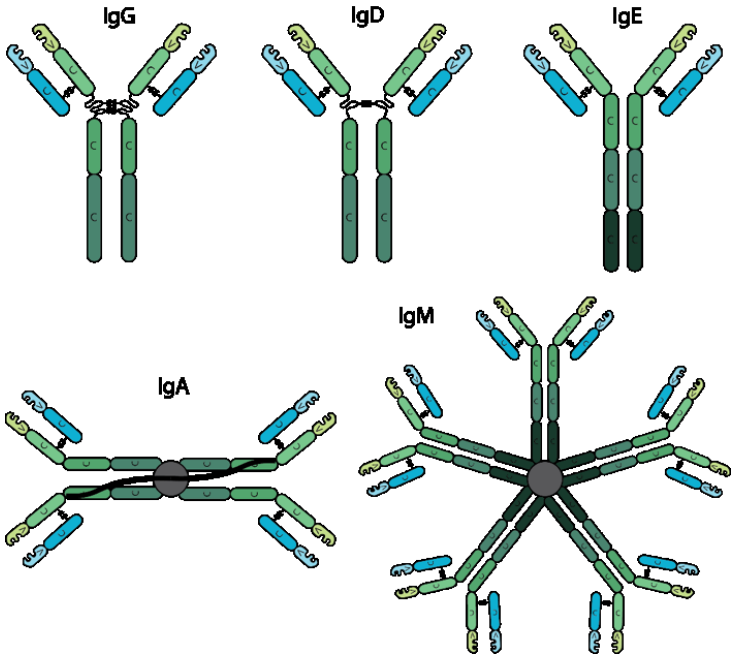

Fig. 3 Schematic of structures of various classes of antibodies (Bxcell, 2018)

The variations in the amino acids present in the variable region, which are antigen specific differ from one antibody to another. Lock and key hypothesis is generally accepted (Notkins, 2004) to explain the binding between antibody and antigen. In practice antibodies are manufactured as monoclonal, polyclonal or recombinant antibodies. Monoclonal antibodies are grown by B cells that have been fused with myeloma cells, whereas polyclonal antibodies are produced by immune reaction of an organism containing multiple immune cells which can recognize a plurality of epitopes, which are subsequently purified (Byrne, Stack, Gilmartin, & O'Kennedy, 2009). Recombinant antibodies are produced by genetic engineering, this allows antibodies to be re-engineered with metal-binding or positively charged amino acids without interfering with the antigen-binding specificity, which in-turn allows control over properties such as orientation on a surface to retain the antigen-binding activity (Zeng, Shen, & Mernaugh, 2012).

3.3 Biosensing Transducer

Many of nature's vast repertoires of physical phenomenon have been used for transduction of sensing events, each of these mechanisms measure specific properties of biomolecules or exploit different physical phenomenon for biosensing. Table 2 shows examples of sensors, the physical property or phenomenon being measured, the transduction mechanism and some examples from literature.

Table 2 Sensors and transduction mechanisms

Sensor	**Property/ Physical phenomenon**	**Perturbing parameter**	**Examples**
Mass	Δ mass after analyte-receptor conjugation	Δ resonance frequency with mass	Quartz crystal microbalance (Hong, Choi, Do Jeong, & Hong, 2009) and resonant cantilever
Acoustic wave	Δ mass after receptor analyte conjugation	Δ velocity of propagation of shear waves	Acoustic wave protein sensing (Battiston et al., 2001)
Electrochemical	Δ redox activity or passivation of the electrode	Δ current, Δ voltage, peak position	Impedance spectroscopy, cyclic voltammetry (Patolsky, Zayats, Katz, & Willner, 1999) and square wave voltammetry
Optical	Δ refractive index	Plasmon resonance shift, interference based techniques like Bio-layer interferometry (Concepcion et al., 2009)	SPR biosensor and SPRi biosensor (Mannelli et al., 2007)
Absorption, emission or Raman spectra	Raman shift, absorption or emission spectra	Raman fingerprint, gold nanoparticle, quantum dots	(Sundaram, Park, Kwon, & Lawrence, 2013)
Electrical	Δ pH	charge on the gate oxide	(Buitrago et al., 2014)

Surface plasmon resonance (SPR) is a charge-density oscillation that may exist at the interface of two media with dielectric constants of opposite signs, for instance, a metal and a dielectric. The charge density wave is associated with an electromagnetic wave, the field vectors of which reach their maxima at the interface and decay evanescently into both media (Sundaram et al., 2013). This surface plasmon wave (SPW) is a TM-polarized wave. These waves are sensitive to the dielectric environment close to the interface. Detection of *Vibrio cholera* O1 (Sundaram et al., 2013) was demonstrated with SPR using gold on BK 7 glass plates functionalised with 11-mercaptoundecanoic acid and hexanethiol, activated with NHS/EDC, protein G and Mab against V. cholerae. The detection range was found to be 10^5/mL to 10^9/mL.

Impedance spectroscopy is a small-signal measurement of the linear electrical response of a material of interest and the subsequent analysis of the response to yield useful information about the physicochemical properties of the system. Analysis is generally carried out in the frequency domain (Macdonald, 1992). *E. coli* are bacteria that naturally occur in the intestinal tracts of humans and warm-blooded animal. One pathogenic strain, *E. coli* O157:H7, produces toxins that damage the lining of the intestine, cause anemia, stomach cramps and bloody diarrhea, and serious complications called hemolytic uremic syndrome (HUS) and thrombotic thrombocytopenic purpura (TTP). Radke et. al. (Radke & Alocilja, 2005) have demonstrated detection of *E. coli* O157:H7 in culture and inoculated food samples, down to 10^4 CFU/mL, using impedance spectroscopy on an inter-digitated electrode array and polyclonal antibody immobilized as the recognition element.

Detection of paramagnetic particles labeled *L. monocytogenes* has been demonstrated by Grossman et. al. using high-critical temperature superconducting quantum interference device (SQUID), which are extremely sensitive to detect magnetic flux. This was used to measure binding between antibody-linked magnetic particles and bacteria, a pulsed magnetic field is used to align the magnetic dipole moments and use a high-critical temperature SQUID, to measure the magnetic relaxation signal when the field is turned off. Unbound particles randomize direction by Brownian rotation too quickly to be detected. In contrast, particles bound to *L. monocytogenes* are effectively immobilized and relax in about 1 s by rotation of the internal dipole moment. This relaxation process is detected by the SQUID. The limit of detection of $5.6 \pm 1.1\ 10^6\ mL^{-1}$ of L. monocytogenes has been demonstrated (Grossman et al., 2004).

Raman spectroscopy is based on inelastic scattering of photons following their interactions with the vibrating molecules of the sample. During this interaction, photons transfer (Stokes)/receive (Anti-Stokes) energy from molecules as vibrational energy. Thus the energy change of the scattered photons correspond to the vibrational energy of the sample molecules (Notingher, 2007). Raman scattering can also be enhanced (~10^{10}) using metal nanostructures, this forms the basis of surface enhanced Raman spectroscopy (SERS). Food safety is dependent upon the ability to detect and differentiate foodborne pathogens that cause severe outbreaks. Major outbreak in food is caused by foodborne pathogenic bacteria such as *Salmonella spp*., *Staphylococcus spp*., *Shigella* and *Escherichia coli*, *Bacillus spp*. and *Clostridium spp*. Sundaram et. al. (Sundaram et al., 2013) have demonstrated silver biopolymer substrate enhanced Raman spectra for food borne

pathogen detection and classification. A summary of detection limits and analysis time for *Legionella pneumophila* is given in table 3.

Table 3 Detection limits and time for analysis for different methods of detecting *Legionella pneumophila.*

Sensor	Detection Limit	Time for analysis	Disadvantages
Fiber based immunosensor (Lin et al., 2007)	10 CFU/mL	1 – 2 hr	Requires specially polished fiber
Surface acoustic wave (Howe & Harding, 2000)	10^6 cells/mL	3 hr	Whole cell. Specially built SAW sensors
SPR (Manera et al., 2013)	10^3 CFU/mL	60 min	Bulky equipment
RTPCR (Ballard et al., 2000)	2.5 CFU/mL	90 min	Bulky equipment
Auto fluorescence of *Legionella* at 450 nm (Ishii et al., 2013)	10^6 /mL	-	Insufficient detection limit and non-specificity
Lateral flow assays (Manera et al., 2013)	9.2×10^3 CFU/mL	20 min	Large variability
Immunofluorescence and solid phase cytometry (Parthuisot et al., 2011)	0.034 /mL	>60 min	Complicated and possibly bulky
Surface enhanced raman spectroscopy (Knauer, Ivleva, Niessner, & Haisch, 2010)	5×10^3 CFU/mL	1 min	Electrokinetic concentration required, the SERS reader is bulky
Culture (Ditommaso, Giacomuzzi, Gentile, & Zotti, 2010)	0.08 CFU/mL	10 days	Slow

Duplan et. al. (Duplan, Frost, & Dubowski, 2011) have demonstrated detection of *E. coli* bacteria using the effect of bacterial electrostatic interaction with GaAs/AlGaAs NH. The biochips were functionalized with self-assembled monolayers of alkanethiols and polyclonal biotinylated antibodies immobilized with neutravidin. A shift in the position of PL maxima was correlated with different concentrations of *E. coli* in the investigated aqueous solutions.

4 GOALS OF THIS WORK

The preliminary work performed in the QS Group was focused on detecting bacteria using GaAs functionalized with various alkanethiol self-assembled monolayers (SAM) used as an anchor for immobilization of antibodies and passivation of the GaAs surface against corrosion. During the experiments that I had undertaken with Elnaz Nazemi, it became obvious that the stability of GaAs/AlGaAs biochips suffered from the photocorrosion effect. Consequently, the question was asked: could the photocorrosion process be controlled with a precision that would allow observing perturbations induced by electrically charged molecules immobilized at the semiconductor surface or in its proximity? This has led us to the discovery of a digital photocorrosion (DIP) based "Photo-electochemical biosensing method" that is a subject of a recently allowed US patent (Jan J Dubowski, Nazemi, Aithal, & Huang, 2018).

The primary goal of this work was to explore DIP dependent PL of GaAs/AlGaAs heterostructures for monitoring *in situ* the decomposition process of these materials with an atomic layer resolution. The goal was also to develop a semi-quantitative model of this process. I was targeting the identification of the relationship between the photocorrosion rate, photon flux and type of aqueous environments employed for supporting the photocorrosion process. I have applied the PL effect for room-temperature metrology of GaAs/AlGaAs NH.

Expecting a difference between the surface potential of GaAs and AlGaAs exposed to the same aqueous environment, I carried out open circuit potential (OCP) measurements of GaAs/AlGaAs photocorroding in water and weak solutions of chlorides. This resulted in the demonstration of an excellent correlation between *in situ* revealed interfaces with PL and those with OCP. The significance of this result is that is suggests the possibility of atomic-level metrology of materials that do not show room-temperature measurable PL.

The final goal of this work was to investigate application of the DIP effect for detection of live *Legionella pneumophila* in water and phosphate buffered saline (PBS) solution. Due to the pathogenic nature of these bacteria, the related experiments were carried out in a dedicated bio-security level 2 laboratory of the Interdisciplinary Institute for Technological Innovation (3IT).

5 EXPERIMENTAL METHODS AND TOOLS

The following sections describe samples investigated in this work, and they provide discussion of the protocols employed for sample preparation and carrying out diagnostics. A brief description of experimental setups is also provided in this chapter.

5.1 Semiconductor samples

Semiconductor wafers were grown either by molecular beam epitaxy (MBE) or metalorganic chemical vapor deposition (MOCVD). MBE allows for atomic layer controlled growth of single crystal semiconductors from vapour phase precursors in ultra-high vacuum. In contrast, MOCVD growth occurs by a chemical reaction of the metal organic precursors under near-atmospheric pressure. The MOCVD growth rates could be four or five times faster than those of MBE, but MBE has better control of background carrier concentration than MOCVD (Sturdivant & Harris, 2015). The investigated GaAs/AlGaAs NH were grown on double side polished semi-insulating GaAs (100) wafers by MBE (Wafers 10-150, v0803 and AXT14-287) and by MOCVD (Wafer 10-413). Each of these wafers have a 200 nm or 500 nm thick epitaxial layer of GaAs, as well as a superlattice with 2.4 nm thick AlAs and 2.4 nm thick GaAs that were grown in each case on GaAs substrates as defect reduction buffer layers (Dawson & Woodbridge, 1984).

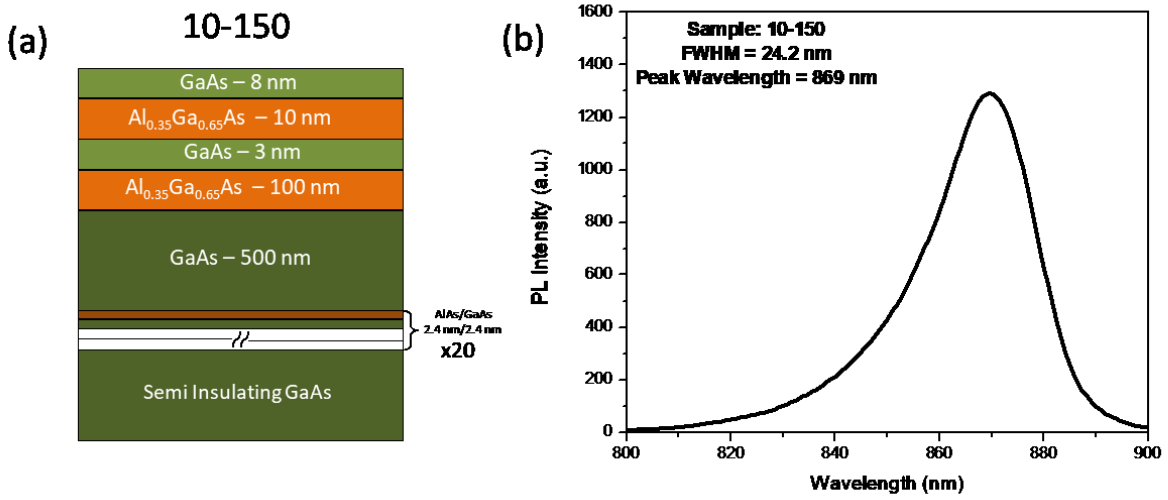

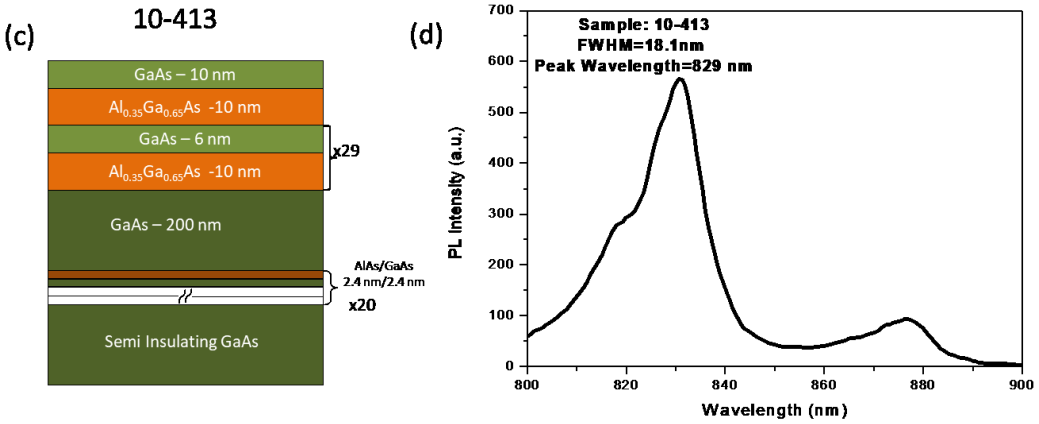
(c)
10-413
GaAs – 10 nm
Al0.35Ga0.65As -10 nm
GaAs – 6 nm
Al0.35Ga0.65As -10 nm
x29
GaAs – 200 nm
AlAs/GaAs
2.4 nm/2.4 nm
x20
Semi Insulating GaAs
(d)
Sample: 10-413
FWHM=18.1nm
Peak Wavelength=829 nm
PL Intensity (a.u.)
Wavelength (nm)

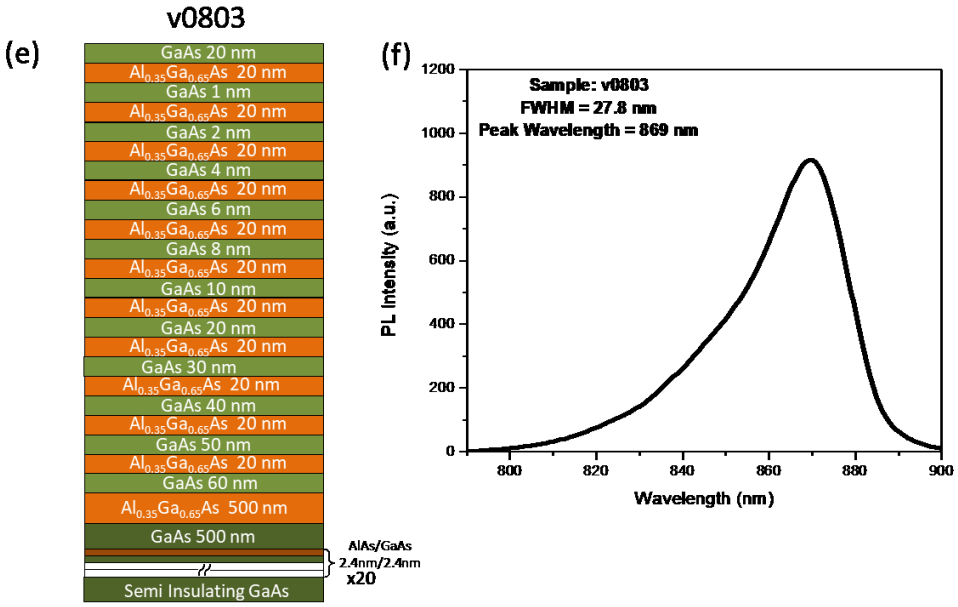
(e)
v0803
GaAs 20 nm
Al0.35Ga0.65As 20 nm
GaAs 1 nm
Al0.35Ga0.65As 20 nm
GaAs 2 nm
Al0.35Ga0.65As 20 nm
GaAs 4 nm
Al0.35Ga0.65As 20 nm
GaAs 6 nm
Al0.35Ga0.65As 20 nm
GaAs 8 nm
Al0.35Ga0.65As 20 nm
GaAs 10 nm
Al0.35Ga0.65As 20 nm
GaAs 20 nm
Al0.35Ga0.65As 20 nm
GaAs 30 nm
Al0.35Ga0.65As 20 nm
GaAs 40 nm
Al0.35Ga0.65As 20 nm
GaAs 50 nm
Al0.35Ga0.65As 20 nm
GaAs 60 nm
Al0.35Ga0.65As 500 nm
GaAs 500 nm
AlAs/GaAs
2.4nm/2.4nm
x20
Semi Insulating GaAs
(f)
Sample: v0803
FWHM = 27.8 nm
Peak Wavelength = 869 nm
PL Intensity (a.u.)
Wavelength (nm)

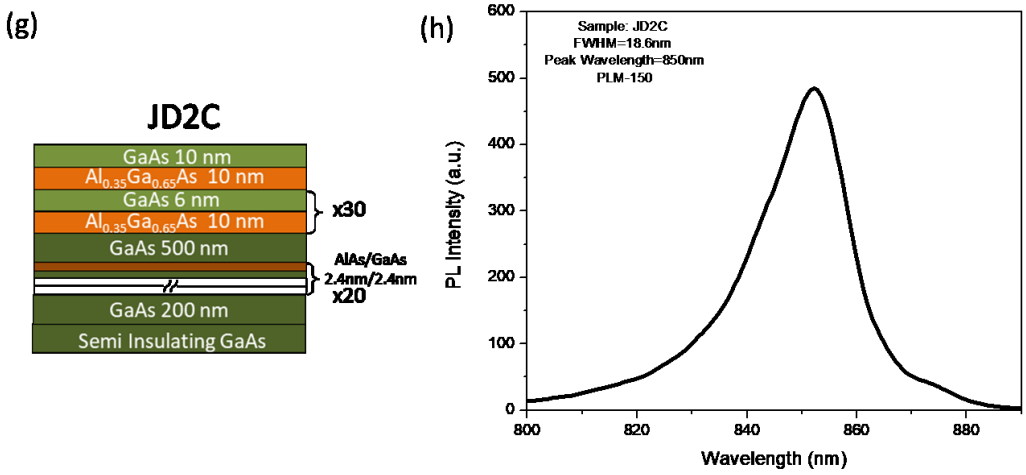
(g)
JD2C
GaAs 10 nm
Al0.35Ga0.65As 10 nm
GaAs 6 nm
Al0.35Ga0.65As 10 nm
x30
GaAs 500 nm
AlAs/GaAs
2.4nm/2.4nm
x20
GaAs 200 nm
Semi Insulating GaAs
(h)
Sample: JD2C
FWHM=18.6nm
Peak Wavelength=850nm
PLM-150
PL Intensity (a.u.)
Wavelength (nm)

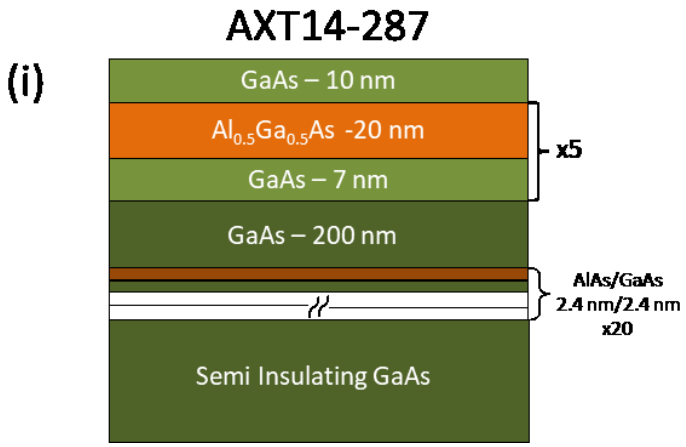

Fig. 4 Schematic of the investigated heterostructures used in this work and their corresponding PL emission spectra. Wafer 10-150 (a), v0803 (e), and AXT14-287 (i) have their PL emission maxima at 869 nm. Wafer 10-413 (c) is a QW microstructure that emits at 829 nm (d). Wafer JD2C (g) a QW microstructure with emission at 850 nm (h).

Wafers 10-150, v0803 and AXT14-287, whose structure are given in figure 5 (a), (b) and (g) have room-temperature PL emission maxima at 869 nm and no quantized emission was observed from these wafers at room temperature. Whereas 10-413, figure 5(c), has its PL maximum at 829 nm that originates from 6-nm thick QWs. A weaker PL emission observed at 869 nm, as shown figure 5 (d), originates from a 200-nm thick GaAs layer. The wafers were spin coated with photoresist (S1813, Shipley), mounted on a carrier tape and diced into 2 mm x 2 mm or 4 mm x 4 mm chips. Such samples, before direct measurements, or before surface functionalization, were sonicated in semiconductor grade OptiClear (National Diagnostics), acetone (ACP Chemicals, Canada) and isopropyl alcohol, to remove photoresist used to reduce particle contamination on samples' surfaces.

5.2 Photoluminescence

5.2.1 Basic principle

Optical excitation of the semiconductors with photons above the bandgap energy (E_g), results in the generation of electron-hole pairs. In direct bandgap semiconductor, excitation can occur without the interaction of a phonon as shown in figure 5, whereas in indirect bandgap semiconductors, the phonon assisted ($h\omega$) excitation is necessary. A well-known example of an indirect bandgap material is Si. All microstructures investigated in this work represent direct bandgap materials.

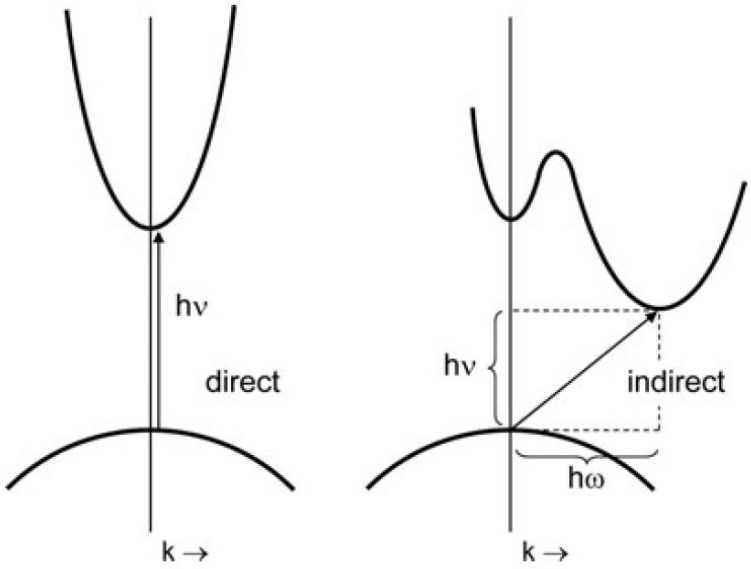

Fig. 5 Energy (E) – momentum (k) diagram showing absorption of photon in a direct bandgap and indirect bandgap semiconductor (Van De Krol, 2012). In this figure, ω is the frequency of a phonon, k is the momentum and v the frequency of the photon.

Lifetime of excited minority charge carriers determine the PL emission efficiency in a semiconductor. Carrier generation and recombination processed determine the carrier lifetime in a semiconductor. PL emission increased follows increased carrier lifetime and vice versa. For a semiconductor with two interfaces, for example, GaAs sandwiched between two AlGaAs layers, minority carrier lifetime, τ could be described by the following equation (Ahrenkiel et al., 1989):

$$\frac{1}{\tau} = \frac{1}{\tau_R} + \frac{1}{\tau_{nR}} + \frac{2S}{d} \qquad \text{Equation 3}$$

where τ_R is the radiative recombination lifetime, τ_{nR} the non-radiative recombination lifetime, S denotes the surface recombination velocity, and d is the depletion width. Except for S and d, the other components in this equation are bulk parameters of the semiconductor. The S represents the non-radiative recombination component due to the break in the translational symmetry of the semiconductor at its surface. Decreased S increases the minority carrier lifetime, and hence the efficiency of PL emission.

Oxidation at GaAs surface has been shown to result in increased efficiency of PL emission from GaAs. While coating GaAs surfaces with oxides of Al-, Si- and Mg resulted in S comparable to that of bare GaAs. i.e., ≈ 10^7 cm/s, the Ga_2O_3-coated GaAs showed S as low as 4000-5000 cm/s. The related PL spectra of GaAs are shown in figure 6 (Passlack, Hong, Mannaerts, Kwo, & Tu, 1996).

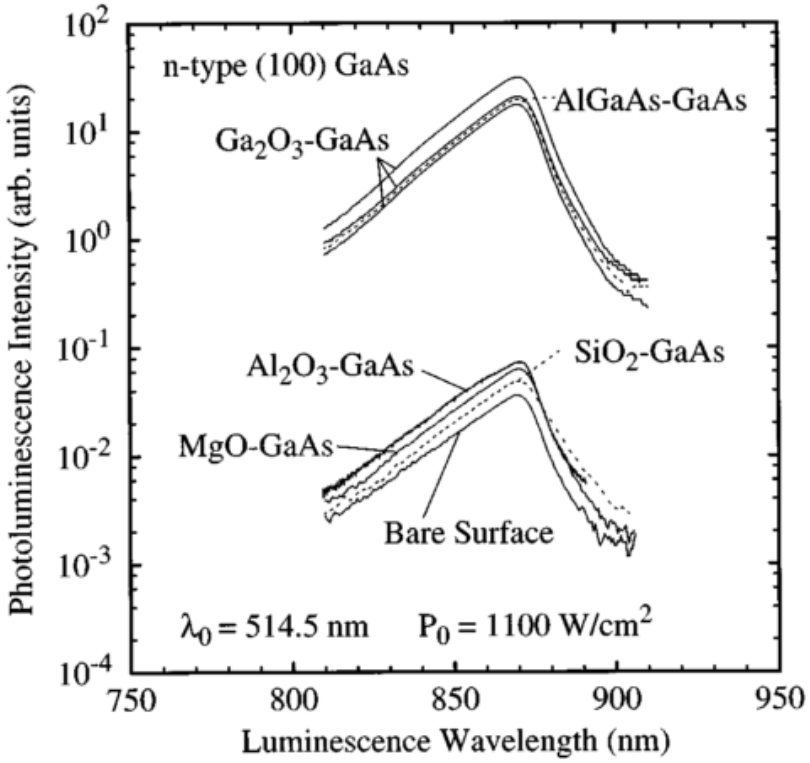

Fig. 6. PL spectra for GaAs and AlGaAs grown with molecular beam epitaxy, coated with various oxides (Passlack et al., 1996).

It can be seen that PL intensities are similar for uncoated GaAs and GaAs coated with Al_2O_3, MgO, SiO_2 oxides. However, Ga_2O_3 coated GaAs and AlGaAs coated GaAs have PL emission about 100 times that of bare GaAs.

In general, PL provides the information about electronic states of a semiconductor with the intensity and spectral characteristics of the emitted photons depending on the radiative and non-radiative processes in the semiconductor. In this work, PL measurements were performed using either a Hyperspectral Imaging Photoluminescence Mapper (HIPLM) or a custom designed Quantum Semiconductor Photonic Biosensor (QSPB) Reader described in (Kim et al., 2009) and (Aziziyan et al., 2016; Nazemi et al., 2015), respectively.

5.2.2 Photocorrosion setup

The experimental setup designed for photocorrosion of samples and simultaneous collection of PL data consists of:

a) A reservoir with investigated fluids (DI H_2O, NH_4OH, PBS and biological targets)
b) A flow cell module for mounting investigated GaAs/AlGaAs microstructures (chips)
c) An optical setup designed to irradiate samples and collect PL signal emitted by the samples
d) A peristaltic pump for injecting fluids to the flow cell

A fluidic flow cell, custom machined from a solid PEEK (Polyetheretherkeone), was designed to hold samples of dimensions up to 4 mm x 4 mm. The flow cell was connected with the reservoir and the peristaltic pump (Masterflex L/S) using Viton tubing, the system block diagram is illustrated in figure 7. The pump allowed for precise flow rate control. Typical flow rates used in these experiments were at 0.1 mL/min.

Fig. 7. Fluidic system block diagram

In the HI-PLM measurement setup, the sample is excited with a continuous wave diode pumped Nd:YAG laser emitting at 532 nm wavelength. Two volume Bragg gratings allow measurement of spatio-spectral emission characteristics of samples. Spectral resolution of 2 nm and spatial resolution under 2 µm can be achieved. The typical excitation power at the sample was 25 $mWcm^{-2}$, temporal variation in laser power is monitored using a photodiode. The samples were excited with intermittent pulses using a shutter. This intermittency was defined by a "duty cycle" (DC) parameter: T_{ON} / (T_{ON} + T_{OFF}).

The excitation in QSPB was provided either by a LED source (625 nm / 660 nm) or by a halogen lamp. An 812-nm cut-off long pass filter (Thorlabs FELH800) was applied in the QSPB Reader to prevent the excitation photons from reaching the CMOS detector employed for detecting PL emission. A schematic of QSPB and flow cell setup for PL measurements is illustrated in figure 8. A dedicated glass window facilitates excitation of samples and collection of PL data. The excitation power density measured at the sample surface in the QSPB systems ranged between 20 - 150 mW/cm^2.

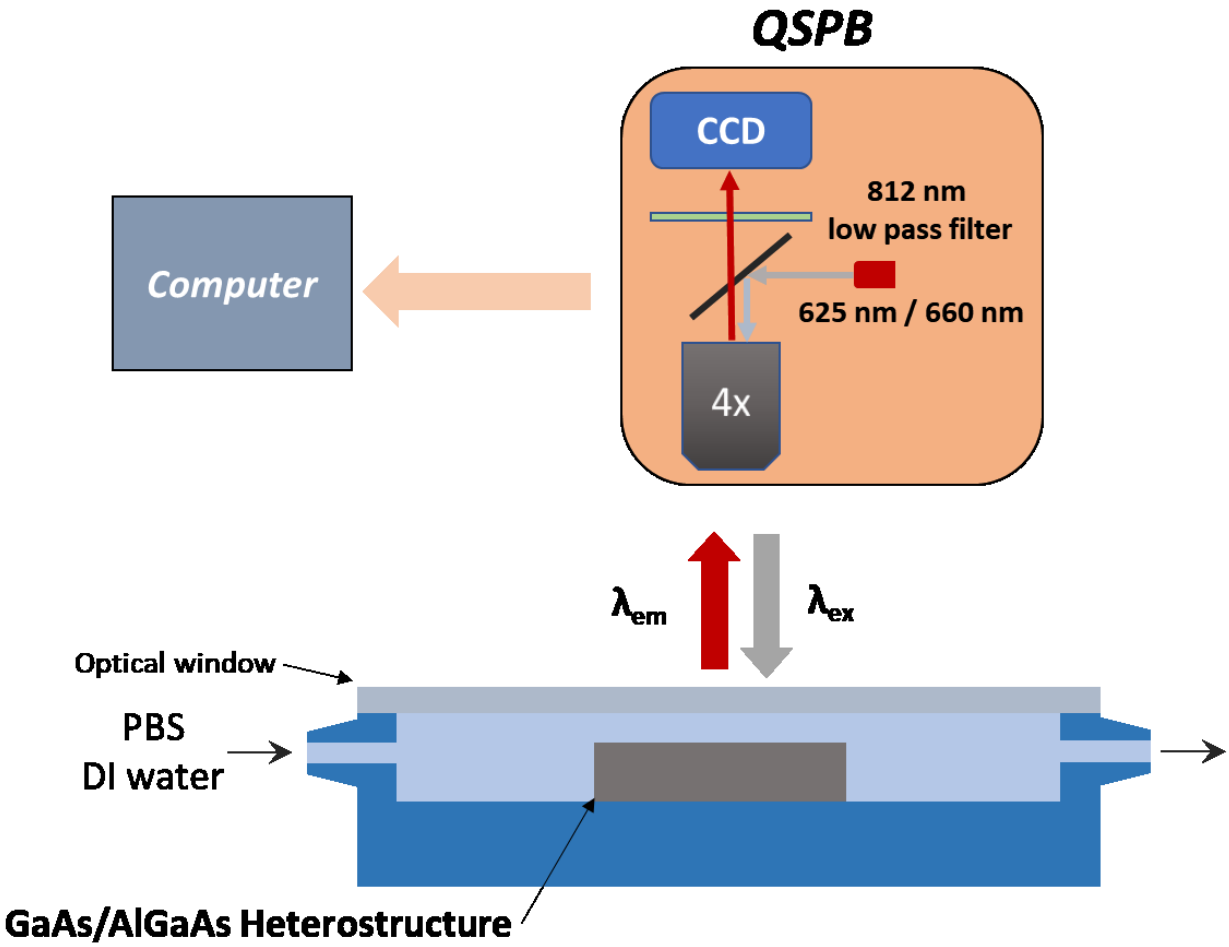

Fig. 8 A schematic view of the QSPB and flow cell setup.

Example of a temporal PL plot collected from a 2 mm x 2 mm chip of the AXT14-287 wafer exposed to an ammonia environment and irradiated with 25 mW/cm^2 at 660 nm for 1 s in each 10 s period (duty cycle 1 s/10 s) is shown in Fig. 8. The chip was cleaned as described in the previous section and placed inside a flow cell with 28% NH_4OH solution. The temporal PL plot of this microstructure reveals 5 maxima clearly observed in figure 9(a) and the PL maxima vs cumulative thickness of the NH is shown in figure 9(b).

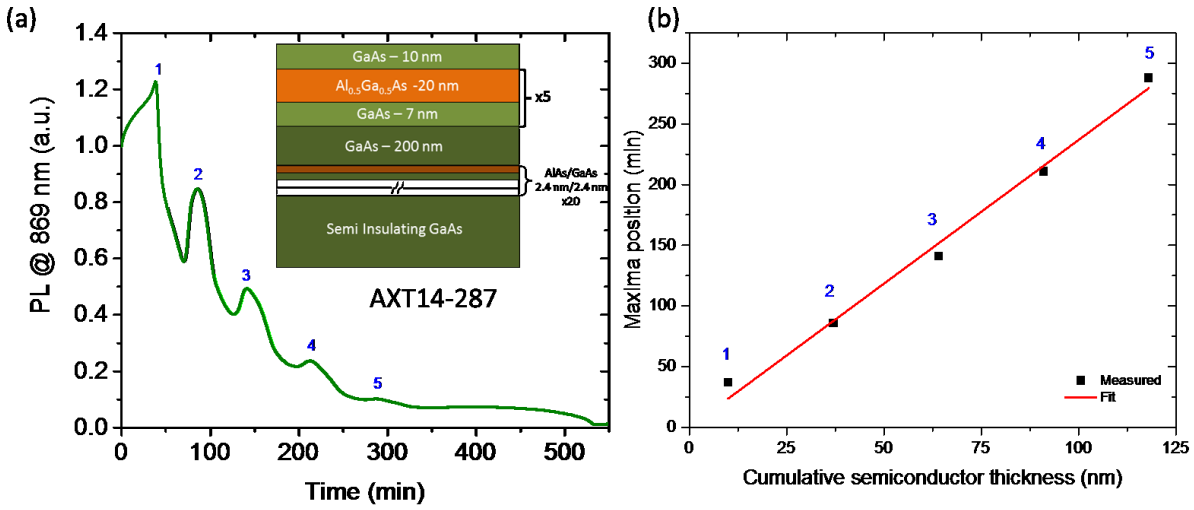

Fig. 9 Time dependent PL emission (at 869 nm) of a GaAs/AlGaAs NH (sample AXT14-287) immersed in NH_4OH and irradiated in QSPB with a 660 nm LED at DC = 1 s/100 s (a), and a plot of the position of PL maxima vs. cumulative thickness of the NH (b).

The maxima positions are linearly correlated with the microstructure thickness up to ~ 120 nm (known from the epitaxial growth parameters). The average etch rate of this chips is estimated at 0.4 nm/min or 0.66 nm per 1 cycle of photo excitation, which corresponds approximately to 2.3 monolayer of the microstructure removed each cycle. Details of this process and interpretation of the observed PL maxima are provided in Chapter 6.

5.2.3 Detection of electrically charged molecules using DIP

The DIP process is driven by the surface concentration of hole (h^+) as discussed in section 2.2.2. The near electric field in the depletion layer of the semiconductor modulates the rate of hole (h^+) transport to the semiconductor surface during DIP (Mannheim, Alkire, & Sani, 1994) (Miller & Richmond, 1997) . Thus, the presence of electrically charged molecules immobilized in the proximity of the semiconductor surface is expected to influence the rate of photocorrosion. A vast majority of bacteria are negatively charged in aqueous environment (A. T. Poortinga et al., 2002) and DIP could be used as a transduction mechanism for detection of this charge. Nazemi et. al. have demonstrated detection at 10^3 CFU/mL of *E. coli* K12 in PBS (Nazemi et al., 2015). The GaAs/AlGaAs samples were coated with *E. coli* antibody using alkanethiols. Such samples were exposed to varying solution concentrations of *E. coli* K12. Fig. 10 illustrates the PL peak position for solutions with different concentrations of *E. coli* K12. A logarithmic response is demonstrated between 10^3 and 10^5 CFU/mL of *E. coli* K12. Additionally, a negative control with *Bacillus subtilis* at 10^5 CFU/mL is also shown. In the current work, this approach is extended to *Legionella pneumophila* pathogenic bacteria.

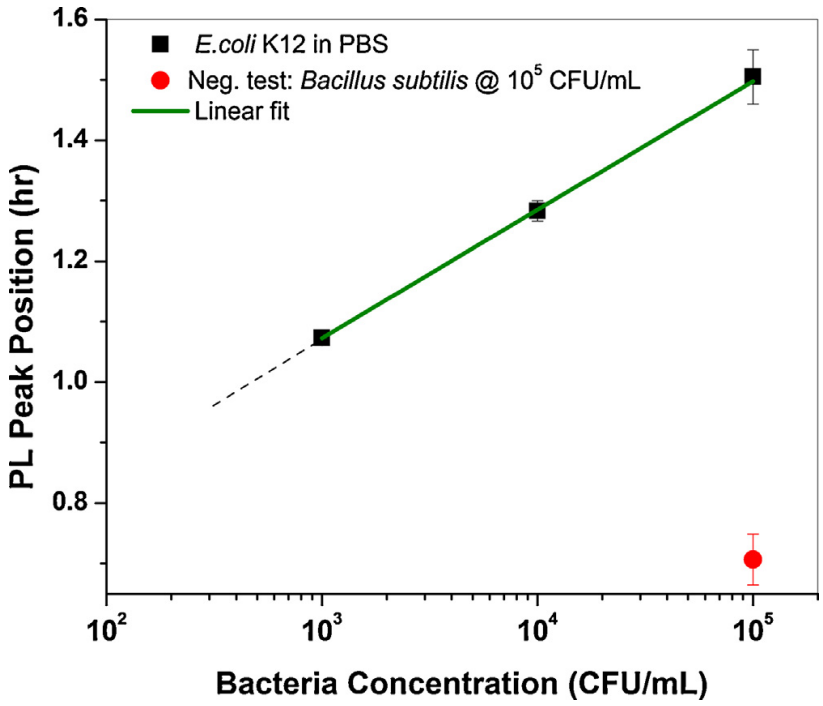

Fig. 10 PL peak position vs. different concentrations of *E. coli K 12* bacteria (Nazemi et al., 2015).

5.3 Biofunctionalization

5.3.1 Sample surface preparation

The GaAs functionalization procedure is based on previously published work by Duplan et. al. (Duplan et al., 2011) and Nazemi et al. (Nazemi et al., 2015) . 2 mm x 2 mm diced samples of the nano-heterostructure are sonicated sequentially in Opticlear, acetone and isopropyl alcohol (IPA), for two minutes each. Subsequently, the native oxide of GaAs is etched with 28% ammonium hydroxide solution for two minutes, transferred to degassed ethanol containing the thiol mixture and incubated overnight in darkness. Preparation of thiol in degassed ethanol is necessary to avoid oxidation of GaAs. The thiolated samples are rinsed with ethanol.

5.3.2 SAMs formation on GaAs

Biorecognition layer is a critical element of a biosensor. In the case of antibody based sensors, one of the most controllable methods of formation of this layer is based on using self-assembled monolayers (SAM) of alkanethiols. Self-assembly of alkanethiols (R-SH) on gold and semiconductors such as GaAs leads to formation of an ordered, compact monolayer on the underlying substrate. This process has been studied for decades (Ding, Moumanis, Dubowski, Tay, & Rowell, 2006; J. J. Dubowski, Voznyy, & Marshall, 2010), and has been applied for biosensing (Wink, J. van Zuilen, Bult, & P. van Bennekom, 1997), photolithography (Tiberio et al., 1993) and

passivation of GaAs (Cuypers et al., 2016). The theoretical maximum surface coverage with alkanethiol SAM on GaAs (100), estimated by density function theory (DFT) calculation was found to be 50 % (Voznyy & Dubowski, 2008). This has an implication for the ability to protect the GaAs surface against corrosion or photocorrosion.

Typically, $Al_{0.35}Ga_{0.65}As$/GaAs QSPB biochips are functionalized with a mixed SAM architecture that consists of a short chain hexadecanethiol (HDT, 15 CH_2 backbone with a terminal CH_3 (methyl)) mixed with a biotinylated polyethylene glycol thiol (PEG-b, 11 CH_2 backbone with 3 ethylene glycol groups and, biotin or Sulphur at each extremities) at 1:14 (v/v). The short chain HDT acts as a spacer to reduce the steric hindrance of the formed self-assembled monolayer. A schematic view of a HDT/PEG-b- architecture employed for attaching neutravidin and biotinylated antibodies is shown in figure 11.

5.3.3 Antibody conjugation

The samples coated with HDT/PEG-b- architectures were rinsed with 1xPBS to remove any residual ethanol and exposed to 0.2 mg/mL of neutravidin for two hours in an environment without light. Next, they were rinsed with 1xPBS, exposed to a 0.1 mg/mL solution of Biotinylated antibody for one hour and, finally, exposed to a PBS solution containing the bacteria. Figure 11 shows a schematic of the architecture after bacterial binding.

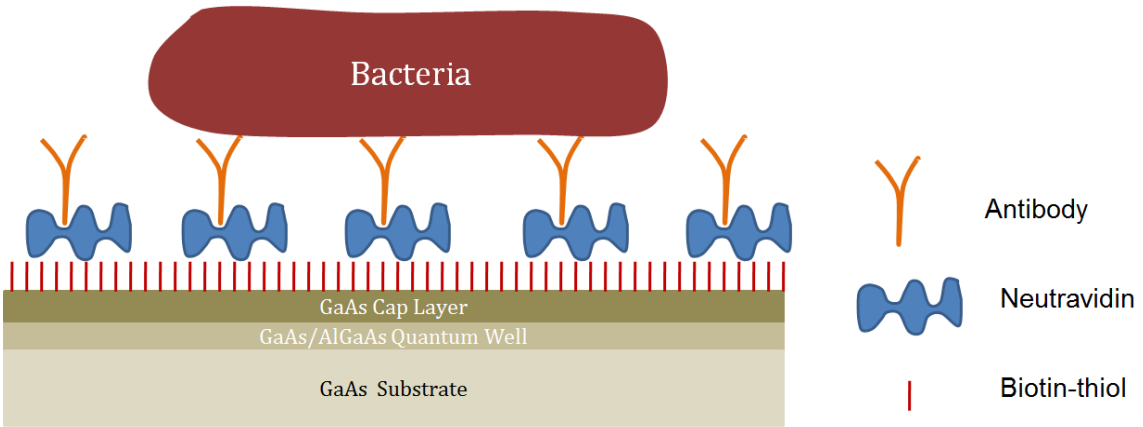

Fig. 11 Functionalization of GaAs with PEG-Biotin, antibody and bacterial binding.

5.4 X-ray photoelectron spectroscopy

X-ray photoelectron spectroscopy (XPS) is a surface analysis technique for determination of composition as well as the chemical states of surface constituents (Turner & Schreifels, 2000). Figure 12 (a) shows a schematic of the method. Monoenergetic soft x-ray photons are absorbed

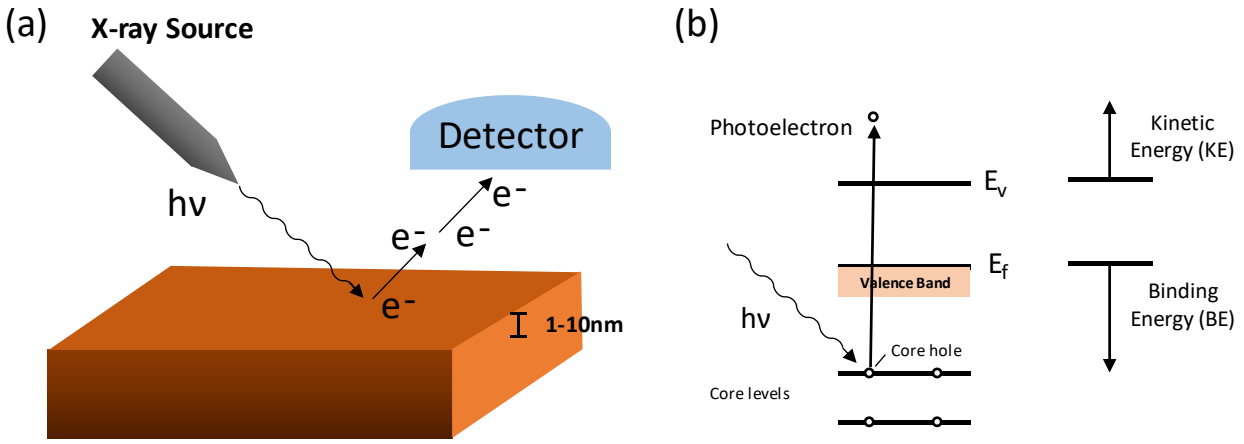

Fig. 12 Schematic of XPS measurement setup (a) and energetics of the XPS process (b).

by core electrons and are ejected from the atoms constituting the sample surface. The x-ray photons have an absorption depth of 1-10 µm and electrons are excited within this range (Moulder, Stickle, Sobol, & Bomben, 2002). A vast majority of these electrons do not leave the material and only the kinetic energy of the electrons emitted from the surface atoms, typically within about 8-10 nm from the surface are measured. The energetics of the emitted electrons are illustrated on figure 12 (b) and relation between energies given by the following equation:

$$KE = h\nu - BE - \phi_s \qquad (4)$$

KE stands for kinetic energy of the emitted electron, $h\nu$ the energy of the x-ray photoelectron, BE the binding energy, h Plank constant and $\phi_s$the spectrometer work function. These measurements are performed under vacuum, usually a low-resolution "survey scan" in performed for the presence of constituent elements, and afterwards a high-resolution scan is performed along the peaks of interest. In semiconductors, XPS is routinely used to measure the constituent elements, contaminations, oxidation states (Liu, Huang, & Dubowski, 2014), thickness of nanometer layers (Huang & Dubowski, 2014) and location of band edges (Nesher et al., 2006). Grazing angle incidence is a technique used to increase depth resolution of XPS (Chester & Jach, 1993). XPS measurements in this work used grazing angle incidence, 60^o from the normal, which allowed to increase depth resolution to under 1 nm (Kerr et al., 2014).

5.5 Fourier transform infrared spectroscopy

Fourier transform infrared spectroscopy (FTIR) is a popular technique for chemical analysis of thin films and studying chemical composition of the surface coating chemical compounds. Infrared (IR) absorption spectra correspond to the vibrational energy of the molecule and the number of absorption peaks correspond to the degrees of freedom of the molecule. IR radiation excite molecules to a higher energy state. The excited states result in the vibrations of molecular bonds occurring at varying wavenumbers in the IR region of the light spectrum. The wavenumber of each IR absorbance peak is determined by the intrinsic physicochemical properties of the corresponding molecule, and is thus diagnostic, like a fingerprint of that particular functional group (Chen et al., 2015). IR spectroscopy has routinely been used to probe the structure of SAMs formed on noble metals and semiconductors (Hostetler, Stokes, & Murray, 1996). The FTIR measurement setup consists of an IR source, beam splitter, stationary and moving mirrors as shown in figure 13. The beam from the interferometer interacts with the sample and is measured by the detector. This signal is processed to obtain the IR absorption spectra.

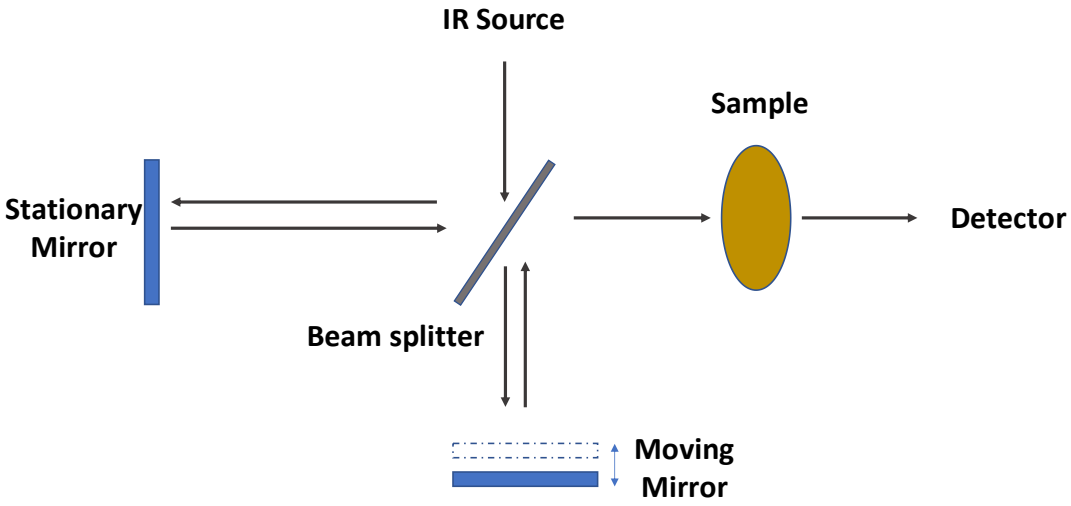

Fig. 13 FTIR setup in the transmission mode.

The fundamental modes of operation are reflectance, transmission and attenuated total reflection (ATR). Reflectance mode of operation is suitable if the sample has a measurable reflection in the IR range of the spectrum (works well for metals), transmission mode could be used if the sample is mostly transparent in the IR and finally ATR is a special mode used to probe surface properties of material. In the ATR mode, the IR radiation undergoes total internal reflection in a crystal that remains in contact with the sample, which allows to probe a sample with an IR evanescent wave that interacts with the sample. In this work, a Bruker Hyperion 2000 FTIR-microscope system has been used in a transmission mode. This system consists of a Bruker RockSolid interferometer, a Globar mid-infrared source with emission between 6000 to 10 cm^{-1}, liquid nitrogen cooled mercury, cadmium, and telluride detector, and a motorized x-y stage. A

15x objective was used to interrogate a 0.5 mm diameter area of the 2 mm x 2 mm sample, each measurement was performed with 4 cm^{-1} resolution and averaged over 256 scans.

The stability of SAMs on a photocorroding surface was studies using FTIR. The thiol SAMs were prepared with mercapto hexadecanoic acid thiols (MHDA), as a model thiol. 2 mm x 2 mm samples of the 10-413 wafer were cleaned with Opticlear, acetone and isopropanol. These samples were dried with nitrogen and etched with ammonium hydroxide for two minutes. After rinsing with degassed ethanol, samples were incubated in 2 mM MHDA overnight and rinsed with degassed ethanol. Photocorrosion was performed on such samples in DI water under QSPB2 with 20 mW/cm^2 excitation intensities and 3 s /25 s DC and photooxides were removed by incubating with NH_4OH for 10 min. IR absorption spectra were measured as described earlier.

An example of FTIR study of the SAM layer of 16-mercaptohexadecanethiol on GaAs, is shown in figure 14 (Huang et al., 2013). This work by Huang et. al. investigated the effect of mixture of solvents on formation of SAM. The high resolution FTIR spectra corresponds to the asymmetric (~2918 cm^{-1}) and symmetric (~2850 cm^{-1}) vibration of CH_2 group for varying mixtures of ethanol/water. Comparison of peak position and absorbance corresponding to CH_2 asymmetric vibrations, provides evidence of increased quality of SAM with addition of water to an ethanol solution.

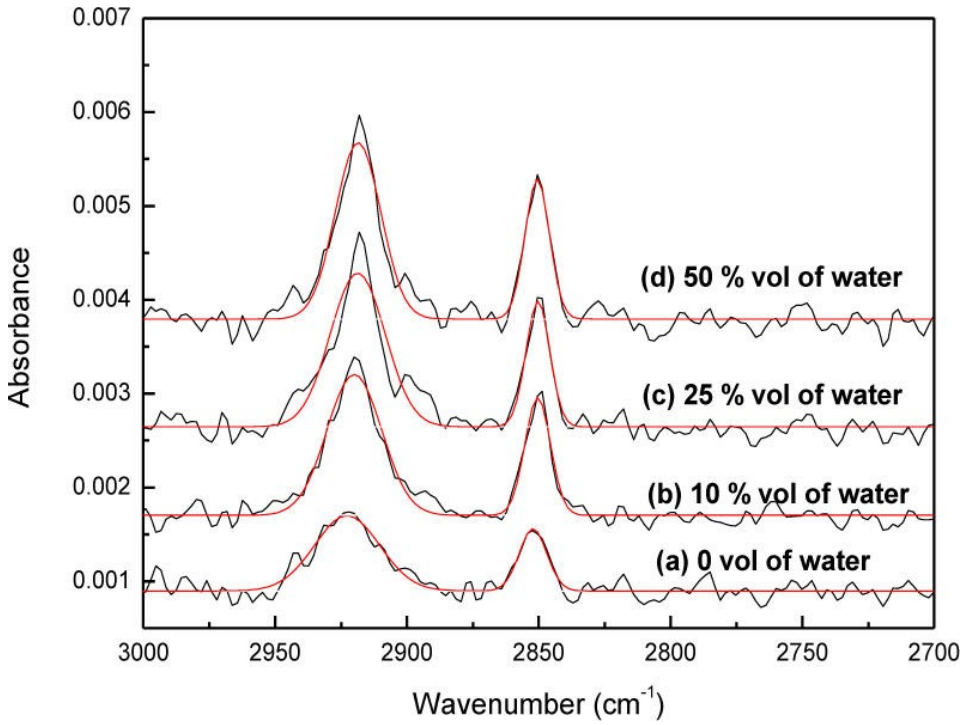

Fig. 14 FTIR spectra of SAM on GaAs corresponding to symmetric and asymmetric vibrations of CH_2 (Huang, Liu, Moumanis, & Dubowski, 2013).

6 RESULTS AND DISCUSSION

In the following section, we describe the results and discussions pertaining to photocorrosion metrology, application of the open circuit potential for monitoring of the digital photocorrosion process and the use of digital photocorrosion for detecting bacteria.

6.1 Foreword: Article 1, Photocorrosion metrology of photoluminescence emitting GaAs/AlGaAs heterostructures

The paper published in Journal of Physics: Applied Physics D demonstrates for the first time, the digital photocorrosion (DIP) dependent photoluminescence (PL) of GaAs/AlGaAs heterostructures for monitoring *in situ* the decomposition process of these materials with an atomic layer resolution. This paper established the relationship between the photocorrosion rate, photon flux and type of aqueous environments employed for supporting the photocorrosion process. Application of DIP for metrology of nanoheterostructures (NHs) has been demonstrated and provides insights into the processes that are applied for detection of bacteria.

Authors:
Srivatsa Aithal: PhD candidate
Neng Liu: PhD candidate
Jan J. Dubowski: Professor

Affiliation:
Laboratory for Quantum Semiconductors and Photon-based BioNanotechnology, Interdisciplinary Institute for Technological Innovation (3IT), Department of Electrical and Computer Engineering, Université de Sherbrooke
Date of publishing: 19 December 2016

Reference:
Aithal, S., Liu, N., Dubowski, J.J., “Photocorrosion metrology of photoluminescence emitting GaAs/AlGaAs heterostructures”, J. Phys. D: Appl. Phys. 50 (2017) 035106 (9pp)

Titre: Métrologie de photocorrosion de photoluminescence des hétérostructures GaAs/AlGaAs

Résumé: La sensibilité élevée de l'effet de photoluminescence (PL) aux états de surface et aux réactions chimiques sur les surfaces de semi-conducteurs émetteurs de PL s'est révélée intéressante pour le monitoring de la micro-structuration photo-induite de tels matériaux. Pour résoudre les problèmes de gravure à des taux d’enlèvement à l’échelle nanométrique, nous avons

étudié les mécanismes de photocorrosion des hétérostructures GaAs/$Al_{0.35}Ga_{0.65}As$ immergées dans de l'eau déionisée ou dans une solution aqueuse de NH_4OH et excitées par un rayonnement au-dessus de la bande interdite. La différence entre les taux de photocorrosion de GaAs et de $Al_{0.35}Ga_{0.65}As$ semble faiblement dépendante de l'énergie de la bande interdite de ces matériaux, et l'intensité du signal PL provenant de puits quantiques GaAs ou d'une couche épitaxiale de GaAs a été retrouvée dominée par les états de surface et par la réactivité chimique des surfaces de l'hétérostructure révélée au cours du processus de photocorrosion. Dans des conditions optimisées de photocorrosion, la méthode a permis la résolution de 1 nm d'épaisseur de GaAs se localisant entre des couches de $Al_{0.35}Ga_{0.65}As$. Nous démontrons que cette approche peut être utilisée comme un outil simple et peu coûteux à température ambiante pour le diagnostic post-croissance d'emplacement d'interface dans des puits quantiques émetteurs de PL et d'autres nano-hétérostructures.

Title: Photocorrosion metrology of photoluminescence emitting GaAs/AlGaAs heterostructures

Abstract: High sensitivity of the photoluminescence (PL) effect to surface states and chemical reactions on surfaces of PL emitting semiconductors has been attractive in monitoring photo-induced microstructuring of such materials. To address the etching at nano-scale removal rates, we have investigated mechanisms of photocorrosion of GaAs/$Al_{0.35}Ga_{0.65}As$ heterostructures immersed either in deionized water or aqueous solution of NH_4OH and excited with above-bandgap radiation. The difference in photocorrosion rates of GaAs and $Al_{0.35}Ga_{0.65}As$ appeared weakly dependent on the bandgap energy of these materials, and the intensity of an integrated PL signal from GaAs quantum wells or a buried GaAs epitaxial layer was found dominated by the surface states and chemical reactivity of heterostructure surfaces revealed during the photocorrosion process. Under optimized photocorrosion conditions, the method allowed resolving a 1 nm thick GaAs sandwiched between $Al_{0.35}Ga_{0.65}As$ layers. We demonstrate that this approach can be used as an inexpensive, and simple room temperature tool for post-growth diagnostics of interface locations in PL emitting quantum wells and other nano-heterostructures.

Keywords: Photocorrosion, GaAs/AlGaAs quantum wells, AFM, X-ray photoelectron spectroscopy, metrology of heterostructures

PACS:
73.20 -r Surface states
73.61 Ey electrical properties of III-V Semiconductors
78.55 Cr Photoluminescence III-V semiconductors
82.45 Bb Corrosion (electrochemistry)

6.1.1 Introduction

Devices based on semiconductor multilayers find a wide range of applications in microelectronics, photonics and consumer market products. Bipolar transistors and high electron mobility transistors (Bhattacharya et al., 2011) that are at the heart of RF technologies applied in ubiquitous devices such as mass-produced cellphones, satellite communication devices and car radars (Pettenpaul, 1998), or multi-junction solar cells developed for concentrated photovoltaics (Dimroth et al., 2014) are examples of devices taking advantage of the heterojunction technology. The successful fabrication of such devices depends on the quality of semiconductor wafers that relies on advanced diagnostic and metrology tools frequently employed as post-growth interrogation about such parameters as layer thickness, interfacial roughness, material composition, density of carriers and interface traps, or Schottky barrier height (Schroder, 2006). The most common methods employed for characterization of physical and chemical properties of semiconductor devices include x-ray diffraction (Gerardi et al., 1997, Nakashima and Tateno, 2004), atomic force microscopy (AFM) (Oliver, 2008), secondary ion mass spectroscopy (SIMS) (Herrmann et al., 2011, Liu and Dubowski, 2013, Gerardi et al., 1997), photo-voltage spectroscopy (Kronik and Shapira, 2001, Masut et al., 1986), Auger electron spectroscopy (Rack et al., 2000), scanning electron microscopy (SEM) (Linkov et al., 2013), transmission electron microscopy (TEM) (Linkov et al., 2013), reflectance spectroscopy (Wośko et al., 2011), monolayer chemical beam etching (Tsang et al., 1993) and x-ray photoelectron spectroscopy (XPS) (Vilar et al., 2005, Hinkle et al., 2009). Furthermore, current-voltage (I-V) and capacitance-voltage (C-V) measurements (Fleetwood et al., 1993) have been employed to investigate device band structure (Watanabe, 1985) and provide information about carrier concentration and distribution by employing electrochemical (Kaniewska and Slomka, 2001) and photo-electrochemical profiling (Blood, 1986). The thickness of layers constituting heterostructure devices is one of the fundamental parameters determining functioning characteristics of quantum well (QW) and other quantum confined microstructure based devices. Typical methods for determining this parameter are based on cross-section SEM or TEM imaging (Perovic et al., 1995), ellipsometric analysis (Erman et al., 1983), depth profiling with Auger electron spectroscopy (J. J. Dubowski et al., 1985), SIMS (Liu et al., 2013) and x-ray diffraction techniques (Tapfer and Ploog, 1986). Electrochemical and photo-electrochemical profiling techniques have been employed to study multi-junction devices due to the ease in revealing location of different interfaces. However, relatively high etch rates induced in such experiments prohibit their application in studying nano-scale interfaces, such as those involving QWs and quantum dots (Fink and Osgood, 1993). Nevertheless, selective etching of cleaved wafers revealed interfaces between ~ 60 nm thick pairs of GaAs and AlGaAs layers using the AFM technique (Pakhomov et al., 2002). Typical etch rates of GaAs and InP achieved with a laser-induced photoetching technique have been reported between 0.1 – 100 μm/min (Ruberto et al., 1991), while fabrication of relatively smooth surfaces of GaAs has been demonstrated with reactive ion etching in $Cl_2/BCl_3/Ar$ plasma at rates exceeding 0.3 μm/min (Nordheden et al., 1999). Generally, surface morphology of etched or photo-etched semiconductors is characterized by average roughness exceeding 15 nm (Kirchner et al., 2002) and, thus, such techniques cannot be readily employed to provide information about location of interfaces in QW or quantum dot heterostructures.

We have recently employed the photocorrosion effect of photoluminescence (PL) emitting GaAs/AlGaAs heterostructures for monitoring surface reactions involving electrically charged molecules that allowed for a rapid detection of bacteria in aqueous solutions (Nazemi et al., 2015, Aziziyan et al., 2016). This was possible thanks to creating conditions for uniform photocorrosion proceeding at rates typically not exceeding ~ 60 nm per hour. In the current work, we investigate the mechanisms of GaAs and AlGaAs photocorrosion in water and aqueous environment of NH_4OH, and we examine the conditions leading to the high-resolution resolving of different material layers contributing to PL emission.

6.1.2 Experimental Section

6.1.2.1 Materials and chemicals reagents

GaAs/AlGaAs heterostructures were grown on double side polished semi-insulating GaAs (100) by molecular beam epitaxy (Wafers 10-150 and v0803) and by metalorganic chemical vapor deposition (Wafer 10-413). A 200 nm thick epitaxial GaAs, as well as a superlattice with 2.4 nm thick AlAs and 2.4 nm thick GaAs were grown in each case on GaAs substrates as defect reduction buffer layers (Dawson and Woodbridge, 1984, Noda et al., 1990). A schematic cross-section of the Wafer 10-150 microstructure is shown in fig. 1a. It consists of a 500 nm thick GaAs epitaxial layer designed to provide PL emission at ~ 869 nm. Additionally, a stack of 100 nm thick $Al_{0.35}Ga_{0.65}As$, 3 nm thick GaAs and 10 nm thick $Al_{0.35}Ga_{0.65}As$, capped with an 8 nm thick GaAs layer, was grown on top of the PL emitting GaAs layer. The room-temperature PL emitted by this microstructure is shown in fig. 1b. Note that due to the quantum confinement effect, the 3 nm thick GaAs QW emits PL at low-temperatures as reported in (Aziziyan et al., 2016), but no such emission could be observed at room temperature. A cross-section of the Wafer 10-413 microstructure is illustrated schematically in fig. 1c. It comprises a stack of 29 GaAs QWs (6 nm thick) surrounded by 10 nm thick $Al_{0.35}Ga_{0.65}As$ barriers grown on a 200 nm thick GaAs buffer layer. This microstructure is capped with a 10 nm thick layer of GaAs. The PL emission of this microstructure at 820 nm originates from the stack of GaAs QWs, as illustrated in fig.1d. A cross section of the Wafer v0803 microstructure is illustrated schematically in fig.1e. A 500 nm $Al_{0.35}Ga_{0.65}As$, overlaid on a 500 nm thick PL emitting epitaxial GaAs layer, forms the base of the heterostructure. There are eleven units of GaAs and $Al_{0.35}Ga_{0.65}As$ grown on the base. The thicknesses of GaAs of these units are 60, 50, 40, 30, 20, 10, 8, 6, 4, 2 and 1 nm for the top layer. The thickness of $Al_{0.35}Ga_{0.65}As$ is 20 nm in each of the eleven layers and the whole structure is capped with a 20 nm thick GaAs layer. A plot of the PL emission at 869 nm that originates from the 500 nm thick GaAs layer in this microstructure is shown in fig. 1f. We have also employed bulk Si-doped ($n=10^{17}$ cm^{-3}) GaAs (AXT, Inc., Fremont, USA) while investigating oxide formation on samples exposed to DI water.

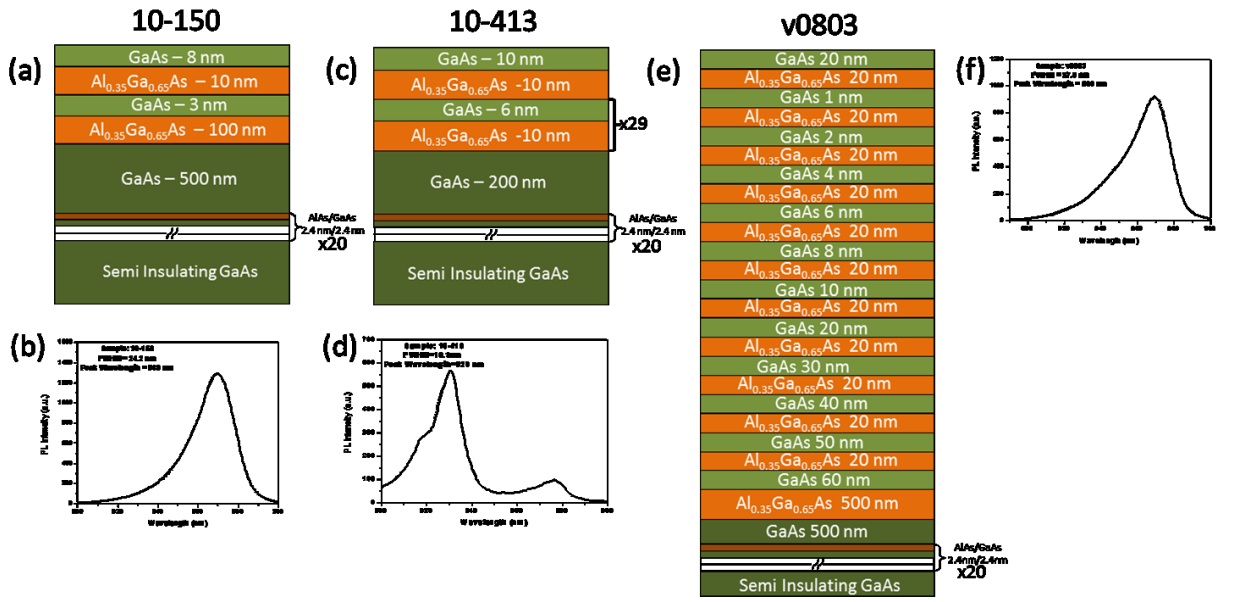

Fig. 1. Schematic cross-sections of the investigated nano-heterostructures. Photoluminescence in the 10-150 sample originates from a 500 nm thick GaAs layer (a), and is centered at 869 nm (b). Photoluminescence on the 10-413 sample originates from a stack of 6 nm quantum wells (c), and is centered at 829 nm (d). Photoluminescence in the v803 sample originates from a 500 nm thick GaAs layer (e), and is centered at 869 nm (f).

Semiconductor grade OptiClear (National Diagnostics), acetone (ACP Chemicals, Canada), isopropyl alcohol and 28% ammonium hydroxide (Anachemia, Canada) were used without further purification. De-ionized (DI) water with a resistivity of 18.2 MΩ-cm was obtained from a MilliQ system. The wafers were spin coated with photoresist (S1813, Shipley), mounted on a carrier tape and diced into 2 mm x 2 mm and 4 mm x 4 mm samples.

6.1.2.2 Photoluminescence measurements

Photoluminescence measurements were performed using either a custom designed Quantum Semiconductor Photonic Biosensor (QSPB) Reader or Hyperspectral Imaging Photoluminescence Mapper (HIPLM) described in (Aziziyan et al., 2016; Nazemi et al., 2015) and (Kim et al., 2009), respectively. The above bandgap excitation in QSPB was provided either by a 625 nm LED source or by a halogen lamp. An 812 nm cut-off long pass filter (Thorlabs FELH800) was applied in the QSPB Reader to prevent the excitation photons from reaching the CMOS detector employed for detecting PL emission. The HIPLM is equipped with a laser emitting at 532 nm, computer controlled volume Bragg gratings, beam homogenizing microlens array and a Peltier cooled high sensitivity CCD camera. The HIPLM allows measurement of spatial-temporal variation of the PL emission from GaAs/AlGaAs heterostructures (Kim et al., 2009). The PL measurements were carried out for samples installed in a flow cell as illustrated schematically in Fig. 2.

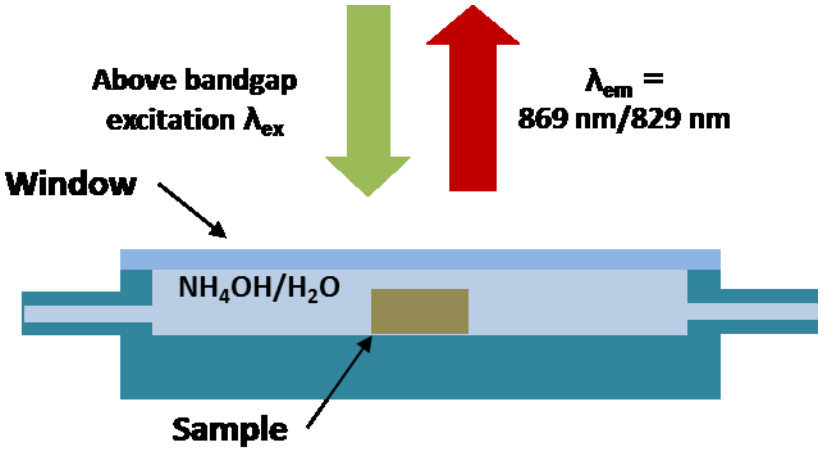

Fig. 2. A schematic view of the flow cell setup.

The flow cell allows a continuous exposure of samples to the photocorrosion supporting solutions that could be refreshed continuously. A dedicated glass window facilitates excitation of samples and collection of PL data. The excitation power density measured at the sample surface in both QSPB and HIPLM systems ranged between 20 - 150 mW/cm^2. In all the measurements, the samples were excited with intermittent pulses to allow a) formation and dissolution of a sufficient thickness surface oxides, and b) diffusion of the photocorrosion products to disperse into the solution between consecutive pulses. The intermittency was defined by a "duty cycle" (DC) parameter: T_{ON} / (T_{ON} + T_{OFF}). The experiments were performed in an open circuit condition.

6.1.2.3 AFM measurements

A Nanoscope IIIa (Digital Instruments, Inc.) was used to carry out atomic force microscopy (AFM) study of surface morphology of the investigated samples. Scans of 5 µm x 5 µm were collected in a tapping mode at ambient conditions. The photocorrosion rates were determined by measuring depths of photocorroded craters. For this, we used 4 mm x 4 mm samples of the 10-413 heterostructure, partially covered with a positive photoresist. The samples were briefly cleaned with isopropanol, placed in the flow cell with DI water and photocorrosion performed for different periods of time. The AFM measurements were performed for samples with removed photoresist, in the areas covering both non-photocorroded and photocorroded surfaces. The AFM measurements were also performed for photocorroded samples that were freshly de-oxidized with NH_4OH.

6.1.2.4 X-ray photoelectron spectroscopy measurements

X-ray photoelectron spectroscopy (XPS) measurements were conducted in the Al 2p region to investigate chemical composition of photocorroded microstructures. The measurements were carried out with a Kratos Analytical AXIS Ultra DLD XPS spectrometer equipped with Al Kα source operating at 150 W. Following the photocorrosion experiments, the samples were de-oxidized for 5 min in a 28% aqueous solution of NH_4OH, dried with gas N_2 and transported in the N_2 ambient to the XPS chamber. The de-oxidization procedure was necessary to remove the surface accumulated oxide layer whose thickness exceeded ~ 10 nm as evidenced by the absence of the Al 2p peak on the photocorroded surfaces. Both surface survey and high-resolution scans were performed for samples mounted in a chamber with the base pressure of 1 × 10−9 Tor. The size of an analyzed area on the investigated samples was set at 220 µm × 220 µm and data were collected at a takeoff angle of 60^o from the surface normal. All XPS results, referenced to the adventitious C 1s peak at the binding energy (BE) of 285.0 eV, were processed using the Casa XPS 2.3.15 software.

6.1.3 Results and discussion

6.1.3.1 PL monitored photocorrosion of bulk n-GaAs

A 2 mm x 2 mm bulk n-GaAs sample, after cleaning with OptiClear, acetone and isopropanol, and deoxidizing with NH4OH was quickly transferred to the flow cell with DI water. The sample was irradiated with the broadband halogen lamp and its PL emission was measured with the QSPB reader. The excitation intensity was 43 mW/cm^2, and the sample was continuously exposed to the radiation (DC = 1, TOFF = 0). A temporal evolution of the PL signal measured at 869 nm is shown in Fig. 3.

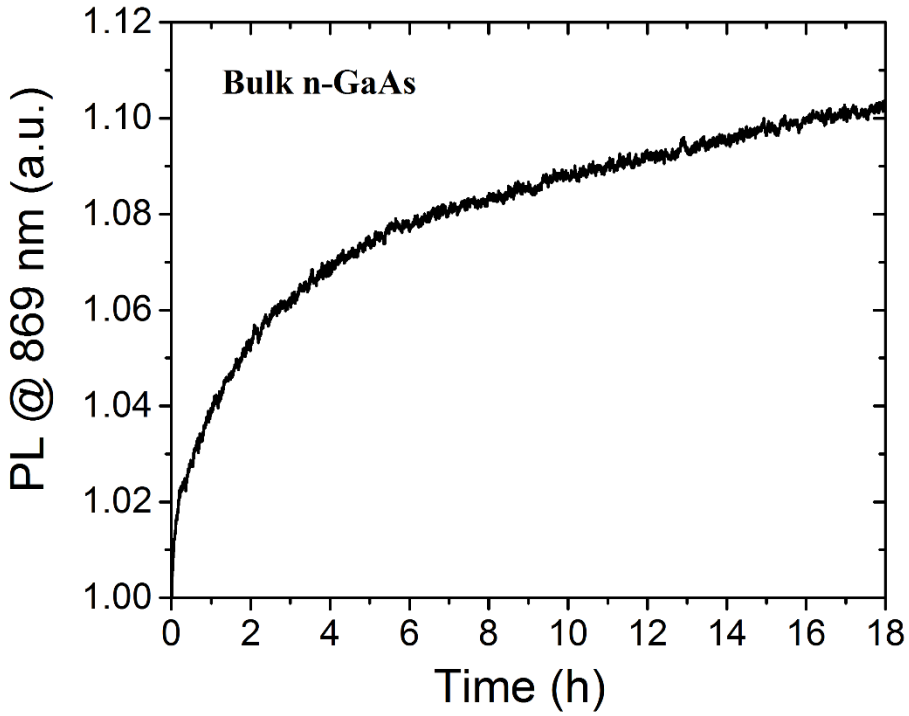

Fig. . 3. Temporal PL intensity of a bulk n-type GaAs (001) emitting at 869 nm while exposed in DI H_2O to a broadband halogen lamp radiation.

It can be seen that PL intensity increases monotonically with time, exhibiting a 10% increase after 18 hours and a tendency towards asymptotic saturation. The origin of this behaviour, referred to as photowashing (Wilmsen et al., 1988, Choi et al., 2002), can be traced down to oxidation of the GaAs surface and photocorrosion (Geisz et al., 1995, Hideki et al., 1988).

The PL emission from a photoexcited semiconductor is a result of the recombination of excited charge carriers, and its efficiency is an index of the lifetime of the minority carriers (holes for an n-type semiconductor): the increase of their lifetime results in the increased PL emission. Minority carrier lifetime, τ, could be described by the following equation (Ahrenkiel et al., 1989):

$$\frac{1}{\tau} = \frac{1}{\tau_R} + \frac{1}{\tau_{nR}} + \frac{2SRV}{d} \qquad (1)$$

where τ_R is the radiative recombination lifetime, τ_{nR} the non-radiative recombination lifetime, SRV denotes the surface recombination velocity, and d is the depletion width. With the exception of SRV and d, the other components in this equation are bulk parameters of the semiconductor. The SRV represents the non-radiative recombination component due to the break in the translational symmetry of the semiconductor at its surface, which results in the formation of surface states

with energy levels in the band gap, and formation of the depletion width region in the semiconductor. Decreased SRV increases the minority carriers' lifetime, and hence the efficiency of PL emission. Furthermore, it is known that the oxidation and photo-decomposition of n-type GaAs could be described by the following equations (Ruberto et al., 1991):

$$\mathbf{GaAs + H_2O + 6h^+ \rightarrow Ga^{3+} + HAsO_2 + 3H^+} \quad (2)$$

$$\mathbf{GaAs + 3}\boldsymbol{e} \mathbf{\rightarrow Ga^0 + As} \quad (3)$$

where h+ represents the holes in the semiconductor and H^+ is the proton in the solution, e represents the electron and Ga^0 denotes a reduced gallium atom. The water environment and excited holes arriving at the semiconductor surface lead to oxidation, and the reactions represented by equations (2) and (3) describe oxidation and dissolution of GaAs upon photo-excitation. As As-oxides are preferentially removed in an aqueous solution (Schwartz et al., 1979), the increased presence of Ga-oxides (Ga_xO_y) develops at the GaAs-solution interface. It has been demonstrated that capping of GaAs with a Ga_2O_3 film results in the reduction of the SRV of minority carriers and, consequently, in the increased PL emission intensity (Passlack et al., 1995, Priyantha et al., 2011). In agreement with these results, and with our XPS data, we argue that it is the predominant formation of a Ga_2O_3 layer and partial dissolution of As-oxides that are responsible for the increasing PL signal observed in Fig. 3. The results reported in that figure were obtained with a white light source, but the same behaviour is expected to take place as long as GaAs is irradiated with photons of energy exceeding the bandgap energy of this material.

PL monitored photocorrosion of nano-heterostructures

Examples of temporal plots of PL emission from GaAs/AlGaAs samples (Wafer 10-150) exposed in the flow cell to continuously flowing DI water and irradiated in the HIPLM system with a CW 532 nm laser at 70 mW/cm^2 are shown in Fig. 4. These experiments were designed to investigate the influence of the irradiation conditions on the average photocorrosion rate of studied microstructures. It can be seen that 1 s irradiation in each 100 s period (DC = 0.01) allows observing the formation of two PL maxima at 80 and 275 min, followed by a slowly decaying signal.

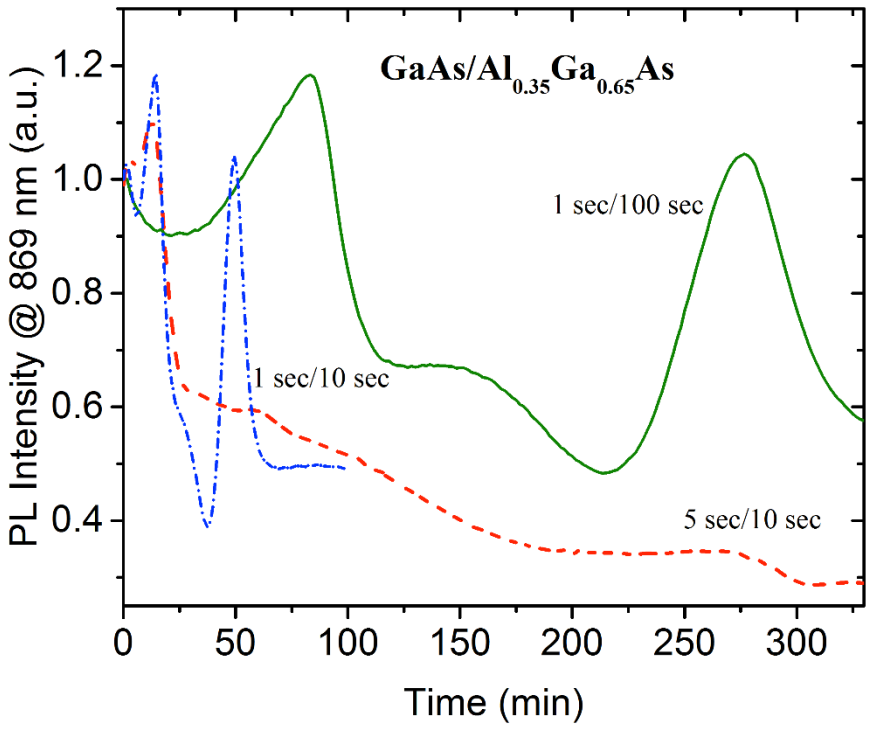

Fig. 4. Temporal PL plots of a GaAs/AlGaAs nano-heterostructure (sample 10-150) emitting at 869 nm while exposed to DI water and irradiated with a 532 nm laser at 70 mW/cm^2 at different duty cycles: 1s/100 s (solid line), 1s/10s (dash-dotted line) and 5s/10 s (dash line).

Similar maxima are observed for the samples irradiated for 1 s in a 10 s period (DC = 0.1). But, in this case, the maxima occur at 15 and 50 min, i.e., they form significantly sooner and they are separated by only 35 min, in comparison to the 195 min separation observed for the sample processed with DC = 0.01. The initial increase of the PL signal observed in theses experiments suggests a similar mechanism of photocorrosion as in the case of bulk GaAs discussed in figure 3. The number of PL maxima observed for low duty cycle experiments (DC=0.1 and 0.01) coincide with the number of GaAs-$Al_{0.35}Ga_{0.65}As$ interfaces in this nano-heterostructure. Furthermore, the region of a slowed down PL decay is observed for DC = 0.01 near 125-140 min, and for DC = 0.1 near 25-40 min. We link this behaviour with a reduced rate of photocorrosion of the 10 nm thick $Al_{0.35}Ga_{0.65}As$ layer. For DC = 0.5, the first maximum occurs around 12 minutes, which suggests an accelerated rate of photocorrosion. Consistent with this was the inability to observe the formation of a second PL maximum.

In figure 5, we plot temporal positions of the 1st maximum observed for the sample 10-150 as a function of the excitation power, P, for DC = 0.01.

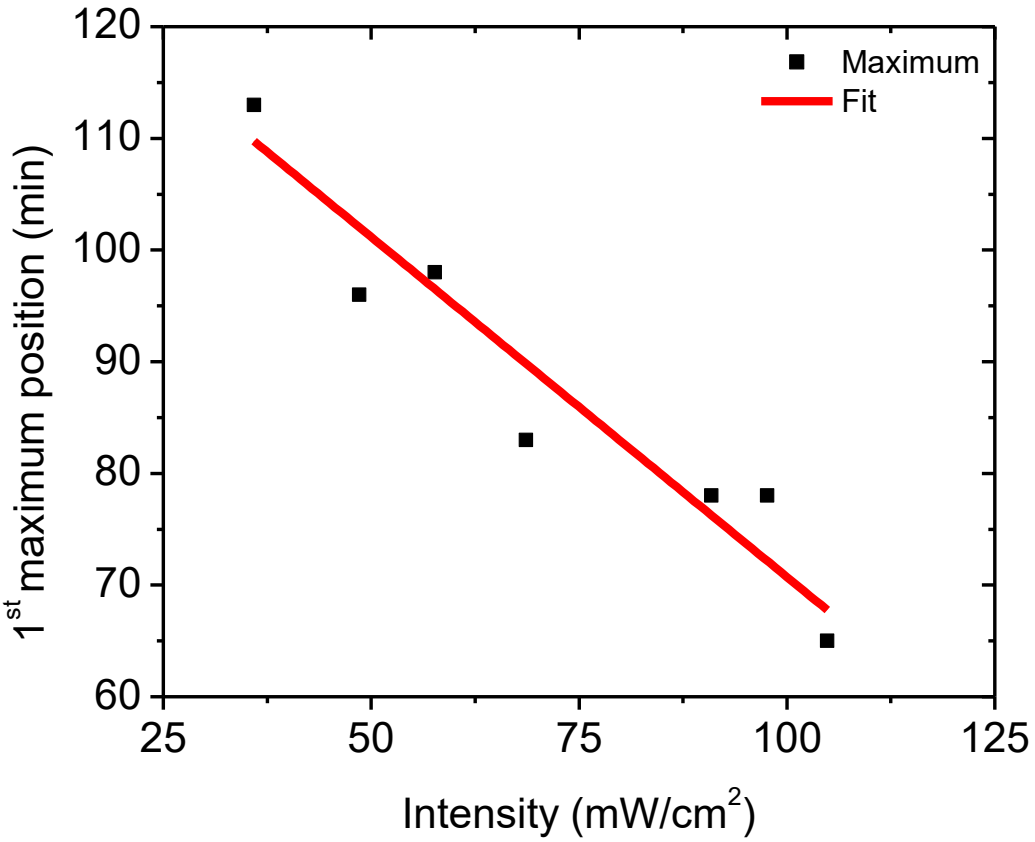

Figure 5. Excitation power dependence of the position of a PL maximum related to the photocorrosion of an 8 nm thick GaAs cap layer (sample 10-150) immersed in DI H2O and irradiated with an uniform beam of the 532 nm laser at DC = 0.01.

It can be seen that the position of this maximum occurs more rapidly with increasing excitation power, and it depends linearly on the excitation power. Thus, the related photocorrosion rate is consistent with the kinetics of a process driven entirely by the availability of photo-excited holes. At P > 105 mW/cm^2, a departure from the linear dependence took place (data not shown), showing significantly delayed positions of the investigated PL maxima. This seems to suggest the onset of a mechanism affected by a greater rate of oxide formation than dissolution.

In Fig. 6a, we present a temporal plot of PL signal measured at 869 nm from the v0803 sample that undergoes photocorrosion in a 28% NH_4OH aqueous solution. The sample was irradiated in the HIPLM system with a 532 nm laser delivering 25 mW/cm^2 power at DC = 0.5 (30 s/60 s). In this experiment, we replaced DI water with an aqueous solution of NH4OH to provide a more efficient means of removing As- and Ga-oxides from photocorroding surface. Such treatment has

been reported to leave only a small amount of Ga-suboxides on the photocorroding surface of GaAs (Lebedev et al., 2004).

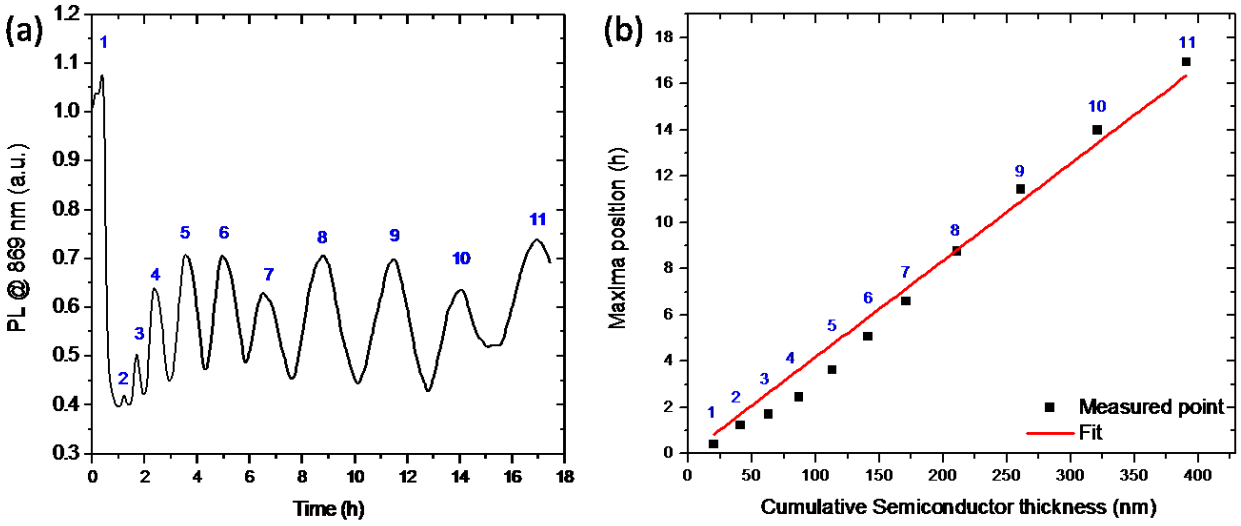

Figure 6. Time dependent PL emission (at 869 nm) of a GaAs/AlGaAs nano-heterostructure (sample v0803) immersed in NH_4OH and irradiated in HIPLM with a 532 nm laser at DC = 30 s/60 s (a), and a plot of the position of PL maxima vs. cumulative thickness of the nano-heterostructure (b).

A series of PL maxima, denoted as 1 to 11, can be distinguished in that figure. Initially, after reaching the first maximum, the PL intensity drops by about 60 %. This is followed by the PL signal modulating between less than 5% for the second maximum (2), to about 30% for the ninth maximum (9). The oxidation and subsequent removal of oxides lead to a continuous thinning of the semiconductor microstructure and switching in situ between interfaces involving GaAs-solution and $Al_{0.35}Ga_{0.65}As$-solution. Figure 6b demonstrates a relationship between the thickness of this microstructure and temporal positions of PL maxima. The thickness was extracted from the known growth parameters of this microstructure (see fig. 1e), and an assumption was made that each maximum coincides with a completely etched GaAs layer and the photocorrosion onset of an AlGaAs layer. It can be seen that there is a reasonable linear correlation between the cumulative microstructure thickness and the number of a consecutive PL maximum. Based on this model, we estimated that the average photocorrosion rate of the microstructure was ~ 0.39 nm/min.

6.1.3.2 AFM Depth Measurements

AFM measurements were performed for samples 10-413 that photocorroded in DI water. The samples were irradiated with a 625 nm LED at 20 mW/cm^2 and DC = 0.075 (3 s/40 s) for a total of

42, 107 and 124 min. The PL runs of these samples are shown in figure 7. We note that the initial attempts to AFM analyse photocorroded craters were unsuccessful due to the presence of a thick oxide layer covering the irradiated surface. It was only after subjecting the samples to ammonium hydroxide etching that we were able to observe clear contrast between non-irradiated (photoresist protected) and photocorroded surface. The results of these measurements are summarized in table 1.

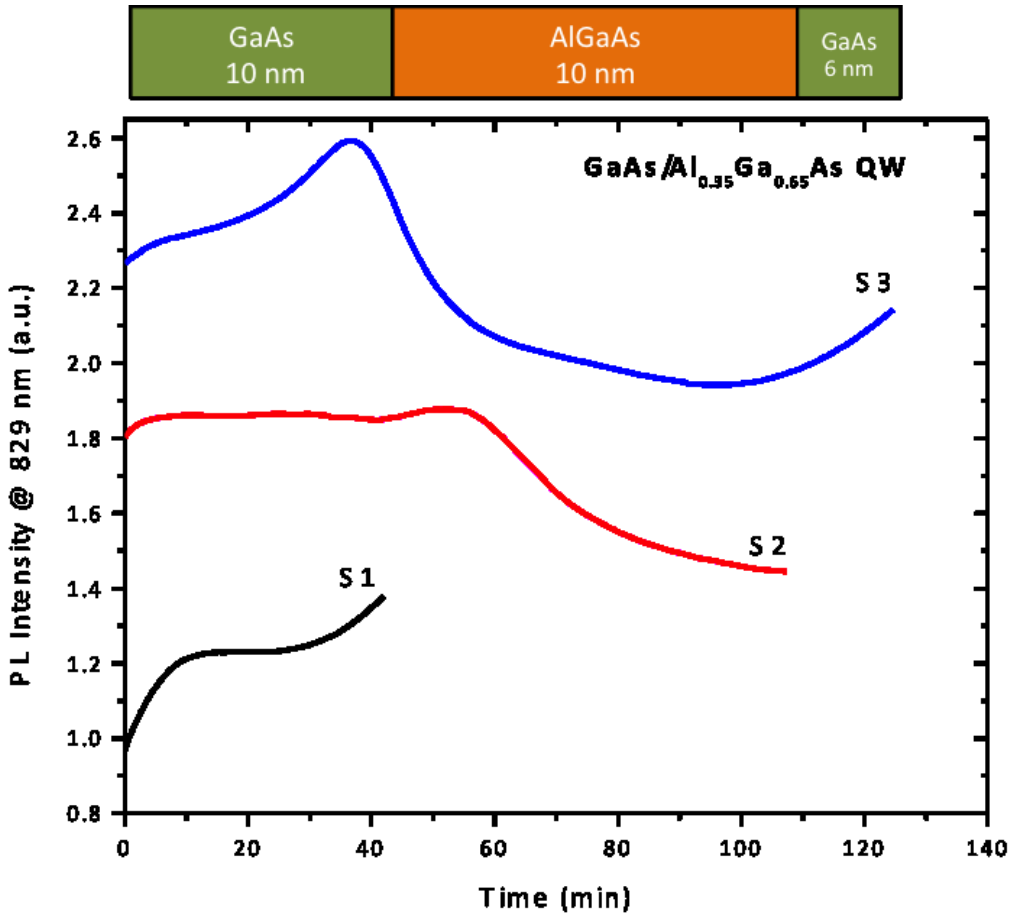

Figure 7. Time dependent PL emission of GaAs/AlGaAs QWs (Wafer 10-413) immersed in DI H_2O and irradiated with a 625 nm LED at 20 mW/cm^2 and DC = 3 s/40 s.

Table 1. AFM determined depths of the craters fabricated by photocorrosion of GaAs/AlGaAs QWs (Wafer 10-413) illustrated in figure7. The samples were irradiated with a 625 nm LED at 20 mW/cm^2 and DC = 0.075 (3 s/40 s).

End Point	Duration of Photocorrosion (min)	Depth (nm)
S1	12	9.8
S2	107	15.7
S3	124	26.7

The estimated depth for the end point S1 is 9.8 nm, hence the photocorrosion has consumed most of the 10 nm thick GaAs cap layer of that sample. For the end point S2, the estimated depth is 15.7 nm, hence the 10 nm GaAs cap layer and 5.7 nm of the first 10 nm AlGaAs layer have photocorroded. For the end point of S3, the estimated depth is 26.7 nm, which indicates that in addition to the entire GaAs cap and the first AlGaAs layer, the second GaAs (QW) layer have photocorroded. These results suggest that the initial PL increase, until the end-point S1 is reached, coincides with the dissolution of a GaAs cap layer. The decrease of a PL signal leading to the end-point S2, coincides with dissolution of the first AlGaAs layer, while the subsequent increase of the PL signal leading to the end point S3, coincides with the second GaAs layer dissolving entirely.

6.1.3.3 XPS Measurements

High resolution XPS scans in the Al 2p peak region for a reference (non-photocorroded) sample 10-413, and for a series of 10-413 samples photocorroded for different period of time, together with the associated PL plots collected in the QSPB reader during their photocorrosion are shown in figures 8a and 8b, respectively. As the photocorrosion proceeds through the GaAs/$Al_{0.35}Ga_{0.65}As$ interface, the XPS determined concentration of Al aluminium increases. Hence, evolution of the Al 2p peak could be used to investigate depth of the photocorroded material, keeping in mind that a typical XPS depth resolution approaches 10 nm (Dallera et al., 2004).

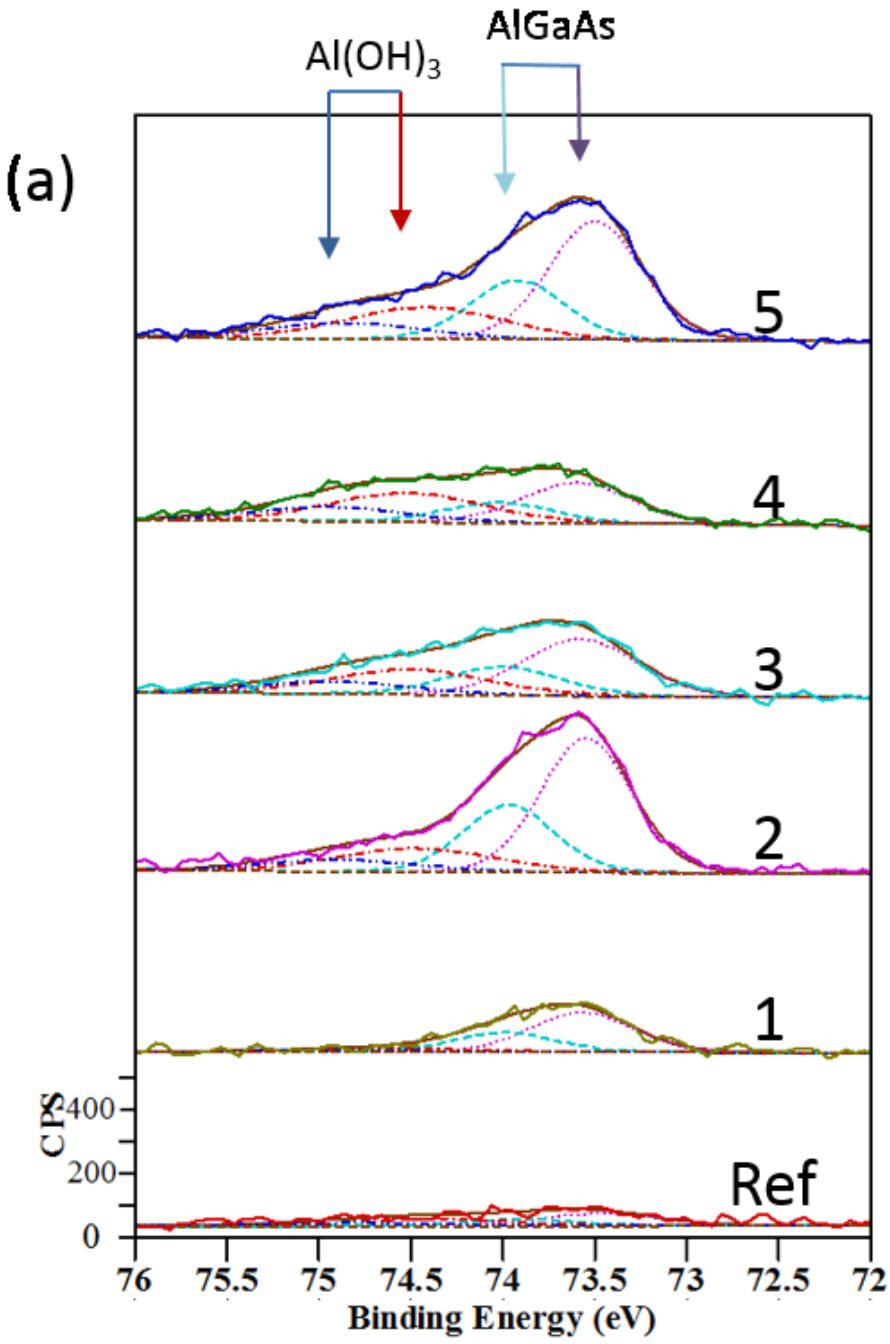
(a)
Al(OH)3
AlGaAs
5
4
3
2
1
Ref
CPS
400
200
0
76
75.5
75
74.5
74
73.5
73
72.5
72
Binding Energy (eV)

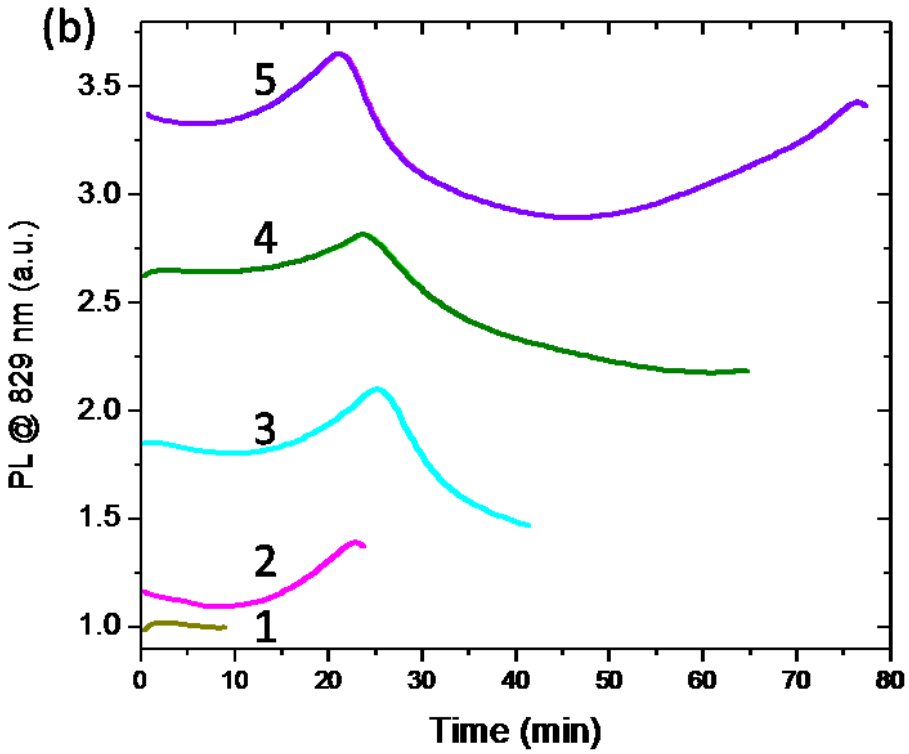

Figure 8. High resolution XPS scans of the Al 2p peak from the 10-413 samples photocorroded for different period of time (a), and associated temporal PL plots for the same samples (b).

Sample 1 that photocorroded for 9 minutes shows a small intensity peak in the region of the elemental Al 2p, suggesting that it originated from the GaAs capped AlGaAs layer. Sample 2 that photocorroded for 25 minutes, and revealed the first PL maximum, shows an increased concentration of the elemental Al 2p. In addition, the presence of some Al 2p oxides in this case suggests a contribution from the AlGaAs layer exposed by photocorrosion. Samples 3 and 4 that photocorroded for 40 and 65 min show decreasing concentration of the elemental Al at the expense of Al-oxides, which is consistent with the increased contribution from the photocorroding AlGaAs layer. Finally, sample 5 that photocorroded until it revealed the second PL maximum, shows an increased concentration of Al originating from the second AlGaAs layer.

The XPS and AFM data confirmed the origin of PL features revealed during photocorrosion of the GaAs/AlGaAs nano-heterostructures. The formation of the 1st PL maximum is consistent with the photocorrosion of GaAs through the formation and dissolution of Ga-oxides, similarly to the photocorrosion of n-GaAs discussed in Section 3.1. Furthermore, the revealing of the AlGaAs surface is associated with the formation of Al-oxides along with As- and Ga-oxides. This affects the intensity of PL signal emitted by the microstructure as the SRV at the Ga-oxide covered GaAs

surface is of the order of 4000-5000 cm/s, whereas that at the Al-oxide covered AlGaAs surface increases to ~10^7 cm/s (Passlack et al., 1996). Hence the formation of PL maxima in these experiments is consistent with the onset of the photocorrosion of AlGaAs, each time the GaAs layer is dissolved, which is also associated with the increased SRV at the revealed surface of AlGaAs.

6.1.4 Conclusions

We have investigated photocorrosion of GaAs/$Al_{0.35}Ga_{0.65}As$ nano-heteostructures immersed in DI water and aqueous solution of NH_4OH. The pulse excitation of such samples with the above bandgap radiation produces photoluminescence of intensity that could be correlated with the sequential formation in situ of different electrochemical junctions. For high duty cycles (DC), defined as the ratio of $T_{ON}/(T_{ON}+T_{OFF})$, and for the excitation power exceeding 105 mW/cm^2, the photocorrosion rates are relatively large, resulting in a poor depth resolution of the process. Under optimized irradiation conditions, described by $P \leq 105$ mW/cm^2 and $DC < 0.5$, the photocorrosion process proceeds at rates of less than 0.2 - 0.4 nm/minute. Such conditions enabled us to observe dissolution of a 1 nm thick layer of GaAs. A linear correlation between photon flux and corrosion rates observed under these conditions is consistent with a pure photo-induced corrosion process. Due to different surface recombination velocities of minority carriers, oxides at the GaAs surface tend to increase PL emission from the GaAs/AlGaAs microstructures, while oxides at the AlGaAs surface reduce that emission. We have demonstrated that PL monitored photocorrosion of the GaAs/AlGaAs heterostructure could be used for post-growth metrology of such architectures with at least a 1 nm depth resolution. The ability to control photodecomposition of PL emitting III-V nano-heterostructures has the potential application for the fabrication of multibandgap devices requiring the regrowth on precisely revealed surfaces prepared, e.g., for the realization of so called butt joint integration architectures.

6.1.4.1 Acknowledgements

This research was supported by the Canada Research Chair in Quantum Semiconductors Program, the Natural Sciences and Engineering Research Council of Canada (NSERC) CRD project CRDPJ 452455 – 13, and the NSERC Discovery Grant RGPIN-2015-04448. We thank Prof. Zbigniew Wasilewski for providing some of the GaAs/AlGaAs microstructures used in this work.

6.1.5 References

Ahrenkiel, R., Dunlavy, D., Keyes, B., Vernon, S., Dixon, T., Tobin, S., Miller, K. & Hayes, R. (1989) Ultralong minority-carrier lifetime epitaxial GaAs by photon recycling. Applied physics letters, 55, 1088-1090

Aziziyan, M. R., Hassen, W. M., Morris, D., Frost, E. H. & Dubowski, J. J. (2016) Photonic biosensor based on photocorrosion of GaAs/AlGaAs quantum heterostructures for detection of Legionella pneumophila. Biointerphases, 11, 019301

Bhattacharya, P., Fornari, R. & Kamimura, H. 2011. Comprehensive Semiconductor Science and Technology, Six-Volume Set, Newnes.

Blood, P. (1986) Capacitance-voltage profiling and the characterisation of III-V semiconductors using electrolyte barriers. Semiconductor Science and Technology, 1, 7

Choi, K. J., Moon, J. K., Park, M., Kim, H. C. & Lee, J. L. (2002) Effects of photowashing treatment on gate leakage current of GaAs metal-semiconductor field-effect transistors. Japanese Journal of Applied Physics Part 1-Regular Papers Brief Communications & Review Papers, 41, 2894-2899

Dallera, C., Duo, L., Braicovich, L., Panaccione, G., Paolicelli, G., Cowie, B. & Zegenhagen, J. (2004) Looking 100 Å deep into spatially inhomogeneous dilute systems with hard X-ray photoemission. Applied physics letters, 85, 4532-4534

Dawson, P. & Woodbridge, K. (1984) Effects of prelayers on minority-carrier lifetime in GaAs/AlGaAs double heterostructures grown by molecular beam epitaxy. Applied Physics Letters, 45, 1227-1229

Dimroth, F., Grave, M., Beutel, P., Fiedeler, U., Karcher, C., Tibbits, T. N., Oliva, E., Siefer, G., Schachtner, M. & Wekkeli, A. (2014) Wafer bonded four-junction GaInP/GaAs//GaInAsP/GaInAs concentrator solar cells with 44.7% efficiency. Progress in Photovoltaics: Research and Applications, 22, 277-282

Erman, M., Theeten, J. B., Vodjdani, N. & Demay, Y. (1983) Chemical and structural analysis of the GaAs/AlGaAs heterojunctions by spectroscopic ellipsometry. Journal of Vacuum Science & Technology B, 1, 328-333

Fink, T. & Osgood, R. M. (1993) Photoelectrochemical Etching of GaAs / AlGaAS Multilayer Structures. Journal of The Electrochemical Society, 140, 2572-2581

Fleetwood, D., Winokur, P., Reber Jr, R., Meisenheimer, T., Schwank, J., Shaneyfelt, M. & Riewe, L. (1993) Effects of oxide traps, interface traps, and ``border traps``on metal-oxide-semiconductor devices. Journal of applied physics, 73, 5058-5074

Geisz, J., Kuech, T. & Ellis, A. (1995) Changing photoluminescence intensity from GaAs/Al0. 3Ga0. 7As heterostructures upon chemisorption of SO2. Journal of applied physics, 77, 1233-1240

Gerardi, C., Giannini, C., Passaseo, A. & Tapfer, L. (1997) High-resolution depth profiling of In(x)Ga(1-x)As/GaAs multiple quantum well structures by combination of secondary ion mass spectrometry and x-ray diffraction techniques. Journal of Vacuum Science & Technology B, 15, 2037-2045

Herrmann, A., Lehnhardt, T., Strauß, M., Kamp, M. & Forchel, A. (2011) Optimization and comparison of depth profiling in GaAs and GaSb with TOF-SIMS. Surface and Interface Analysis, 43, 673-675

Hideki, H., Toshiya, S., Seiichi, K., Hirotatsu, I. & Hideo, O. (1988) Correlation between Photoluminescence and Surface-State Density on GaAs Surfaces Subjected to Various Surface Treatments. Japanese Journal of Applied Physics, 27, L2177

Hinkle, C. L., Milojevic, M., Brennan, B., Sonnet, A. M., Aguirre-Tostado, F. S., Hughes, G. J., Vogel, E. M. & Wallace, R. M. (2009) Detection of Ga suboxides and their impact on III-V passivation and Fermi-level pinning. Applied Physics Letters, 94, 62101-62101

J. J. Dubowski, D. F. Williams, P. B. Sewell & Norman, P. (1985) Epitaxial growth of (100)CdTe on (100)GaAs induced by pulsed laser evaporation Appl. Phys. Lett. , 46, 1081-1883

Kaniewska, M. & Slomka, I. (2001) C-V profiling of GaAs using electrolyte barriers. Crystal Research and Technology, 36, 1113-1118

Kim, C.-K., Marshall, G. M., Martin, M., Bisson-Viens, M., Wasilewski, Z. & Dubowski, J. J. (2009) Formation dynamics of hexadecanethiol self-assembled monolayers on (001) GaAs observed with photoluminescence and Fourier transform infrared spectroscopies. Journal of Applied Physics, 106, 083518

Kirchner, C., George, M., Stein, B., Parak, W. J., Gaub, H. E. & Seitz, M. (2002) Corrosion Protection and Long-Term Chemical Functionalization of Gallium Arsenide in an Aqueous Environment. Advanced Functional Materials, 12, 266-276

Kronik, L. & Shapira, Y. (2001) Surface photovoltage spectroscopy of semiconductor structures: at the crossroads of physics, chemistry and electrical engineering. Surface and Interface Analysis, 31, 954-965

Lebedev, M. V., Ensling, D., Hunger, R., Mayer, T. & Jaegermann, W. (2004) Synchrotron photoemission spectroscopy study of ammonium hydroxide etching to prepare well-ordered GaAs (100) surfaces. Applied surface science, 229, 226-232

Linkov, P., Artemyev, M., Efimov, A. E. & Nabiev, I. (2013) Comparative advantages and limitations of the basic metrology methods applied to the characterization of nanomaterials. Nanoscale, 5, 8781-8798

Liu, N. & Dubowski, J. J. (2013) Chemical evolution of InP/InGaAs/InGaAsP microstructures irradiated in air and deionized water with ArF and KrF lasers. Applied Surface Science, 270, 16-24

Liu, N., Poulin, S. & Dubowski, J. J. (2013) Enhanced photoluminescence emission from bandgap shifted InGaAs/InGaAsP/InP microstructures processed with UV laser quantum well intermixing. J. Phys. D: Appl. Phys., 46, 445103

Masut, R. A., Roth, A. P., Dubowski, J. J. & Lenchyshyn, L. C. (1986) Characterisation of CdTe/GaAs heterojunctions with photovoltage measurements. Semiconductor Science and Technology, 1, 226-229

Nakashima, K. & Tateno, K. (2004) X-ray diffraction analysis of GaInNAs double-quantum-well structures. Journal of Applied Crystallography, 37, 14-23

Nazemi, E., Aithal, S., Hassen, W. M., Frost, E. H. & Dubowski, J. J. (2015) GaAs/AlGaAs heterostructure based photonic biosensor for rapid detection of Escherichia coli in phosphate buffered saline solution. Sensors and Actuators B: Chemical, 207, 556-562

Noda, T., Tanaka, M. & Sakaki, H. (1990) Correlation length of interface roughness and its enhancement in molecular beam epitaxy grown GaAs/AlAs quantum wells studied by mobility measurement. Applied Physics Letters, 57, 1651-1653

Nordheden, K. J., Hua, X. D., Lee, Y. S., Yang, L. W., Streit, D. C. & Yen, H. C. (1999) Smooth and anisotropic reactive ion etching of GaAs slot via holes for monolithic microwave integrated circuits using Cl(2)/BCl(3)/Ar plasmas. Journal of Vacuum Science & Technology B, 17, 138-144

Oliver, R. A. (2008) Advances in AFM for the electrical characterization of semiconductors. Reports on Progress in Physics, 71, 076501

Pakhomov, G. L., Vostokov, N. V., Daniltsev, V. M. & Shashkin, V. I. (2002) AFM study of dry etched cleavages of the Al(x)Ga(1-x)As/GaAs heterostructures. Physics of Low-Dimensional Structures, 5-6, 247-253

Passlack, M., Hong, M., Mannaerts, J., Kwo, J. & Tu, L. (1996) Recombination velocity at oxide–GaAs interfaces fabricated by in situ molecular beam epitaxy. Applied physics letters, 68, 3605-3607

Passlack, M., Hong, M., Schubert, E. F., Kwo, J. R., Mannaerts, J. P., Chu, S. N. G., Moriya, N. & Thiel, F. A. (1995) In situ fabricated Ga2O3–GaAs structures with low interface recombination velocity. Applied Physics Letters, 66, 625-627

Perovic, D., Castell, M., Howie, A., Lavoie, C., Tiedje, T. & Cole, J. (1995) Field-emission SEM imaging of compositional and doping layer semiconductor superlattices. Ultramicroscopy, 58, 104-113

Pettenpaul, E. (1998) GaAs a key RF technology - Industrialisation \& competition. 2, 368--373

Priyantha, W., Radhakrishnan, G., Droopad, R. & Passlack, M. (2011) In-situ XPS and RHEED study of gallium oxide on GaAs deposition by molecular beam epitaxy. Journal of Crystal Growth, 323, 103-106

Rack, M., Thornton, T., Ferry, D., Roberts, J. & Westhoff, R. (2000) Characterization of strained silicon quantum wells and Si1-xGex heterostructures using Auger electron spectroscopy and spreading resistance profiles of bevelled structures. Semiconductor science and technology, 15, 291

Ruberto, M. N., Zhang, X., Scarmozzino, R., Willner, A. E., Podlesnik, D. V. & Osgood, R. M. (1991) The Laser-Controlled Micrometer-Scale Photoelectrochemical Etching of III–V Semiconductors. Journal of the Electrochemical Society, 138, 1174-1185

Schroder, D. K. 2006. Semiconductor material and device characterization, John Wiley & Sons.

Schwartz, G., Gualtieri, G., Kammlott, G. & Schwartz, B. (1979) An X-Ray Photoelectron Spectroscopy Study of Native Oxides on GaAs. Journal of The Electrochemical Society, 126, 1737-1749

Tapfer, L. & Ploog, K. (1986) Improved assessment of structural properties of AlxGa1− xAs/GaAs heterostructures and superlattices by double-crystal x-ray diffraction. Physical review. B, Condensed matter, 33, 5565-5574

Tsang, W. T., Chiu, T. H. & Kapre, R. M. (1993) Monolayer chemical beam etching: Reverse molecular beam epitaxy. Applied Physics Letters, 63, 3500-3502

Vilar, M. R., El Beghdadi, J., Debontridder, F., Artzi, R., Naaman, R., Ferraria, A. M. & do Rego, A. M. B. (2005) Characterization of wet-etched GaAs (100) surfaces. Surface and Interface Analysis, 37, 673-682

Watanabe, M. O. a. Y. J. a. M. M. a. N. T. a. H. A. (1985) Band discontinuity for GaAs/AlGaAs heterojunction determined by C-V profiling technique. Journal of Applied Physics, 57, 5340

Wilmsen, C. W., Kirchner, P. D. & Woodall, J. M. (1988) Effects of N2, O2, and H2O on GaAs passivated by photowashing or coating with Na2S.9H2O. J. Appl. Phys., 64, 3287-3289

Wośko, M., Paszkiewicz, B., Tarnowski, K., Ściana, B., Radziewicz, D., Salejda, W., Paszkiewicz, R. & Tłaczała, M. (2011) Reverse engineering of AlxGa1− xAs/GaAs structures composition by reflectance spectroscopy. Opto-Electronics Review, 19, 418-424

6.2 Foreword: Article 2, Open circuit potential monitored digital photocorrosion of GaAs/AlGaAs quantum well microstructures

The second journal paper published in Applied Physics Letters establishes the correlation between open circuit potential (OCP) and PL, during DIP *in situ* involving interfaces of AlAs and AlGaAs. The results reported in this work suggests the possibility to expand the atomic-level metrology technique to materials without room-temperature measurable PL.

Authors:
Srivatsa Aithal: PhD candidate
Jan J. Dubowski: Professor

Affiliation:
Laboratory for Quantum Semiconductors and Photon-based BioNanotechnology, Interdisciplinary Institute for Technological Innovation (3IT), Department of Electrical and Computer Engineering, Université de Sherbrooke

Date of publishing: March 2018

Reference:
Aithal, S. and Dubowski, J.J., "Open circuit potential monitored digital photocorrosion of GaAs/AlGaAs quantum well microstructures", Appl. Phys. Lett., 2018; 112:153102

Titre: Suivi de photocorrosion digitale des microstructures à puits quantiques GaAs/AlGaAs par potentiel en circuit ouvert

Résumé:
La nano-structuration de gaufres semi-conducteurs avec une résolution de profondeur au niveau atomique est une tâche ardue, principalement en raison de la disponibilité limitée d'instruments de monitoring *in situ* de tels processus. La gravure digitale conventionnelle repose sur des procédures de calibration et des diagnostics complexe appliqués entre les cycles de gravure ou à la fin de ceux-ci. Nous avons développé un processus à base de photoluminescence (PL) pour le monitoring de la photocorrosion digitale *in situ* (DPC) de microstructures GaAs/AlGaAs à des taux inférieures à 0,2 nm par cycle. Dans cette communication, nous démontrons que le DPC des microstructures GaAs/AlGaAs peut être suivi avec le potentiel en circuit ouvert (OCP) mesuré entre la surface de photocorrosion d'une microstructure et une électrode de référence Ag/AgCl installée dans la chambre à échantillon. L'excellente corrélation entre la position des maxima PL et OCP indique que le processus DPC pourrait être suivi *in situ* pour les matériaux qui ne présentent pas nécessairement une émission de PL mesurable.

Abstract:
Nanostructuring of semiconductor wafers with an atomic level depth resolution is a challenging task, primarily due to the limited availability of instruments for *in situ* monitoring of such processes. Conventional digital etching relies on calibration procedures and cumbersome diagnostics applied between or at the end of etching cycles. We have developed a photoluminescence (PL) based process for monitoring *in situ* digital photocorrosion (DPC) of GaAs/AlGaAs microstructures at rates below 0.2 nm per cycle. In this communication, we demonstrate that DPC of GaAs/AlGaAs microstructures could be monitored with open circuit potential (OCP) measured between the photocorroding surface of a microstructure and an Ag/AgCl reference electrode installed in the sample chamber. The excellent correlation between the position of both PL and OCP maxima indicates that the DPC process could be monitored *in situ* for materials that do not necessary exhibit measurable PL emission.

Digital etching (DE) of Si was introduced almost 30 years ago as a method designed to fabricate microstructures with minimized damage of etched surfaces, typically associated with the use of reactive ion etching and conventional wet etching techniques (Hiroyuki et al., 1990). The so called atomic bilayer etching of GaAs has also been introduced (Maki & Ehrlich, 1989) and, subsequently, the concept of DE has been reported for GaAs (Ref. (Meguro et al., 1990; Meguro et al., 1993)), GaAs/AlGaAs microstructures (Fink & Osgood, 1993), GaAs p-n junctions (van de Ven & Kelly, 2001), $Ge_{1-x}Si_x$ (Ref. (Shang et al., 2016)) , SiO_2 (Ref. (Metzler et al., 2017)) and SiN (Ref. (Shinoda et al., 2017)). The DE process consists of a series of 2-phase cycles, each involving a limited or self-limited reaction step followed by a step designed to remove reaction products from processed surfaces. Typically, 0.1– 1.5 nm of material is removed in each cycle, which, due to the general lack of diagnostic allowing to monitor this process *in situ*, is calculated based on post-processing measurements (e.g., Ref. (Lin, Zhao, Antoniadis, & Alamo, 2014)). We have investigated the process of photocorrosion of GaAs/AlGaAs microstructures in aqueous solutions that is driven by photo-holes (h^+) generated on the surface of such microstructures (Nazemi, Aithal, Hassen, Frost, & Dubowski, 2015). The exposure of water-immersed GaAs to radiation exciting e-h^+ pairs results in oxidation of this material and, under proper conditions, a dilution of the products of oxidation. With a negligible dark corrosion, this approach allows a step removal of the material with a sub-monolayer precision (Aithal, Neng, & Jan, 2017). We have explored this feature for etching of multilayer GaAs/$Al_{0.35}Ga_{0.65}As$ microstructures, and we demonstrated that a photoluminescence (PL) monitored digital photocorrosion (DPC) allows resolving *in-situ* the removal of individual layers thinner than 1 nm. The advantage of DPC over conventional DE process is that it does not require changing of the processing environment that normally is required between two steps of a DE cycle. Water environment is attractive for both formation and dissolution of As-based oxides, while the removal of other products of reaction would require dedicated solutions, such as ammonium hydroxide used for removing Ga-oxides (Aithal et al., 2017). Generally, the photocorrosion process and depth resolution of DPC depend on pH of the corrosion inducing solution (Sharma, Moumanis, & Dubowski, 2016).

Due to the strong sensitivity to the presence of surface states, the PL effect has frequently been used to diagnose reaction of PL-emitting semiconductor microstructures to different environments (Gfroerer, 2000). For instance, we have observed the increased intensity of PL emission associated with the reduction of non-radiative recombination centers during DPC of n-type GaAs in water, while the opposite was observed with the corrosion front was passing through $Al_{0.35}Ga_{0.65}As$ (Nazemi et al., 2015; Sharma et al., 2016; Aithal et al., 2017). This allowed determining with a high precision the location of GaAs/$Al_{0.35}Ga_{0.65}As$ interfaces, and interrogate *in situ* about the dynamics and the propagation of the corrosion front. Since the nature of the surface states and the type of a surrounding environment affect the semiconductor surface electrical potential, we postulated that an open circuit potential (OCP) could also be employed for monitoring *in situ* the DPC process. In this report, we discuss DPC of GaAs/$Al_{0.35}Ga_{0.65}As$ quantum well (QW) nano-heterostructures monitored with OCP that is measured concurrently with the PL signal generated by the investigated samples.

The investigated GaAs/AlGaAs nano-heterostructure was grown on a double side polished semi-insulating GaAs (100) wafer using metal-organic chemical vapor deposition (Wafer10-150, Azastra Inc.). An AlAs/GaAs (2.4 nm/2.4 nm) superlattice was grown to minimize defect propagation from the GaAs substrate. This was followed by a 200 nm thick GaAs layer and 30 pairs of 10 nm $Al_{0.35}Ga_{0.65}As$ barriers and 6 nm GaAs quantum wells (QWs). The microstructure was capped with 10 nm thick GaAs. A cross-section view of the nano-heterostructure is shown in Fig. 1a. The wafer was coated with a surface protecting layer of photoresist and diced into 4 mm x 4 mm samples. The room temperature PL spectral emission from the wafer was measured using a commercial PL mapper (Philips PLM-150) equipped with a 532 nm laser excitation source and an InGaAs array detector. As it can be seen in Fig. 1b, the PL emission is dominated by the 829 nm peak originating from GaAs QWs, while a weak feature at 879 nm corresponds to emission from the GaAs substrate. Semiconductor grade OptiClear (National Diagnostics), acetone (ACP Chemicals, Canada), isopropyl alcohol and 28% ammonium hydroxide (NH_3 (aq)), Anachemia, Canada) were used without further purification. De-ionized (DI) water with a resistivity of 18.2 MΩ-cm was obtained from a MilliQ system.

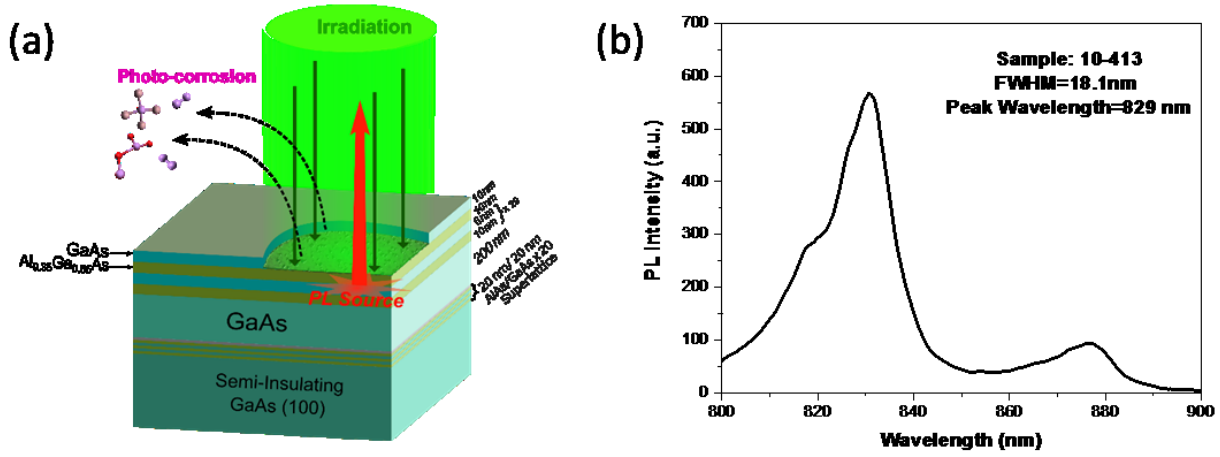

FIG. 1. Schematic cross-section view of the GaAs/$Al_{0.35}Ga_{0.65}As$ QW nano-heterostructure used for a digital photocorrosion study (a), and a room temperature PL spectrum of the nano-heterostructure excited with a 532 nm laser (b).

The bottom electric contact to the sample was obtained by depositing a thin layer of gold from a gold chloride ($HAuCl_4$) solution using the galvanic displacement process (Pham, Park, Lee, & Oh, 2014). For this, the sample was first sonicated in OptiClear, acetone and IPA, each for five minutes. Next, the sample was deoxidized with an aqueous solution of ammonium hydroxide (28%) for two minutes, rinsed with DI water and blown dry with nitrogen and sonicated in OptiClear, acetone and IPA, each for five minutes. A continuous layer of Au was obtained after 5 min exposure of the sample in 1µL of 2 mM $HAuCl_4$.

The PL measurements from photocorroding GaAs/AlGaAs microstructures were performed *in situ* using a custom built Quantum Semiconductor Photonic Biosensor (QSPB) Reader (Aziziyan, Hassen, Morris, Frost, & Dubowski, 2016; Aithal et al., 2017). The above bandgap irradiation was provided by a 625 nm light-emitting diode (LED) source, and the PL emission from the sample was measured, after passing through an 812 nm cut-off long pass filter (Thorlabs FELH800), with a CMOS detector (CMLN-13S2M, Point Grey). The OCP measurements were performed using the CHI604C potentiostat (CH Instruments Inc., Austin, USA). A 1 mm diameter chlorided silver wire (Ag/AgCl) was used as a reference electrode. The sample was connected to the working electrode terminal through the galvanic Au contact on the backside. The potentiostat was used in a voltage open circuit configuration whose input impedance was greater than 10^{12} Ω. A schematic view of the setup employed for the simultaneous measurements of PL and OCP from DPC GaAs/$Al_{0.35}Ga_{0.65}As$ QW nano-heterostructure is shown Fig. 2. The flow cell has an entry and an exit port to continuously pass DI water or phosphate buffer saline (PBS) solution, although in these experiments a stagnant etching environment was applied. Samples were fixed on the bottom of the flow cell with solvent resistant acrylic adhesive tape (300LSE, 3M^{TM} Adhesive Transfer Tape). The DPC cycle consisted of a 3 s irradiation in each 60 s period. The samples were irradiated with a spatially homogenized LED source delivering power of 25 mW/cm^2 at their surface.

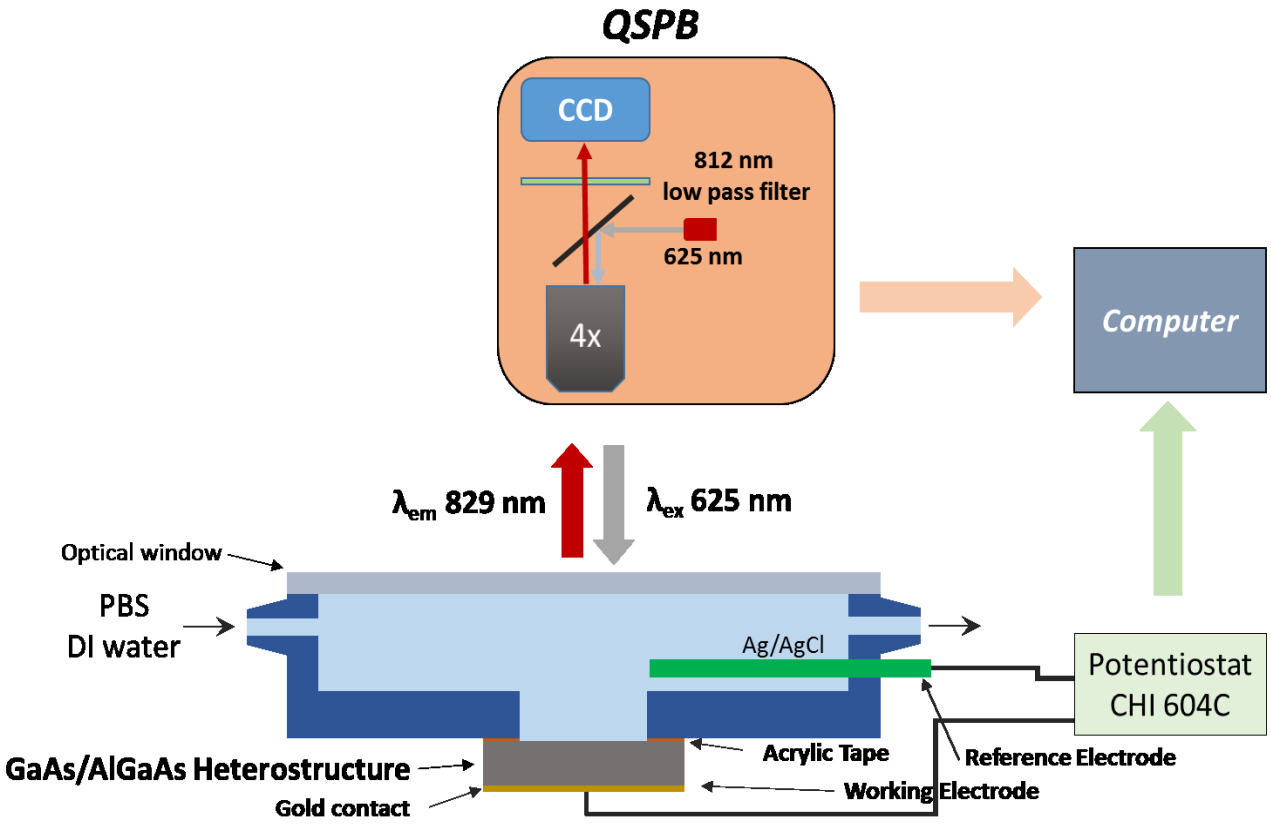

FIG. 2. Schematic view of the setup for simultaneous PL and OCP measurements during digital photocorrosion of GaAs/$Al_{0.35}Ga_{0.65}As$ QW nano-heterostructures.

An example of the PL signal measured during DPC of a GaAs/$Al_{0.35}Ga_{0.65}As$ QW nano-heterostructure is shown in Fig. 3. The sample was irradiated with a 625 nm LED delivering power of 25 mW/cm^2. The intermittent photo-excitation of the sample (3 s irradiation in each 60 s period) resulted in its oxidation and decomposition that allowed observing the formation of three PL maxima denoted as 'interface 1', 'interface 2' and 'interface 3'. Each of these maxima corresponds to the onset of formation of an AlGaAs-DI water interface as reported previously.[13] Reduced dynamics of the PL signal could also be seen following the revealing of the 'interface 3'. This observation suggests that slowing down of the DPC process is related to the surface accumulation of the corrosion resisting oxides that are weakly soluble in DI water.[13,14] Nevertheless, it can be seen that a 52 nm thick material (10 nm GaAs, 10 nm $Al_{0.35}Ga_{0.65}As$ and 2 GaAs QWs, 6 nm each, separated by 10 nm $Al_{0.35}Ga_{0.65}As$ barriers) has been removed with 300 cycles, corresponding to an average of 0.17 nm of material removed per single DPC cycle.

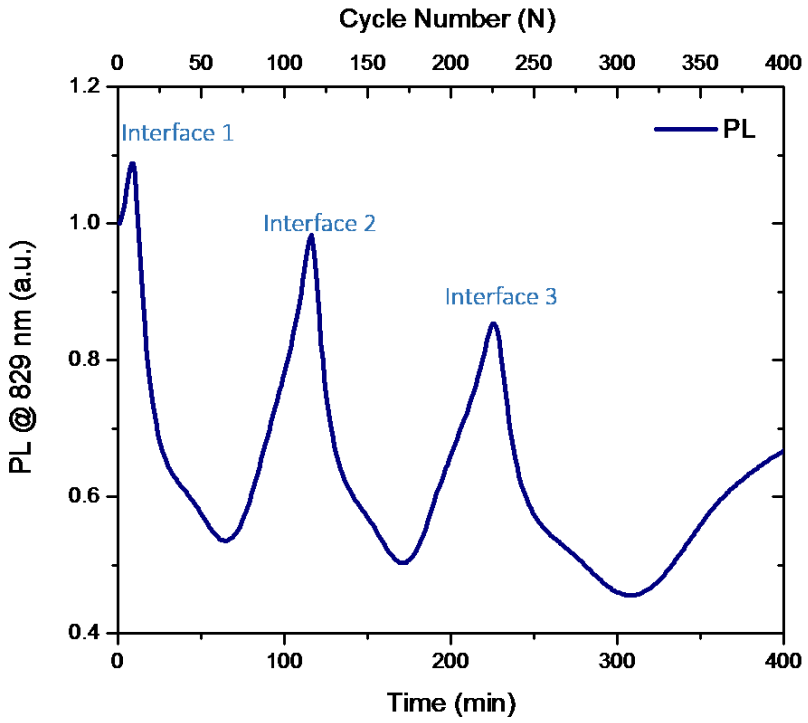

FIG. 3. Temporal evolution of the integrated PL signal of the GaAs/$Al_{0.35}Ga_{0.65}As$ QW nano-heterostructure digitally photocorroding in DI water (λ_{ex} = 625 nm, P_{ex} = 25 mW/cm^2).

In Fig. 4a, we compare the evolution of both OCP and PL signals measured simultaneously during DPC of a GaAs/$Al_{0.35}Ga_{0.65}As$ nano-heterostructure irradiated intermittently, 2 s in each 10 s period, with 25 mW/cm^2 power. To assure the proper functioning of an Ag/AgCl reference electrode, this experiment was carried out in a PBS solution that provided the necessary chloride ions. Under these conditions, the presence of 4 GaAs/$Al_{0.35}Ga_{0.65}As$ interfaces has been revealed with 4 PL maxima within 300 min (1800 cycles). This corresponds to a total of 68 nm thick material removed with an average rate of 0.04 nm per a single DPC cycle. As it can be seen, the OCP maxima are aligned very well with the PL maxima. Thus, it is clear that both PL and OCP oscillations (Δ_{OCP}) allow monitoring *in situ* DPC of the investigated nano-heterostructure. Fig. 4b illustrates OCP variations (δ_{OCP}) for the sample illuminated and remaining in darkness between the 348th - 351st photocorrosion cycles that generate δ_{OCP} ~ 30 mV. This value is determined by the dynamic of photoexcited carriers and no significant difference is expected for δ_{OCP} characterizing GaAs-PBS and $Al_{0.35}Ga_{0.65}As$-PBS interfaces. However, we observed that δ_{OCP} was reduced from ~ 30 to 25 mV over 2400 cycles. Reduced dynamics of the PL amplitude was also observed as shown in Fig. 4a. We associate this behavior with the growing surface accumulation of the photocorrosion products insoluble in PBS that leads to the increased surface roughness of the photocorroding material (Aithal et al., 2017). This could also be responsible for a reduced coupling efficiency of the PL exciting illumination.

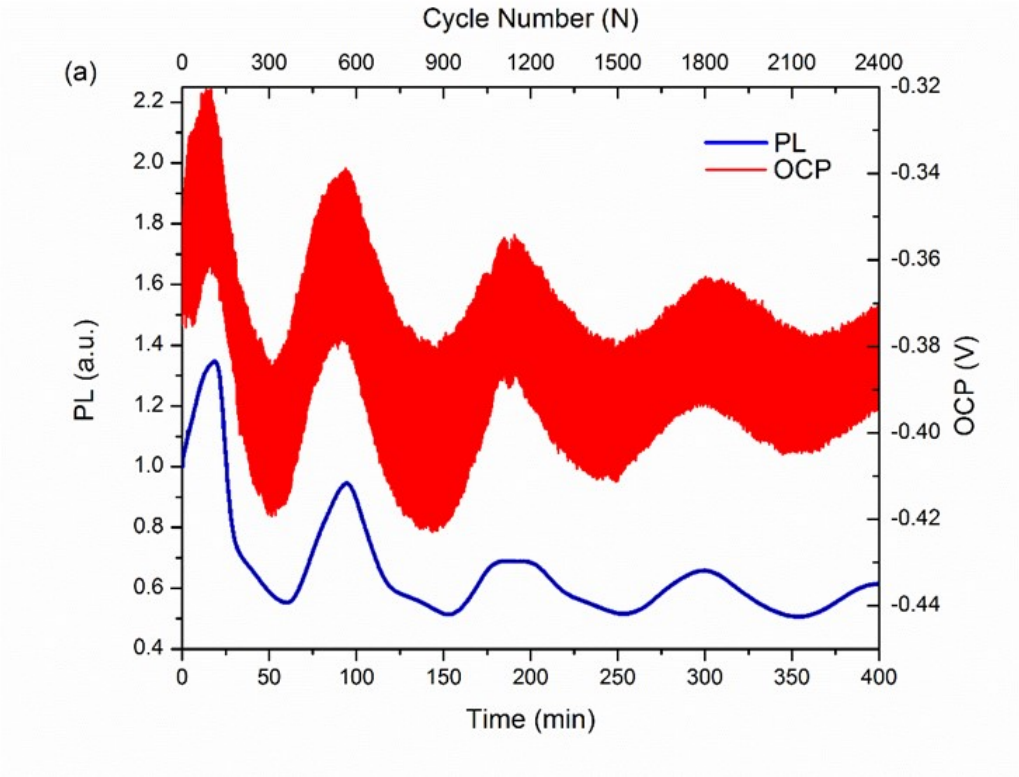

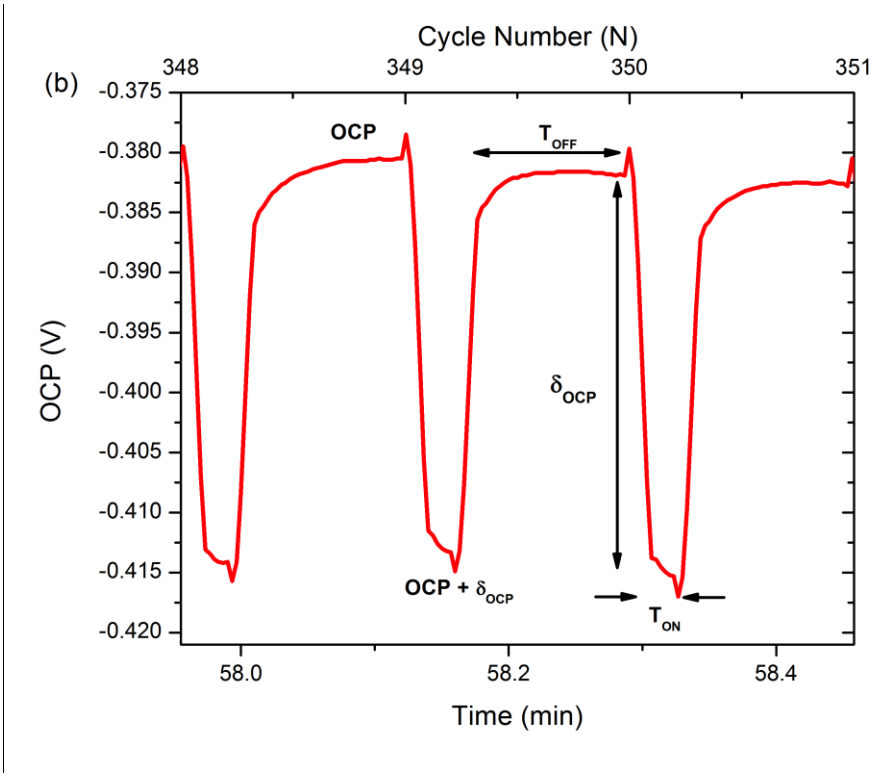

FIG. 4. OCP and PL of GaAs/$Al_{0.35}Ga_{0.65}As$ QW nano-heterostructure during a 400-min digital photocorrosion in PBS (a). A fragment of OCP measurements collected between 348 and 351 cycles (b).

We were not able to observe OCP oscillations (Δ_{OCP}) in an aqueous solution of ammonia (NH_3:H_2O) that normally is used for removing As- and Ga-oxides (Clawson, 2001). Under these conditions, we measured $\delta_{OCP} \approx 200$ mV. Thus, we hypothesize that the failure to observe δ_{OCP} oscillations is likely related to a constantly refreshed oxide-free surface.

A qualitative model of photocorroding n-type GaAs/AlGaAs nano-heterostructure is presented in Fig. 5. The photoexcitation process of an n-type semiconductor generates the excess carriers up to the optical penetration depth (L_D). The minority carriers (holes) in the space charge region (L_{SCR}) and within their diffusion depth (L_{diff}) drift towards the surface due to the electric field in the SCR. These minority carriers induce surficial reactions, perturb the equilibrium both in the SCR and at the semiconductor electrolyte-interface, and modify the surface charge through carrier trapping (Kronik & Shapira, 1999). The net result of the photoexcitation is the reduction of the L_{SCR} and split of the Fermi level into two quasi-Fermi levels (E_{fn} and E_{fp}), which is measured as the perturbation δ_{OCP}. In darkness, there are no photo-carriers and the OCP is at its equilibrium potential.

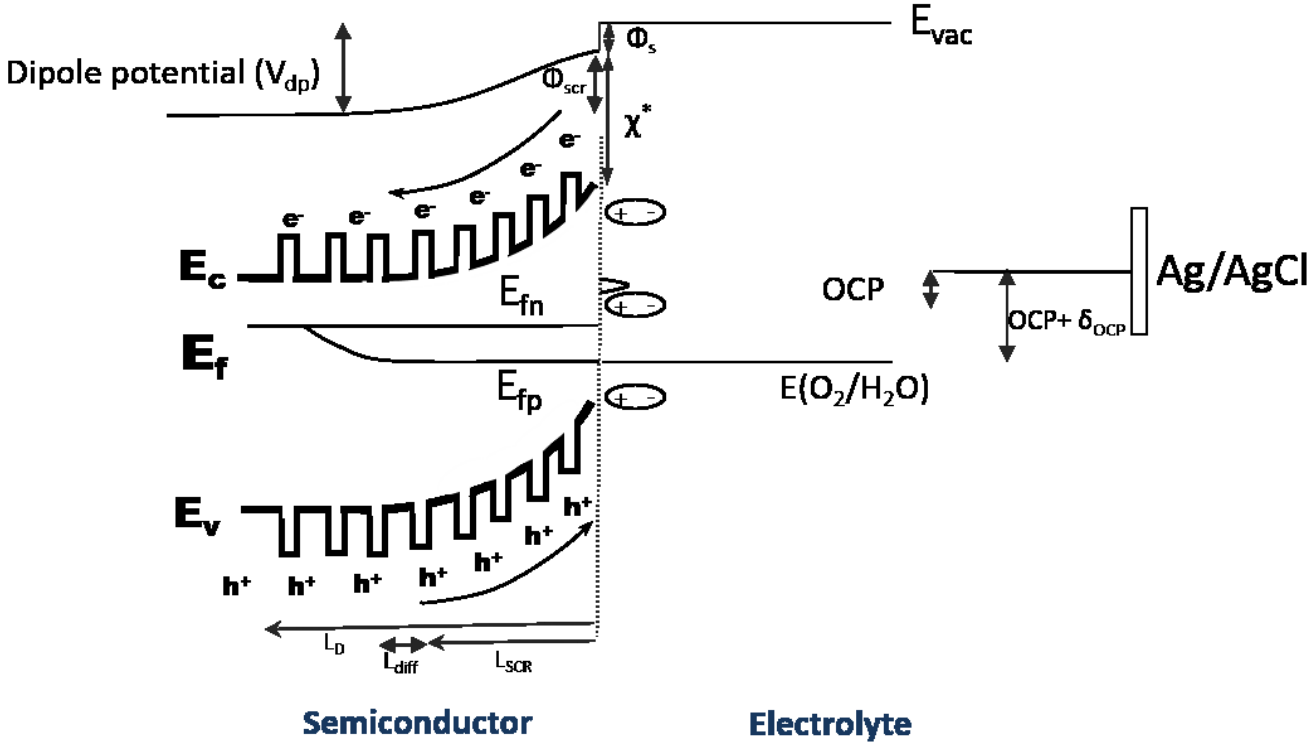

FIG. 5. Energy band diagram of the GaAs/AlGaAs QW nano-heterostructure exposed to an aqueous electrolyte solution.

The energy band alignment at the semiconductor-electrochemical interface is determined by the electron affinity of the semiconductor, χ^*, chemical potential of the electrolyte, $E(O_2/H_2O)$, and interfacial dipole potential, $V_{dp,}$ affected by SCR dipole (Φ_{SCR}), surface states, adsorbed ions and

oxides. This interfacial dipole potential is widely used to tune the band edge alignment of semiconductor devices (Ref. (Ratcliff et al., 2013),(Hikita et al., 2016),(Shyam, Kyung-Young, Azwar, Yuhei, & Shuzi, 2011) (Chakrapani et al., 2007)). The residual photocorrosion products cyclically shift this band edge alignment during photocorrosion. The composition of the photocorrosion product (oxides) varies depending on whether GaAs or AlGaAs is being oxidized. Some common photocorrosion products, such as Ga_2O_3, Al_2O_3 and $GaAl_2O_4$ have their isoelectric points, respectively, around pH=9 (Ref. (Kosmulski, 2001)), between pH=8-~9 in 0.1M NaCl (Ref. (Kosmulski, 2014)), and at pH=4.2. At pH=7.4 of the PBS electrolyte, Ga_2O_3 and Al_2O_3 carry a positive charge, while $GaAl_2O_4$ carries a negative charge. This is consistent with the oscillation of the net interfacial dipole formed by the photo-oxides during photocorrosion, in phase with the composition of the nano-heterostructure. It should be emphasized that to assure the proper functioning of an Ag/AgCl reference electrode, the photocorrosion had to be carried out in a solution that provided the necessary chloride ions. Furthermore, the monitoring of DPC with OCP required retaining some amount of photo-oxides on the surface of photocorroding GaAs/$Al_{0.35}Ga_{0.65}As$ samples, although the excessive accumulation of surface oxides would inhibit digital photocorrosion. For instance, we have observed that the photocorrosion of such nano-heterostructures at a moderate pH 10.2 resulted in a series of well-defined PL maxima each time the photocorrosion front passed from the GaAs to $Al_{0.35}Ga_{0.65}As$ surface, while at 11< pH < 7 the measurements suggested that either the excessive accumulation of oxides (inhibited photocorrosion) or a rapidly progressing photocorrosion take place (Sharma et al., 2016). Thus, we argue that with the proper selection of a photocorrosion environment and its pH, the OCP measurements could be successfully employed to monitor DPC of semiconductor nano-heterostructure photocorroding in excess of hundreds of nm.

In conclusion, we have investigated digital photocorrosion of GaAs/$Al_{0.35}Ga_{0.65}As$ QW nano-heterostructures in DI H_2O, NH_4OH and PBS solutions. The method allows sub-monolayer removal of material per cycle. An excellent correlation between PL and OCP maxima, indicating location of GaAs-$Al_{0.35}Ga_{0.65}As$ interfaces, has been observed *in situ* for samples photocorroding in water environment. The OCP technique of monitoring digital corrosion is particularly attractive for materials with measurable PL emission. A relatively oxide-free surface of GaAs/$Al_{0.35}Ga_{0.65}As$ produced in an NH_4OH environment did not show OCP maxima (oscillations), while they were easily detected with PL measurements. Thus, the presence of surface oxide plays an important role in the ability to monitor digital photocorrosion with OCP. An excessive oxide accumulation at the photocorroding surface leads to both PL and OCP reduced amplitudes. A careful choice of both the chemical composition and pH of the photocorrosion solution should allow using the OCP measurements for monitoring *in situ* the removal of material with sub-monolayer precision in excess of 80 nm reported in this communication.

Acknowledgements

This research was supported by the Canada Research Chair in Quantum Semiconductors Program (Grant No 950-220304) and the NSERC Discovery Grant RGPIN-2015-04448. The fabrication of GaAs/AlGaAs wafers was subsidized by the CMC Microsystems (Kingston, Canada). The authors

are indebted to Dr. Khalid Moumanis for collecting wavelength dependent PL spectra of the GaAs/AlGaAs wafers. The help provided by Dr. Walid M. Hassen and technical staff of the Université de Sherbrooke Interdisciplinary Institute for Technological Innovation (3IT) is also greatly appreciated.

References

Aithal, S., Neng, L., & Jan, J. D. (2017). Photocorrosion metrology of photoluminescence emitting GaAs/AlGaAs heterostructures. Journal of Physics D: Applied Physics, 50(3), 035106. Retrieved from http://stacks.iop.org/0022-3727/50/i=3/a=035106

Aziziyan, M. R., Hassen, W. M., Morris, D., Frost, E. H., & Dubowski, J. J. (2016). Photonic biosensor based on photocorrosion of GaAs/AlGaAs quantum heterostructures for detection of Legionella pneumophila. Biointerphases, 11(1), 019301. doi:doi:http://dx.doi.org/10.1116/1.4941983

Chakrapani, V., Angus, J. C., Anderson, A. B., Wolter, S. D., Stoner, B. R., & Sumanasekera, G. U. (2007). Charge Transfer Equilibria Between Diamond and an Aqueous Oxygen Electrochemical Redox Couple. Science, 318(5855), 1424-1430. doi:10.1126/science.1148841

Clawson, A. (2001). Guide to references on III–V semiconductor chemical etching. Materials Science and Engineering: R: Reports, 31(1), 1-438.

DeSalvo, G. C., Bozada, C. A., Ebel, J. L., Look, D. C., Barrette, J. P., Cerny, C. L. A., . . . Via, G. D. (1996). Wet Chemical Digital Etching of GaAs at Room Temperature. Journal of The Electrochemical Society, 143(11), 3652-3656. doi:10.1149/1.1837266

Fink, T., & Osgood, R. M. (1993). Photoelectrochemical Etching of GaAs / AlGaAS Multilayer Structures. Journal of the Electrochemical Society, 140(9), 2572-2581. doi:10.1149/1.2220865

Gfroerer, T. H. (2000). Photoluminescence in Analysis of Surfaces and Interfaces, Encyclopedia of analytical chemistry : applications, theory and instrumentation, Ed. R.A. Meyers. Chichester: John Wiley.

Hikita, Y., Nishio, K., Seitz, L. C., Chakthranont, P., Tachikawa, T., Jaramillo, T. F., & Hwang, H. Y. (2016). Band Edge Engineering of Oxide Photoanodes for Photoelectrochemical Water Splitting: Integration of Subsurface Dipoles with Atomic-Scale Control. Advanced Energy Materials, 6(7).

Hiroyuki, S., Seiji, I., Kazushi, A., Jirou, Y., Masataka, H., & Yasuhiro, H. (1990). Atomic Layer Controlled Digital Etching of Silicon. Japanese Journal of Applied Physics, 29(11R), 2648. Retrieved from http://stacks.iop.org/1347-4065/29/i=11R/a=2648

Kosmulski, M. (2001). Pristine Points of Zero Charge of Gallium and Indium Oxides. Journal of colloid and interface science, 238(1), 225-227. doi:http://dx.doi.org/10.1006/jcis.2001.7484

Kosmulski, M. (2014). The pH dependent surface charging and points of zero charge. VI. Update. Journal of colloid and interface science, 426, 209-212. doi:http://dx.doi.org/10.1016/j.jcis.2014.02.036

Kronik, L., & Shapira, Y. (1999). Surface photovoltage phenomena: theory, experiment, and applications. Surface science reports, 37(1), 1-206.

Lin, J., Zhao, X., Antoniadis, D. A., & Alamo, J. A. d. (2014). A Novel Digital Etch Technique for Deeply Scaled III-V MOSFETs. Ieee Electron Device Letters, 35(4), 440-442. doi:10.1109/LED.2014.2305668

Maki, P. A., & Ehrlich, D. J. (1989). Laser bilayer etching of GaAs surfaces. Applied Physics Letters, 55(2), 91-93. doi:10.1063/1.102097

Meguro, T., Hamagaki, M., Modaressi, S., Hara, T., Aoyagi, Y., Ishii, M., & Yamamoto, Y. (1990). Digital etching of GaAs: New approach of dry etching to atomic ordered processing. Applied Physics Letters, 56(16), 1552-1554. doi:10.1063/1.103171

Meguro, T., Ishii, M., Kodama, K., Yamamoto, Y., Gamo, K., & Aoyagi, Y. (1993). Surface processes in digital etching of GaAs. Thin Solid Films, 225(1–2), 136-139. doi:http://dx.doi.org/10.1016/0040-6090(93)90142-C

Metzler, D., Li, C., Engelmann, S., Bruce, R. L., Joseph, E. A., & Oehrlein, G. S. (2017). Characterizing fluorocarbon assisted atomic layer etching of Si using cyclic Ar/C4F8 and Ar/CHF3 plasma. The Journal of Chemical Physics, 146(5), 052801. doi:10.1063/1.4961458

Nazemi, E., Aithal, S., Hassen, W. M., Frost, E. H., & Dubowski, J. J. (2015). GaAs/AlGaAs heterostructure based photonic biosensor for rapid detection of Escherichia coli in phosphate buffered saline solution. Sensors and Actuators B-Chemical, 207, 556-562. Retrieved from <Go to ISI>://CCC:000345895200071

Pham, N. D., Park, S. J., Lee, J. P., & Oh, I. (2014). Galvanic displacement of gallium arsenide surface: a simple and low-cost method to deposit metal nanoparticles and films. Journal of Chemistry, 2014.

Ratcliff, E. L., Garcia, A., Paniagua, S. A., Cowan, S. R., Giordano, A. J., Ginley, D. S., . . . Olson, D. C. (2013). Investigating the influence of interfacial contact properties on open circuit voltages in organic photovoltaic performance: work function versus selectivity. Advanced Energy Materials, 3(5), 647-656.

Shang, C. K., Wang, V., Chen, R., Gupta, S., Huang, Y.-C., Pao, J. J., . . . Harris, J. S. (2016). Dry-wet digital etching of Ge1−xSnx. Applied Physics Letters, 108(6), 063110. doi:10.1063/1.4941800

Sharma, H., Moumanis, K., & Dubowski, J. J. (2016). pH-Dependent Photocorrosion of GaAs/AlGaAs Quantum Well Microstructures. The Journal of Physical Chemistry C, 120(45), 26129-26137. doi:10.1021/acs.jpcc.6b08844

Shinoda, K., Miyoshi, N., Kobayashi, H., Miura, M., Kurihara, M., Maeda, K., . . . Hori, M. (2017). Selective atomic-level etching using two heating procedures, infrared irradiation and ion bombardment, for next-generation semiconductor device manufacturing. Journal of Physics D: Applied Physics, 50(19), 194001. Retrieved from http://stacks.iop.org/0022-3727/50/i=19/a=194001

Shyam, S. P., Kyung-Young, L., Azwar, H., Yuhei, O., & Shuzi, H. (2011). Investigating the Role of Dye Dipole on Open Circuit Voltage in Solid-State Dye-Sensitized Solar Cells. Japanese Journal of Applied Physics, 50(6S), 06GF08. Retrieved from http://stacks.iop.org/1347-4065/50/i=6S/a=06GF08

Van de Ven, J., & Kelly, J. J. (2001). Galvanic Effects in the Etching of Semiconductor p/n Structures. Journal of the Electrochemical Society, 148(1), G10-G15. doi:10.1149/1.1344556

6.3 Digital photocorrosion based biosensing

In the following section, we explore the application of digital photocorrosion for detection of *Legionella pneumophila*. Results and discussion pertaining to the stability of SAM during photocorrosion, bacterial binding density on the functionalized semiconductor surface and the PL response have been presented.

6.3.1 Stability of SAM during photocorrosion

The ability of antibody to remain anchored to the GaAs surface during photocorrosion crucially depends on the stability of thiols on the GaAs surface during photocorrosion. AFM and XPS studies discussed in section 6.1 have demonstrated the conversion of GaAs into its oxide and a partial dissolution of such oxides during photocorrosion. To study the variation of thiol coverage during various stages of photooxidation, infrared absorption spectra are measured before and after DIP, and after etching with NH_4OH. The general procedure for SAM formation on GaAs samples has been discussed in section 5.4.2. The temporal PL response of the MHDA coated 10-413 is shown in figure 15. The 1st maximum occurs around 40 minutes and represents the oxidation of the top layer of GaAs, the next three maxima occur at 75 minutes, 160 minutes and 220 minutes, respectively.

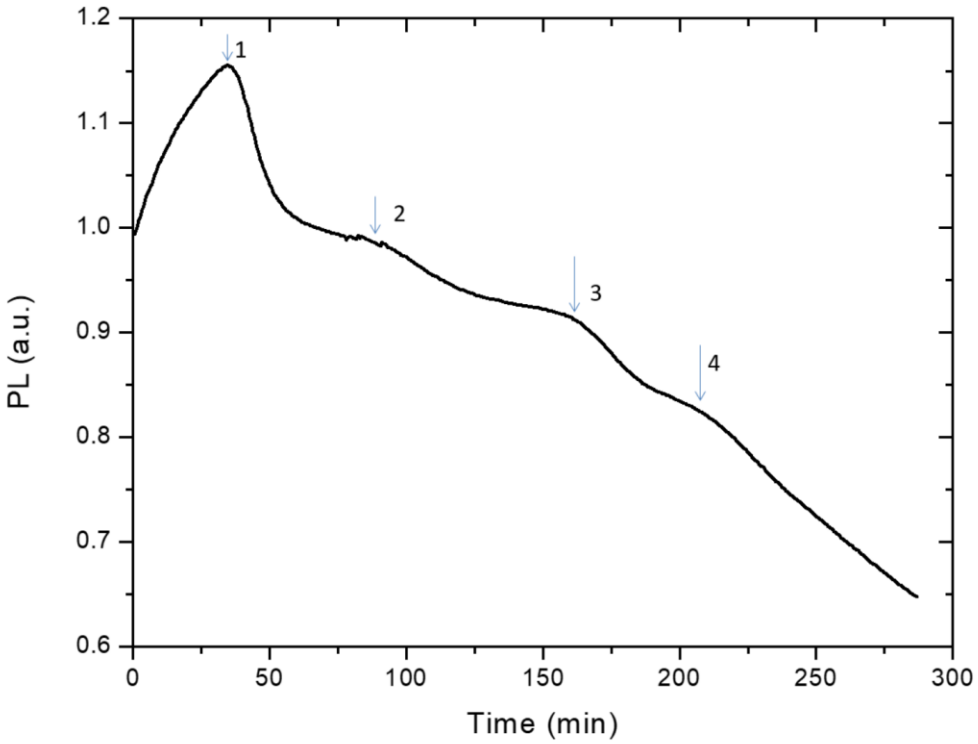

Fig. 15 Temporal PL reponse of MHDA SAM coated 10-413 sample digitally photocorroding in DI water. The arrows indicate approximate positions of the GaAs/AlGaAs interfaces.

It is hypothesized that accumulation of oxide owing to pH of DI water (~6.3), results in reduced difference in peaks occurring through 2nd to 4th maxima. This is consistent with the pH dependent oxide accumulation as reported by Sharma et. al. (Sharma, Moumanis, & Dubowski, 2016).

Figure 16 illustrates FTIR spectrum corresponding to a freshly MHDA SAM functionalized sample (wafer No 10-413). The FTIR spectrum for the sample photocorroded (P = 20 mW/cm^2, DC = 3 s/25 s, for 672 cycles at 280 min) in DI water (48 nm of material removed) is also shown in this figure. As reported previously, IR spectral peaks corresponding to the asymmetric stretching peaks (ν_{as}) of CH_2 ~2920 cm^{-1} (Ref. (Huang & Dubowski, 2014)) have been used as an index of the quality of alkanethiol SAMs. It can be seen that the freshly thiolated and photocorroded samples (Fig. 16a and b) have ν_{as} peak intensities of 7 x 10^{-4} (a.u.) and 7 x 10^{-4} (a.u.), and the peak positions (ν_{as}) are 2922.6 cm^{-1} and 2921.9 cm^{-1}, respectively. These results indicate that there is no measurable reduction in the intensity of the asymmetric peaks, even after the photocorrosion front moved 48 nm deep into the nano-heterostructure. The mechanism of SAM to remain intact on the surface of a digitally photocorroding nano-heterostructure is unclear. It seems possible that SAM either remained attached to the original GaAs surface, or it followed the recessing surfaces of GaAs and AlGaAs.

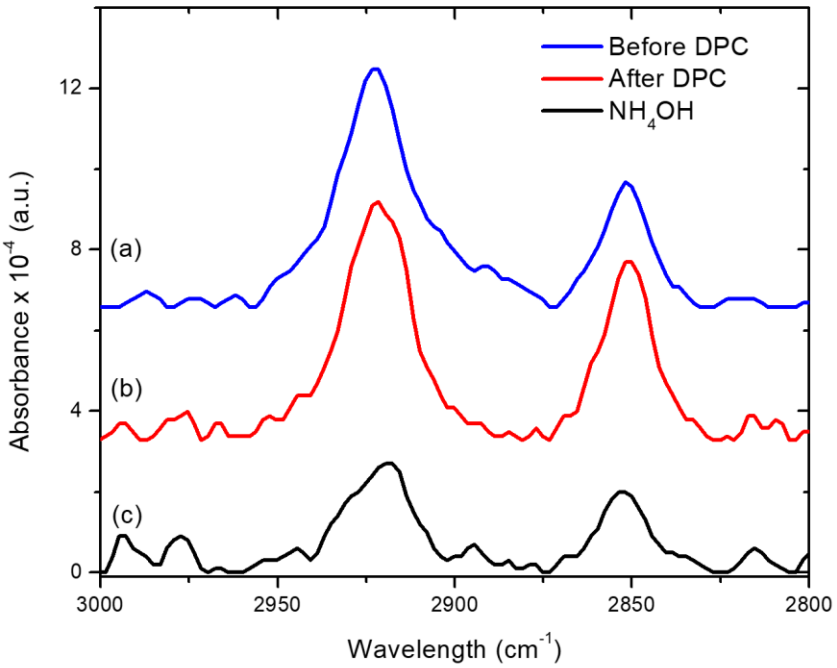

Fig. 16 Transmission FTIR spectra of 10-413 MHDA SAMs formed in ethanol before DPC(a), post DPC in DI water (b) and after deoxidation with NH_4OH (c).

DIP results in the formation of Ga-, Al- and As-oxides only on one side of the sample exposed photons. Etching by immersing for 10 minutes in an oxide etching NH_4OH solution, results in the

reduction of v_{as} peak intensity to about half of freshly thiolated sample. The nano-heterostructure samples, which are grown on top of double side polished GaAs, have SAM formed on both top and bottom surfaces. Hence, reduction in peak intensity to half of a freshly thiolated sample could indicates complete removal of thiol from top surface of the sample. Although this stability has been demonstrated here for MHDA, it is reasonable to expect a similar effect for PEG-B/HDT thiols used in this work.

6.3.2 Reproducibility of the thiolation process

Reproducibility of the thiolation process was investigated by functionalizing four samples of 10-413 as described in the previous section. IR absorption spectra were measured using a Hyperion 2000 FTIR-microscope with 4 cm^{-1} resolution and 256 scans. Figure 17 shows the absorbance spectra for each of the four samples (S1, S2, S3 and S4).

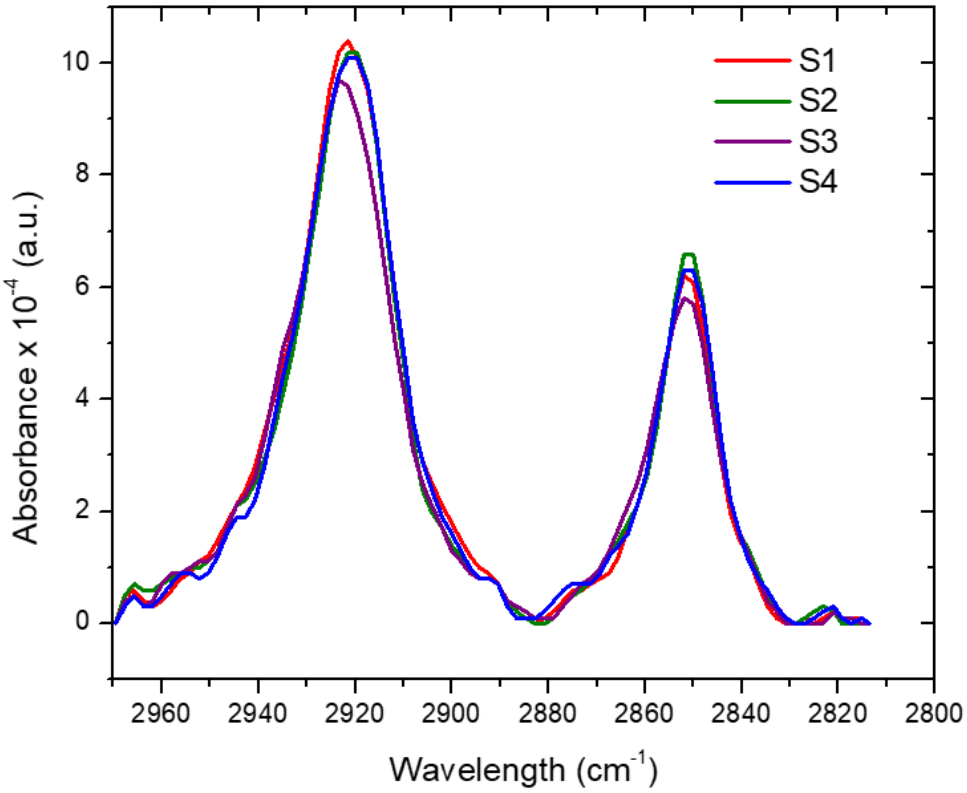

Fig. 17 Transmission FTIR spectra of 10-413 MHDA SAMs formed in ethanol for four samples; sample 1 (S1), sample 2 (S2), sample 3 (S3) and sample 4 (S4).

Intensity of v_{as} varies between $9.5x10^{-4}$ to $10x10^{-4}$. The peak position is rather reproducible except for sample 3, which is slightly shifted towards lower energy. Overall, from the measured spectra, the amount of thiols on a functionalized surface is fairly reproducible.

6.3.3 Surface coverage of bacterial binding: Fluorescent microscopy study

As discussed in 5.2.3, DIP is sensitive to bacteria that are in the immediate vicinity and immobilized on the antibody functionalized surface of the sensor. A 1 mL solution containing the target bacteria is applied onto the sensor and these bacteria are immobilized on the antibody coated surface of the biosensor. Although optical imaging of these surficial bacterial is possible, to increase specificity, antibodies with fluorescent labels are used to specifically tag the target bacteria. This scheme has been schematically illustrated in figure 18.

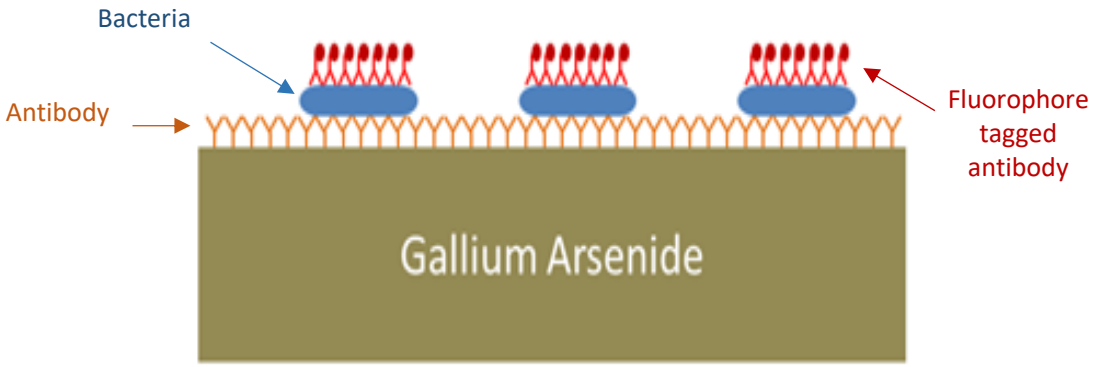

Fig. 18 Illustration of the scheme to fluorescently tag immobilized bacteria.

As discussed in 5.4.1, bulk GaAs samples were cleaned successively with Opticlear, acetone and IPA. Such samples were etched with NH_4OH and thiolate overnight in PEG-B/HDT (1:15 molar ration) in ethanol. After ethanol rinse and drying with nitrogen. Neutravidin and *Legionella* antibody were coated onto the sample. The samples were placed in a flow cell and 1mL of lab cultured *Legionella pneumophila* were exposed to the sample for 30 minutes. Fluorescence iso-thiocyanide (FITC) tagged *Legionella pneumophila* Ab at 50 µg/ml was used to react with the sample surface for 30 minutes. Unconjugated FITC were washed with 1xPBS, DI water and decontaminated with iso-propanol sequentially. Images of the sample were taken with an inverted Zeiss microscope with a 10x objective in the fluorescent mode and such images were processed using ImageJ software to identify objects with a nominal dimension of 1 µm x 0.5 µm, the nominal dimensions of *E. coli* bacteria. The results are shown in table 4 for two concentrations of lab cultured *Legionella pneumophila,* grown in buffered charcoal yeast extract (BCYE) agar and resuspended in 1xPBS. The bacteria concentration was quantified with optical density measurements. The control sample was not exposed to *Legionella pneumophila* but exposed to the fluorescent antibody staining step.

Table 4 Solution concentration of *L. pneumophila* and surficial density of immobilization studied by fluorescent antibody staining.

Solution concentration of bacteria (CFU/ml)	Number of bacteria in each image			Average	%Standard deviation	Coverage 1/mm^2
3.3x10^3	**13**	**8**	**12**	**11.0**	**2,2**	**8.8**
3.3x10^4	**17**	**17**	**49**	**27.7**	**15.1**	**22.1**
Control	**7**	**11**	**31**	**16.3**	**10.5**	

The maximum number of bacteria that could bind to the GaAs surface is 1 mL x solution concentration of bacteria. Ratio of maximum number of bacteria to the total bacteria immobilized on the GaAs surface represents the bacterial capture efficiency (BCE). The number fluorescent spots measured in control sample is subtracted before calculating the BCE ratio. With fluorescence, the number of bacteria immobilized on GaAs for a solution concentration of 3.3 x 10^3 mL^{-1} is indistinguishable from control. For a solution concentration of 3.3 x 10^4 mL^{-1}, 46 bacteria are immobilized on the surface. Which represents a BCE of 0.14%. It is hypothesized that a relatively low capture efficiency could be a result of the bacteria flowing through the flow cell without sufficient interaction with the sample surface. Schemes such as improving flow cell design and chemotaxis have been investigated to increase bacterial surficial binding, as demonstrated by Hassen et. al. from the QS group, but this has not been the focus of this work (W. M. Hassen et al., 2016).

6.3.4 Photocorrosion based sensing of live *Legionella pneumophila*

Fresh culture of *L. pneumophila* grown in a BCYE medium, was resuspended into 0.1xPBS. A 10-fold dilution of PBS has been employed to reduce the Debye screening length of the bacterial charge.(Aziziyan et al., 2016) The JD2C samples were functionalized with PEGB/HDT SAMs, neutravidin and *Legionella* antibody as discussed in section 6.3.2. Various concentrations of live *Legionella pneumophila* suspension are brought in contact with such functionalized sample located in a flow cell. Simultaneously, the PL is measured in the QSPB2 system with 8 mW/cm^2 incident light and DC of 3 s/8 s. Fig. 19 shows temporal PL curves for two runs of detection experiments performed. Each temporal PL plot is characterized by a clear maximum within 60 minutes from the beginning of the measurement. A summary of these experiments is given in Table 5.

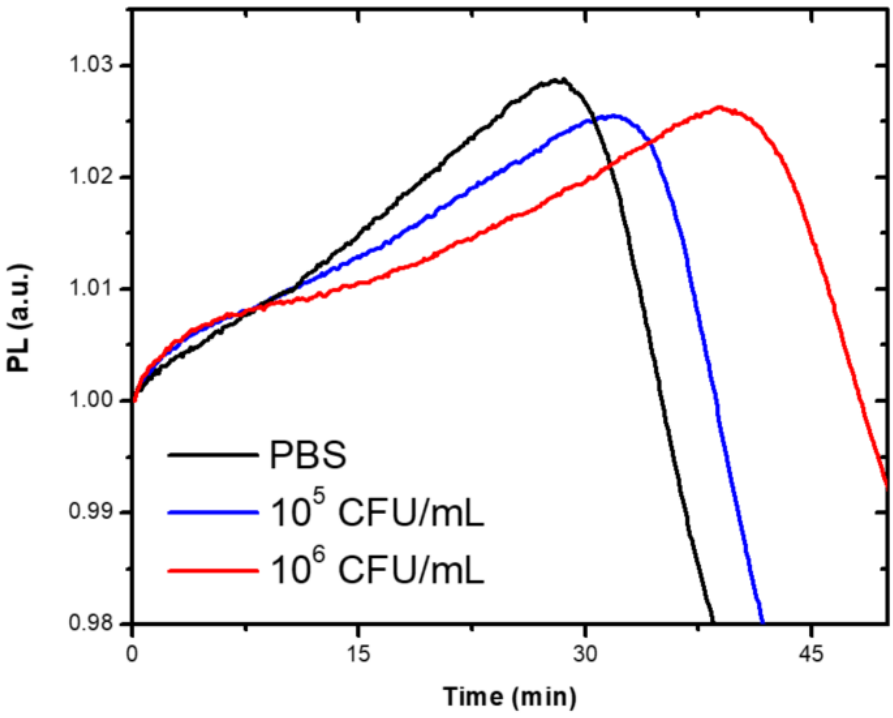

Fig. 19 Representative temporal PL curves for biochip functionalized with *Legionella* antibody exposed to freshly prepared live *Legionella pneumophila at* 10^6 and 10^5 CFU/mL, and to PBS solution.

Table 5 PL maxima positions for live *Legionella pneumophila* detection runs (n represents replicates).

Concentration (CFU/mL)	Average Maximum (min)
10^6	41.4 (n=2)
10^5	32.3 (n=2)
PBS	29.2 (n=7)

There are clear differences in the PL maxima positions corresponding to PBS and to bacterial solutions in PBS at 10^5 and 10^6 CFU/mL. The detection of *Legionella pneumophila* at 10^5 CFU/mL is rather modest in comparison to that of 10^4 CFU/mL already published by the QS Group (Aziziyan et al., 2016). This may be related to the relatively weak efficiency of capturing bacteria with the applied biosensing architecture as discussed in the previous section. It should be underlined however that the goal of this experiment was to demonstrate for the first time a direct detection of live *Legionella pneumophila* in PBS rather than optimize the process. Other approaches addressing enhanced detection involving heat killed *Legionella*, decorating *Legionella* with negatively charged molecules and application of the chemotaxis effect to increase the efficiency

of surface immobilized bacteria are the subject of an on-going research. The electrostatic nature of a DIP biosensor appears also potentially attractive for enhanced detection of bacteria lysed with an electric field or surfactants, such as Tween or SDS.

7 CONCLUSION

La recherche entreprise dans le cadre de ce projet s'est concentrée sur l'exploration de la réponse des biosenseurs à base de semi-conducteur III-V fonctionnalisés par des anticorps, pour la détection de bactéries, en se basant sur la photoluminescence. En s'appuyant sur les expériences reliées à ce sujet, il est devenu évident que la photocorrosion de GaAs/AlGaAs des biopuces a joué un rôle important dans le processus de détection. Ainsi, le besoin urgent est apparu d'étudier les mécanismes de photocorrosion GaAs/AlGaAs et de déterminer les conditions affectant les taux de photocorrosion. La photoluminescence des échantillons irradiés d'une façon intermittente et exposés à différentes solutions de PBS avec les bactéries, a montré une forte dépendance à la concentration de bactéries. L'importance de cette découverte a été reconnue immédiatement et nous (Dubowski, Nazemi, Aithal, Huang) avons déposé, en janvier de 2014, un brevet pour protéger cette découverte (US 2016/0349258 A1, « Photo-electrochemical biosensor and semiconductor heterostructure sensing method », publiée le 1 décembre 2017).

La première partie de cette thèse concerne l'étude de la photocorrosion intermittente (digitale), pour le développement d'une méthode convenable pour le monitoring de l'enlèvement de la matière de semi-conducteur in situ à température ambiante. L'utilité de la PL, comme un outil utile pour caractériser d'une façon digitale la profondeur de la matière enlevée (DIP), a été démontrée. Il a aussi été démontré que cette approche est suffisante pour effectuer la gravure d'une couche de GaAs aussi mince que 1 nm. Ceci est impressionnant, considérant la simplicité et la facilité pour la préparation des échantillons, ainsi qu'en tenant compte du faible coût du setup. La capacité de contrôler l'enlèvement du matériel in situ au niveau de la monocouche et sans contact (la photoluminescence), confirme que cette méthode est potentiellement attrayante pour la fabrication de nano-dispositifs avancés. Cette approche pourrait aussi être utilisée régulièrement pour localiser les interfaces dans des dispositifs à base de multicouches, sans le besoin d'utiliser des équipements sophistiqués tels que SEM, TEM et XPS qui exigent un système de vide et qui impliquent une procédure onéreuse pour la préparation des échantillons.

Dans la deuxième partie de cette thèse, j'ai démontré la corrélation entre le potentiel à circuit ouvert (OCP) et la photoluminescence, pour détecter les positions de la photocorrosion dans les nano-heterostructures GaAs/AlGaAs. Grâce à ceci, j'ai démontré que le OCP est extrêmement sensible aux propriétés physico-chimiques de surfaces de semi-conducteur et cela permet le monitoring des changements avec une résolution de l'ordre de sous-monocouche. La conséquence importante de cet accomplissement est que cela démontre le potentiel pour le monitoring in situ de la photocorrosion digitale de matériel qui n'émet pas de photoluminescence mesurable à température ambiante.

La troisième partie de ce travail a été consacrée à l'étude de la détection de L. pneumophila avec DIP des biopuces à base de GaAs/AlGaAs. Vu les résultats déjà obtenus par des expériences reliées au sujet et déjà publiées, j'ai démontré un niveau modeste de détection à 105 CFU/mL. Cela semble être relié à l'efficacité limitée de capturer des bactéries avec l'architecture employée dans

le biosenseur à anticorps utilisée dans mes tests. Au cours de ces expériences, j'ai été capable de démontrer la stabilité d'un alcanethiol SAM sur la surface subissant la photocorrosion de GaAs/AlGaAs des biopuces. Il semble que les SAM sont restés attachés à la surface de GaAs originale, ou ont suivi les surfaces « en retrait » de couches de GaAs et de AlGaAs. L'analyse détaillée de ce phénomène exige des études plus poussées qui s'étendent au-delà des limites de cette thèse.

SUMMARY AND PROSPECTS

The research undertaken in the frame of this project was originally focused on exploring the response of antibody functionalized III-V semiconductor devices for photoluminescence-based detection of bacteria. Over the course of related experiments, it became obvious that photocorrosion of GaAs/AlGaAs biochips played important role in the detection process. Thus, the urgent need arose to investigate the mechanisms of GaAs/AlGaAs photocorrosion and to determine conditions affecting photocorrosion rates. The photoluminescence of intermittently irradiated samples exposed to different PBS solutions with bacteria showed a strong dependence on the concentration of bacteria. The importance of this discovery was recognized immediately and we (Dubowski, Nazemi, Aithal, Huang) applied in January 2014 for a patent to protect this discovery (US 2016/0349258 A1, Photo-electrochemical biosensor and semiconductor heterostructure sensing method, published December 1st 2017). Subsequently, the first part of this thesis concerned investigation of the intermittent (digital) photocorrosion for the development of a method suitable for room temperature *in situ* monitoring of semiconductor material removal. The utility of PL as a useful tool for characterizing the depth of digitally photocorroding (DIP) material was demonstrated. It was also demonstrated that this approach is sufficient to resolve the etching of a GaAs layer as thin as 1 nm. This is impressive considering the simplicity, minimal sample preparation and cost of the setup. The ability to monitor *in situ* material removal at the monolayer level with a non-contact (photoluminescence) method is potentially attractive for fabrication of advanced nanodevices. This approach could also be routinely used for detecting interface locations in multilayered devices, without the need of using sophisticated equipment such as SEM, TEM and XPS that require vacuum, and which could involve an expensive sample preparation procedure.

In the second part of this thesis, I demonstrated the correlation between open circuit potential (OCP) and photoluminescence detected positions of the photocorrosion front in GaAs/AlGaAs nano-heterostructures. With this, I have demonstrated that OCP is extremely sensitive to the physico-chemical properties of semiconductor surfaces, and it allows monitoring related changes with a sub-monolayer resolution. The important consequence of this achievement is that it demonstrates the potential for monitoring *in situ* digital photocorrosion of materials that do not exhibit measurable photoluminescence at room-temperature.

The third part of this work was devoted to investigate detection of live *L. pneumophila* with DIP GaAs/AlGaAs biochips. In view of the results already obtained in related experiments published by others, I have demonstrated a modest level of detection at 10^5 CFU/mL. This seems to be related to the limited efficiency of capturing bacteria with the employed architecture of an antibody biosensor used in my experiments. In the course of these experiments, I was able to demonstrate the stability of an alkanethiol SAM on the photocorroding surface of a GaAs/AlGaAs biochip. It seems that SAM either remained attached to the original GaAs surface, or it followed

the recessing surfaces of GaAs and AlGaAs layers. Detailed analysis of this phenomenon requires studies extending beyond the scope of this thesis.

REFERENCES

Ahrenkiel, R., Dunlavy, D., Keyes, B., Vernon, S., Dixon, T., Tobin, S., . . . Hayes, R. (1989). Ultralong minority-carrier lifetime epitaxial GaAs by photon recycling. *Applied Physics Letters, 55*(11), 1088-1090.

Akke, M., & Forsén, S. (2004). Protein stability and electrostatic interactions between solvent exposed charged side chains. *Proteins: Structure, Function, and Bioinformatics, 8*(1), 23-29. doi:10.1002/prot.340080106

Aziziyan, M. R., Hassen, W. M., Morris, D., Frost, E. H., & Dubowski, J. J. (2016). Photonic biosensor based on photocorrosion of GaAs/AlGaAs quantum heterostructures for detection of Legionella pneumophila. *Biointerphases, 11*(1), 019301.

Ballard, A., Fry, N., Chan, L., Surman, S., Lee, J., Harrison, T., & Towner, K. (2000). Detection of Legionella pneumophilausing a real-time PCR hybridization assay. *Journal of clinical microbiology, 38*(11), 4215-4218.

Battiston, F., Ramseyer, J.-P., Lang, H., Baller, M., Gerber, C., Gimzewski, J., . . . Güntherodt, H.-J. (2001). A chemical sensor based on a microfabricated cantilever array with simultaneous resonance-frequency and bending readout. *Sensors and Actuators B: Chemical, 77*(1), 122-131.

Berk, S., Gunderson, J., Newsome, A., Farone, A., Hayes, B., Redding, K., . . . Farsian, M. (2006). Occurrence of infected amoebae in cooling towers compared with natural aquatic environments: implications for emerging pathogens. *Environmental science & technology, 40*(23), 7440-7444.

Bhattacharya, P., Fornari, R., & Kamimura, H. (2011a). *Comprehensive Semiconductor Science and Technology, Six-Volume Set* (Vol. 5). UK: Elsevier Science.

Bhattacharya, P., Fornari, R., & Kamimura, H. (2011b). *Comprehensive Semiconductor Science and Technology, Six-Volume Set* (Vol. 1): Newnes.

Blood, P. (1986). Capacitance-voltage profiling and the characterisation of III-V semiconductors using electrolyte barriers. *Semiconductor Science and Technology, 1*(1), 7. Retrieved from http://stacks.iop.org/0268-1242/1/i=1/a=002

Bloomfield, V., & Crothers, D. M. (2000). *Nucleic acids: structures, properties and functions*.

Buitrago, E., Badia, M. F.-B., Georgiev, Y. M., Yu, R., Lotty, O., Holmes, J. D., . . . Ionescu, A. M. (2014). Electrical characterization of high performance, liquid gated vertically stacked SiNW-based 3D FET biosensors. *Sensors and Actuators B: Chemical, 199*, 291-300.

Burlage, R. S., & Tillmann, J. (2017). Biosensors of bacterial cells. *Journal of Microbiological Methods, 138*, 2-11. doi:https://doi.org/10.1016/j.mimet.2016.12.023

Bxcell. (2018, 2018). Guide to the structure and classification of antibodies. Retrieved from https://bxcell.com/antibody-structure/

Byrne, B., Stack, E., Gilmartin, N., & O'Kennedy, R. (2009). Antibody-based sensors: Principles, problems and potential for detection of pathogens and associated toxins. *Sensors, 9*(6), 4407-4445.

Chen, Y., Zou, C., Mastalerz, M., Hu, S., Gasaway, C., & Tao, X. (2015). Applications of micro-fourier transform infrared spectroscopy (FTIR) in the geological sciences—a review. *International journal of molecular sciences, 16*(12), 30223-30250.

Chester, M. J., & Jach, T. (1993). Grazing-incidence x-ray photoelectron spectroscopy from multilayer media: Oxidized GaAs(100) as a case study. *Physical Review B, 48*(23), 17262-17270. Retrieved from https://link.aps.org/doi/10.1103/PhysRevB.48.17262

Chu, X., Wang, Y., Gan, L., Bai, Y., Han, W., Wang, E., & Wang, J. (2012). Importance of Electrostatic Interactions in the Association of Intrinsically Disordered Histone Chaperone Chz1 and Histone H2A.Z-H2B. *PLOS Computational Biology, 8*(7), e1002608. doi:10.1371/journal.pcbi.1002608

Clark, L. C., & Lyons, C. (1962). Electrode systems for continuous monitoring in cardiovascular surgery. *Annals of the New York Academy of sciences, 102*(1), 29-45.

Concepcion, J., Witte, K., Wartchow, C., Choo, S., Yao, D., Persson, H., . . . Ma, W. (2009). Label-free detection of biomolecular interactions using BioLayer interferometry for kinetic characterization. *Combinatorial chemistry & high throughput screening, 12*(8), 791-800.

Cuypers, D., Fleischmann, C., van Dorp, D. H., Brizzi, S., Tallarida, M., Müller, M., . . . Adelmann, C. (2016). Sacrificial Self-Assembled Monolayers for the Passivation of GaAs (100) Surfaces and Interfaces. *Chemistry of Materials, 28*(16), 5689-5701. doi:10.1021/acs.chemmater.6b01732

Dawson, P., & Woodbridge, K. (1984). Effects of prelayers on minority-carrier lifetime in GaAs/AlGaAs double heterostructures grown by molecular beam epitaxy. *Applied physics letters, 45*(11), 1227-1229.

DeSalvo, G. C., Bozada, C. A., Ebel, J. L., Look, D. C., Barrette, J. P., Cerny, C. L. A., . . . Via, G. D. (1996). Wet Chemical Digital Etching of GaAs at Room Temperature. *Journal of The Electrochemical Society, 143*(11), 3652-3656. doi:10.1149/1.1837266

Dimroth, F., Grave, M., Beutel, P., Fiedeler, U., Karcher, C., Tibbits, T. N., . . . Wekkeli, A. (2014). Wafer bonded four-junction GaInP/GaAs//GaInAsP/GaInAs concentrator solar cells with 44.7% efficiency. *Progress in Photovoltaics: Research and Applications, 22*(3), 277-282.

Ding, X., Moumanis, K., Dubowski, J. J., Tay, L., & Rowell, N. L. (2006). Fourier-transform infrared and photoluminescence spectroscopies of self-assembled monolayers of long-chain thiols on (001) GaAs. *Journal of Applied Physics, 99*(5), 054701. doi:10.1063/1.2178659

Ditommaso, S., Giacomuzzi, M., Gentile, M., & Zotti, C. (2010). Evaluation of the usefulness of a new direct immunofluorescence assay (ScanVIT-Legionella [trade mark sign]) for monitoring hospital water systems contaminated with Legionella spp. *Letters in applied microbiology*.

Dubowski, J. J., Nazemi, E., Aithal, S., & Huang, X. (2018). Photo-electrochemical biosensor and semiconductor heterostructure-based sensing method: US Patent App. 15/114,660.

Dubowski, J. J., Voznyy, O., & Marshall, G. M. (2010). Molecular self-assembly and passivation of GaAs (001) with alkanethiol monolayers: A view towards bio-functionalization. *Applied Surface Science, 256*(19), 5714-5721. doi:https://doi.org/10.1016/j.apsusc.2010.03.090

Duplan, V., Frost, E., & Dubowski, J. J. (2011). A photoluminescence-based quantum semiconductor biosensor for rapid in situ detection of Escherichia coli. *Sensors and Actuators B: Chemical, 160*(1), 46-51.

Erman, M., Theeten, J. B., Vodjdani, N., & Demay, Y. (1983). Chemical and structural analysis of the GaAs/AlGaAs heterojunctions by spectroscopic ellipsometry. *Journal of Vacuum Science & Technology B, 1*(2), 328-333. doi:doi:http://dx.doi.org/10.1116/1.582551

Fink, T., & Osgood, R. M. (1993). Photoelectrochemical Etching of GaAs / AlGaAS Multilayer Structures. *Journal of The Electrochemical Society, 140*(9), 2572-2581. doi:10.1149/1.2220865

Fleetwood, D., Winokur, P., Reber Jr, R., Meisenheimer, T., Schwank, J., Shaneyfelt, M., & Riewe, L. (1993). Effects of oxide traps, interface traps, and ``border traps``on metal-oxide-semiconductor devices. *Journal of Applied Physics, 73*(10), 5058-5074.

Fologea, D., Ledden, B., McNabb, D. S., & Li, J. (2007). Electrical characterization of protein molecules by a solid-state nanopore. *Applied physics letters, 91*(5), 053901. doi:10.1063/1.2767206

Franke, T., Kreutzer, P., Zacher, T., Naumann, W., & Anton, R. (1998). In situ RHEED, AFM, and REM investigations of the surface recovery of MBE-grown GaAs(001)-layers during growth interruptions. *Journal of Crystal Growth, 193*(4), 451-459. Retrieved from <Go to ISI>://000076725000002

Fritz, J., Cooper, E. B., Gaudet, S., Sorger, P. K., & Manalis, S. R. (2002). Electronic detection of DNA by its intrinsic molecular charge. *Proceedings of the National Academy of Sciences, 99*(22), 14142-14146. doi:10.1073/pnas.232276699

Gerardi, C., Giannini, C., Passaseo, A., & Tapfer, L. (1997). High-resolution depth profiling of In(x)Ga(1-x)As/GaAs multiple quantum well structures by combination of secondary ion mass spectrometry

and x-ray diffraction techniques. *Journal of Vacuum Science & Technology B, 15*(6), 2037-2045. Retrieved from <Go to ISI>://CCC:000071103100032

Grossman, H., Myers, W., Vreeland, V., Bruehl, R., Alper, M., Bertozzi, C., & Clarke, J. (2004). Detection of bacteria in suspension by using a superconducting quantum interference device. *Proceedings of the National Academy of Sciences, 101*(1), 129-134.

Hamm, C. W., Goldmann, B. U., Heeschen, C., Kreymann, G., Berger, J., & Meinertz, T. (1997). Emergency room triage of patients with acute chest pain by means of rapid testing for cardiac troponin T or troponin I. *New England Journal of Medicine, 337*(23), 1648-1653.

Hassen, W., Sanyal, H., Hammood, M., Moumanis, K., Frost, E., & Dubowski, J. (2016). Chemotaxis for enhanced immobilization of Escherichia coli and Legionella pneumophila on biofunctionalized surfaces of GaAs. *Biointerphases, 11*(2), 021004.

Hassen, W. M., Sanyal, H., Hammood, M., Moumanis, K., Frost, E. H., & Dubowski, J. J. (2016). Chemotaxis for enhanced immobilization of Escherichia coli and Legionella pneumophila on biofunctionalized surfaces of GaAs. *Biointerphases, 11*(2), 021004.

Herrmann, A., Lehnhardt, T., Strauß, M., Kamp, M., & Forchel, A. (2011). Optimization and comparison of depth profiling in GaAs and GaSb with TOF-SIMS. *Surface and Interface Analysis, 43*(1-2), 673-675.

Ho, C. K., Robinson, A., Miller, D. R., & Davis, M. J. (2005). Overview of sensors and needs for environmental monitoring. *Sensors, 5*(1), 4-37.

Hong, S.-R., Choi, S.-J., Do Jeong, H., & Hong, S. (2009). Development of QCM biosensor to detect a marine derived pathogenic bacteria Edwardsiella tarda using a novel immobilisation method. *Biosensors and Bioelectronics, 24*(6), 1635-1640.

Hostetler, M. J., Stokes, J. J., & Murray, R. W. (1996). Infrared Spectroscopy of Three-Dimensional Self-Assembled Monolayers: N-Alkanethiolate Monolayers on Gold Cluster Compounds. *Langmuir, 12*(15), 3604-3612. doi:10.1021/la960249n

Howe, E., & Harding, G. (2000). A comparison of protocols for the optimisation of detection of bacteria using a surface acoustic wave (SAW) biosensor. *Biosensors and Bioelectronics, 15*(11), 641-649.

Huang, X., & Dubowski, J. J. (2014). Solvent-mediated self-assembly of hexadecanethiol on GaAs (001). *Applied Surface Science, 299*, 66-72. doi:https://doi.org/10.1016/j.apsusc.2014.01.187

Huang, X., Liu, N., Moumanis, K., & Dubowski, J. J. (2013). Water-Mediated Self-Assembly of 16-Mercaptohexadecanoic Acid on GaAs (001). *The Journal of Physical Chemistry C, 117*(29), 15090-15097. doi:10.1021/jp402653n

Ishii, H., Sawada, K., Ishida, M., Machida, K., Iida, K.-I., Saito, M., & Yoshida, S.-i. (2013). Bio-MEMS Chip for Bacteria Detection-A Challenge of Si Technology to Biomedical Field. *ECS Transactions, 58*(9), 125-133.

J. J. Dubowski, D. F. Williams, P. B. Sewell, & Norman, P. (1985). Epitaxial growth of (100)CdTe on (100)GaAs induced by pulsed laser evaporation. *Appl. Phys. Lett., 46*(11), 1081-1883.

Kaniewska, M., & Slomka, I. (2001). C-V profiling of GaAs using electrolyte barriers. *Crystal Research and Technology, 36*(8-10), 1113-1118. Retrieved from <Go to ISI>://CCC:000171958300039

Kerr, A. J., Chagarov, E., Gu, S., Kaufman-Osborn, T., Madisetti, S., Wu, J., . . . Kummel, A. C. (2014). Preparation of gallium nitride surfaces for atomic layer deposition of aluminum oxide. *The Journal of Chemical Physics, 141*(10), 104702. doi:10.1063/1.4894541

Kim, C.-K., Marshall, G. M., Martin, M., Bisson-Viens, M., Wasilewski, Z., & Dubowski, J. J. (2009). Formation dynamics of hexadecanethiol self-assembled monolayers on (001) GaAs observed with photoluminescence and Fourier transform infrared spectroscopies. *Journal of Applied Physics, 106*(8), 083518. doi:doi:http://dx.doi.org/10.1063/1.3248370

Kirchner, C., George, M., Stein, B., Parak, W. J., Gaub, H. E., & Seitz, M. (2002). Corrosion Protection and Long-Term Chemical Functionalization of Gallium Arsenide in an Aqueous Environment. *Advanced Functional Materials, 12*(4), 266-276.

Knauer, M., Ivleva, N. P., Niessner, R., & Haisch, C. (2010). Optimized Surface-enhanced Raman Scattering (SERS) Colloids for the Characterization of Microorganisms. *Analytical Sciences, 26*(7), 761-766. doi:10.2116/analsci.26.761

Kronik, L., & Shapira, Y. (2001). Surface photovoltage spectroscopy of semiconductor structures: at the crossroads of physics, chemistry and electrical engineering. *Surface and Interface analysis, 31*(10), 954-965.

Lin, H.-Y., Tsao, Y.-C., Tsai, W.-H., Yang, Y.-W., Yan, T.-R., & Sheu, B.-C. (2007). Development and application of side-polished fiber immunosensor based on surface plasmon resonance for the detection of Legionella pneumophila with halogens light and 850nm-LED. *Sensors and Actuators A: Physical, 138*(2), 299-305.

Linkov, P., Artemyev, M., Efimov, A. E., & Nabiev, I. (2013). Comparative advantages and limitations of the basic metrology methods applied to the characterization of nanomaterials. *Nanoscale, 5*(19), 8781-8798.

Liu, N., & Dubowski, J. J. (2013). Chemical evolution of InP/InGaAs/InGaAsP microstructures irradiated in air and deionized water with ArF and KrF lasers. *Applied Surface Science, 270*, 16-24.

Liu, N., Huang, X., & Dubowski, J. J. (2014). Selective area in situ conversion of Si (0 0 1) hydrophobic to hydrophilic surface by excimer laser irradiation in hydrogen peroxide. *Journal of Physics D: Applied Physics, 47*(38), 385106.

Liu, N., Poulin, S., & Dubowski, J. J. (2013). Enhanced photoluminescence emission from bandgap shifted InGaAs/InGaAsP/InP microstructures processed with UV laser quantum well intermixing. *J. Phys. D: Appl. Phys., 46*(44), 445103. Retrieved from http://stacks.iop.org/0022-3727/46/i=44/a=445103

Lynch, S. V., & Pedersen, O. (2016). The Human Intestinal Microbiome in Health and Disease. *New England Journal of Medicine, 375*(24), 2369-2379. doi:10.1056/NEJMra1600266

Macdonald, J. R. (1992). Impedance spectroscopy. *Annals of biomedical engineering, 20*(3), 289-305.

Manera, M. G., Montagna, G., Cimaglia, F., Chiesa, M., Poltronieri, P., Santino, A., & Rella, R. (2013). SPR based immunosensor for detection of Legionella pneumophila in water samples. *Optics Communications, 294*, 420-426.

Mannelli, I., Lecerf, L., Guerrouache, M., Goossens, M., Millot, M.-C., & Canva, M. (2007). DNA immobilisation procedures for surface plasmon resonance imaging (SPRI) based microarray systems. *Biosensors and Bioelectronics, 22*(6), 803-809.

Mannheim, E., Alkire, R. C., & Sani, R. L. (1994). Modeling of Charge Carrier Transport in Photoetching of Gallium Arsenide. *141*(2), 546-554.

Masut, R. A., Roth, A. P., Dubowski, J. J., & Lenchyshyn, L. C. (1986). Characterisation of CdTe/GaAs heterojunctions with photovoltage measurements. *Semiconductor Science and Technology, 1*(3), 226-229. Retrieved from <Go to ISI>://000202875400011

Meguro, T., & Aoyagi, Y. (1997). Digital etching of GaAs. *Applied Surface Science, 112*, 55-62. doi:https://doi.org/10.1016/S0169-4332(96)00996-8

Michen, B., & Graule, T. (2010). Isoelectric points of viruses. *Journal of Applied Microbiology, 109*(2), 388-397. doi:10.1111/j.1365-2672.2010.04663.x

Miller, E. A., & Richmond, G. L. (1997). Photocorrosion of n-GaAs and Passivation by Na 2 S: A Comparison of the (100), (110), and (111)B Faces. *The Journal of Physical Chemistry B, 101*(14), 2669-2677. doi:10.1021/jp962852k

Moulder, J., Stickle, W., Sobol, P., & Bomben, K. (2002). Handbook of X-ray Photoelectron Spectroscopy (Perkin-Elmer, Eden Prairie, MN, 1992). *Google Scholar*, 128.

Murga, R., Forster, T. S., Brown, E., Pruckler, J. M., Fields, B. S., & Donlan, R. M. (2001). Role of biofilms in the survival of Legionella pneumophila in a model potable-water system. *Microbiology, 147*(11), 3121-3126.

Nagel, B., Dellweg, H., & Gierasch, L. (1992). Glossary for chemists of terms used in biotechnology (IUPAC Recommendations 1992). *Pure and Applied Chemistry, 64*(1), 143-168.

Nakashima, K., & Tateno, K. (2004). X-ray diffraction analysis of GaInNAs double-quantum-well structures. *Journal of Applied Crystallography, 37*, 14-23. Retrieved from <Go to ISI>://CCC:000188225100003

Nazemi, E., Aithal, S., Hassen, W. M., Frost, E. H., & Dubowski, J. J. (2015). GaAs/AlGaAs heterostructure based photonic biosensor for rapid detection of Escherichia coli in phosphate buffered saline solution. *Sensors and Actuators B: Chemical, 207*, 556-562.

Nesher, G., Vilan, A., Cohen, H., Cahen, D., Amy, F., Chan, C., . . . Kahn, A. (2006). Energy Level and Band Alignment for GaAs−Alkylthiol Monolayer−Hg Junctions from Electrical Transport and Photoemission Experiments. *The Journal of Physical Chemistry B, 110*(29), 14363-14371. doi:10.1021/jp062181i

Notingher, I. (2007). Raman spectroscopy cell-based biosensors. *Sensors, 7*(8), 1343-1358.

Notkins, A. L. (2004). Polyreactivity of antibody molecules. *Trends in immunology, 25*(4), 174-179.

Oliver, R. A. (2008). Advances in AFM for the electrical characterization of semiconductors. *Reports on Progress in Physics, 71*, 076501. doi:10.1088/0034-4885/71/7/076501

Parthuisot, N., Binet, M., Touron-Bodilis, A., Pougnard, C., Lebaron, P., & Baudart, J. (2011). Total and viable Legionella pneumophila cells in hot and natural waters as measured by immunofluorescence-based assays and solid-phase cytometry. *Applied and environmental microbiology, 77*(17), 6225-6232.

Passlack, M., Hong, M., Mannaerts, J. P., Kwo, J. R., & Tu, L. W. (1996). Recombination velocity at oxide–GaAs interfaces fabricated by in situ molecular beam epitaxy. *Applied physics letters, 68*(25), 3605-3607. doi:10.1063/1.116652

Patolsky, F., Zayats, M., Katz, E., & Willner, I. (1999). Precipitation of an insoluble product on enzyme monolayer electrodes for biosensor applications: characterization by faradaic impedance spectroscopy, cyclic voltammetry, and microgravimetric quartz crystal microbalance analyses. *Analytical chemistry, 71*(15), 3171-3180.

Perovic, D., Castell, M., Howie, A., Lavoie, C., Tiedje, T., & Cole, J. (1995). Field-emission SEM imaging of compositional and doping layer semiconductor superlattices. *Ultramicroscopy, 58*(1), 104-113.

Pettenpaul, E. (1998). *GaAs a key RF technology-Industrialisation & competition.* Paper presented at the Microwave Conference, 1998. 28th European.

Pettenpaul, E. (1998). GaAs a key RF technology - Industrialisation \& competition. *2*, 368--373. doi:10.1109/EUMA.1998.338180

Poortinga, A., Bos, R., & Busscher, H. (1999). Measurement of charge transfer during bacterial adhesion to an indium tin oxide surface in a parallel plate flow chamber. *Journal of microbiological methods, 38*(3), 183-189.

Poortinga, A. T., Bos, R., Norde, W., & Busscher, H. J. (2002). Electric double layer interactions in bacterial adhesion to surfaces. *Surface science reports, 47*(1), 1-32. doi:https://doi.org/10.1016/S0167-5729(02)00032-8

Radke, S. M., & Alocilja, E. C. (2005). A high density microelectrode array biosensor for detection of E. coli O157: H7. *Biosensors and Bioelectronics, 20*(8), 1662-1667.

Rowe, C. A., Scruggs, S. B., Feldstein, M. J., Golden, J. P., & Ligler, F. S. (1999). An array immunosensor for simultaneous detection of clinical analytes. *Analytical chemistry, 71*(2), 433-439.

Ruberto, M. N., Zhang, X., Scarmozzino, R., Willner, A. E., Podlesnik, D. V., & Osgood, R. M. (1991). The Laser-Controlled Micrometer-Scale Photoelectrochemical Etching of III–V Semiconductors. *Journal of The Electrochemical Society, 138*(4), 1174-1185. doi:10.1149/1.2085737

Salgin, S., Salgin, U., & Bahadir, S. (2012). Zeta potentials and isoelectric points of biomolecules: the effects of ion types and ionic strengths. *Int. J. Electrochem. Sci, 7*(12), 12404-12414.

Salis, A., Boström, M., Medda, L., Cugia, F., Barse, B., Parsons, D. F., . . . Monduzzi, M. (2011). Measurements and Theoretical Interpretation of Points of Zero Charge/Potential of BSA Protein. *Langmuir, 27*(18), 11597-11604. doi:10.1021/la2024605

Sarangadharan, I., Chu, C. H., Hsu, C.-P., & Wang, Y.-L. (2015). Early Detection of Lung Cancer Using High Electron Mobility Transistors. *ECS Transactions, 66*(7), 145-149.

Schroder, D. K. (2006). *Semiconductor material and device characterization*: John Wiley & Sons.

Sharma, H., Moumanis, K., & Dubowski, J. J. (2016). pH-Dependent Photocorrosion of GaAs/AlGaAs Quantum Well Microstructures. *The Journal of Physical Chemistry C, 120*(45), 26129-26137. doi:10.1021/acs.jpcc.6b08844

Sharp, K. A. (2002). Electrostatic interactions in proteins *Computational Approaches to Biochemical Reactivity* (pp. 199-235): Springer.

Simpson, B. H., & Rodríguez-López, J. (2015). Electrochemical Imaging and Redox Interrogation of Surface Defects on Operating SrTiO3 Photoelectrodes. *Journal of the American Chemical Society, 137*(47), 14865-14868.

Soni, K. A., Balasubramanian, A. K., Beskok, A., & Pillai, S. D. (2008). Zeta potential of selected bacteria in drinking water when dead, starved, or exposed to minimal and rich culture media. *Current Microbiology, 56*(1), 93-97.

Stølhaug, A., & Bergh, K. (2006). Identification and differentiation of Legionella pneumophila and Legionella spp. with real-time PCR targeting the 16S rRNA gene and species identification by mip sequencing. *Applied and environmental microbiology, 72*(9), 6394-6398.

Sturdivant, R., & Harris, M. (2015). *Transmit Receive Modules for Radar and Communication Systems*: Artech House.

Subramanian, P., Lesniewski, A., Kaminska, I., Vlandas, A., Vasilescu, A., Niedziolka-Jonsson, J., . . . Szunerits, S. (2013). Lysozyme detection on aptamer functionalized graphene-coated SPR interfaces. *Biosensors and Bioelectronics, 50*, 239-243.

Sundaram, J., Park, B., Kwon, Y., & Lawrence, K. C. (2013). Surface enhanced Raman scattering (SERS) with biopolymer encapsulated silver nanosubstrates for rapid detection of foodborne pathogens. *International journal of food microbiology, 167*(1), 67-73.

Takashi, M., Masashi, I., Hirokazu, K., Manabu, H., Tamio, H., Yasuhiro, Y., & Yoshinobu, A. (1990). Layer-By-Layer Controlled Digital Etching by Means of an Electron-Beam-Excited Plasma System. *Japanese Journal of Applied Physics, 29*(10R), 2216. Retrieved from http://stacks.iop.org/1347-4065/29/i=10R/a=2216

Tapfer, L., & Ploog, K. (1986). Improved assessment of structural properties of AlxGa1− xAs/GaAs heterostructures and superlattices by double-crystal x-ray diffraction. *Physical review. B, Condensed matter, 33*(8), 5565-5574.

Tiberio, R. C., Craighead, H. G., Lercel, M., Lau, T., Sheen, C. W., & Allara, D. L. (1993). Self-assembled monolayer electron beam resist on GaAs. *Applied physics letters, 62*(5), 476-478. doi:10.1063/1.108938

Turner, N. H., & Schreifels, J. A. (2000). Surface Analysis: X-ray Photoelectron Spectroscopy and Auger Electron Spectroscopy. *Analytical chemistry, 72*(12), 99-110. doi:10.1021/a10000110

Van De Krol, R. (2012). Principles of photoelectrochemical cells *Photoelectrochemical hydrogen production* (pp. 13-67): Springer.

Vartoukian, S. R., Palmer, R. M., & Wade, W. G. (2010). Strategies for culture of 'unculturable'bacteria. *FEMS microbiology letters, 309*(1), 1-7.

Voznyy, O., & Dubowski, J. J. (2008). Structure of Thiol Self-Assembled Monolayers Commensurate with the GaAs (001) Surface. *Langmuir, 24*(23), 13299-13305. doi:10.1021/la8010635

Wang, J. (2002). Electrochemical nucleic acid biosensors. *Analytica Chimica Acta, 469*(1), 63-71.

Wilson, W. W., Wade, M. M., Holman, S. C., & Champlin, F. R. (2001). Status of methods for assessing bacterial cell surface charge properties based on zeta potential measurements. *Journal of Microbiological Methods, 43*(3), 153-164. doi:https://doi.org/10.1016/S0167-7012(00)00224-4

Wink, T., J. van Zuilen, S., Bult, A., & P. van Bennekom, W. (1997). Self-assembled Monolayers for Biosensors. *Analyst, 122*(4), 43R-50R. doi:10.1039/A606964I

Wośko, M., Paszkiewicz, B., Tarnowski, K., Ściana, B., Radziewicz, D., Salejda, W., . . . Tłaczała, M. (2011). Reverse engineering of AlxGa1− xAs/GaAs structures composition by reflectance spectroscopy. *Opto-Electronics Review, 19*(4), 418-424.

Zeng, X., Shen, Z., & Mernaugh, R. (2012). Recombinant antibodies and their use in biosensors. *Analytical and bioanalytical chemistry, 402*(10), 3027-3038.

Zhang, Y., Yang, M., Portney, N. G., Cui, D., Budak, G., Ozbay, E., . . . Ozkan, C. S. (2008). Zeta potential: a surface electrical characteristic to probe the interaction of nanoparticles with normal and cancer human breast epithelial cells. *Biomedical microdevices, 10*(2), 321-328.

Zourob, M., Elwary, S., & Turner, A. P. (2008). *Principles of bacterial detection: biosensors, recognition receptors and microsystems*: Springer Science & Business Media.

Conference and poster presentations during PhD thesis

- Open Circuit Potential Oscillations of Digitally Photocorroding GaAs/AlGaAs Nano-Heterostructures, **S. Aithal**, and J.J. Dubowski, Canadian Semiconductor Science and Technology, August 20-24, 2017, Waterloo, Canada
- Biginelli Compound Functionalized Biosensors: GaAs/AlGaAs Biochips for Enhanced Detection of Bacteria, **S. Aithal**, H. Sharma, A. Singh, N. Singh, and JJ. Dubowski, IC-IMPACTS Research Conference, June 9-10, 2017, Vancouver, Canada
- Quasi-continuous Detection of Bacteria with GaAs/AlGaAs Nano-Heterostructures, **S. Aithal**, W. M. Hassen, J.J. Dubowski, 17th Canadian Semiconductor Science and Technology Conference, August 16 – 21, 2015, Sherbrooke, Quebec, Canada
- GaAs-based photonic biosensor: pH sensitivity and detection of E. coli, **S. Aithal**, E. Nazemi, M.W. Hassen, E. Frost and J.J. Dubowski, SSP'2013, Krakow, Poland, September 8 -12, 2013

Journal publications

- **S. Aithal**, N. Liu, JJ. Dubowski, Photocorrosion metrology of photoluminescence emitting GaAs/AlGaAs heterostructures. Journal of Physics D: Applied Physics. 2016;50(3):035106
- E. Nazemi, **S. Aithal**, WM. Hassen, EH. Frost, JJ. Dubowski, GaAs/AlGaAs heterostructure based photonic biosensor for rapid detection of Escherichia coli in phosphate buffered saline solution. Sensors and Actuators B: Chemical. 2015;207:556-62
- **S. Aithal**, JJ. Dubowski, Open circuit potential monitored digital photocorrosion of GaAs/AlGaAs quantum well microstructures, Applied Physics Letters, 2018;112:153102

Patent

- Photo-electrochemical biosensor and semiconductor heterostructure-based sensing method, Jan J. Dubowski, Elnaz Nazemi, **Srivatsa Aithal**, Xiaohuan Huang, PCT/CA2015/050073